Titre: Title:	Evaluation of Time-Domain and Phasor-Domain Methods for Power System Transients
Auteur: Author:	Reza Hassani
Date:	2022
Type:	Mémoire ou thèse / Dissertation or Thesis
Référence: Citation:	Hassani, R. (2022). Evaluation of Time-Domain and Phasor-Domain Methods for Power System Transients [Ph.D. thesis, Polytechnique Montréal]. PolyPublie. https://publications.polymtl.ca/10299/

URL de PolyPublie: PolyPublie URL:	https://publications.polymtl.ca/10299/
Directeurs de recherche: Advisors:	Jean Mahseredjian
Programme: Program:	Génie électrique

POLYTECHNIQUE MONTRÉAL

affiliée à l'Université de Montréal

Evaluation of time-domain and phasor-domain methods for power system transients

REZA HASSANI

Département de génie électrique

Thèse présentée en vue de l'obtention du diplôme de *Philosophiæ Doctor*

Génie électrique

Avril 2022

POLYTECHNIQUE MONTRÉAL

affiliée à l'Université de Montréal

Cette thèse intitulée :

Evaluation of time-domain and phasor-domain methods for power system transients

présentée par **Reza HASSANI**

en vue de l'obtention du diplôme de *Philosophiæ Doctor*

a été dûment acceptée par le jury d'examen constitué de :

Houshang KARIMI, président
Jean MAHSEREDJIAN, membre et directeur de recherche
Antoine LESAGE-LANDRY, membre
Ali ABUR, membre externe

DEDICATION

To my parents

ACKNOWLEDGEMENTS

It is my pleasure to express gratitude to all the people whom I had the honor to work and communicate with during this project:

Foremost, I would like to express my very great appreciation to my supervisor Prof. Jean Mahseredjian for accepting me as his Ph.D. student, and for the support and meaningful discussions.

To Tshibain Tshibungu for his collaborators and knowledge, he was a great help to me.

To Aboutaleb Haddadi for his guidance.

To Tarek Ould-Bachir for his meaningful discussions.

To the late Prof. Akihiro Ametani for encouragement and inspiration.

All colleagues at the department for their friendship and support. To those who already left: Isabel Lafaia, Younes Seyedi, Baki Çetindağ, Thomas Kauffmann, Mohsen Ghafouri, Haoyan Xue, Ming Cai, Anas Abousalah, Anton Stepanov, Aramis Trevisan, Diane Desjardins, François Gauthier, Jesus Morales Rodrigues, Masashi Natsui, Miguel Cervantes Martinez, Serigne Seye, Xiaopeng Fu, Amir Sadati, Hossein Chalangar, Danial Jafari, Alireza Masoum, Reza Ramezanpour, and Willy Nzale, Maryam Torabi. To those who will continue: Sadegh Rahimi, Milad Hosseini, and others.

RÉSUMÉ

Les chercheurs et les ingénieurs utilisent largement la méthode des transitoires électromagnétiques (EMT) dans les études des systèmes électriques. La méthode EMT prend en charge la simulation des modèles en détail. Cependant, la vitesse de simulation est compromise en raison de la taille des pas de temps d'intégration.

La thèse utilise la méthode Dynamic Phasor (DP) pour tenter d'accélérer les simulations transitoires des systèmes électriques. La méthode DP permet d'utiliser de grands pas de temps pour simuler avec précision la dynamique du système électrique dans une bande de fréquence centrée autour de la fréquence souhaitée.

La thèse présente et améliore les méthodes de simulation disponibles pour les transitoires du système électrique, à savoir : Domaine de phaseur (PD), Domaine de phaseur triphasé (3pPD), EMT et DP. Ensuite, les résultats de simulation et les temps de simulation des méthodes sont comparés pour les cas de test pratiques présentés. De nouvelles démonstrations et comparaisons non disponibles auparavant sont effectuées.

Parmi les améliorations apportées aux modèles, la thèse propose un nouveau modèle de machine synchrone basé sur la méthode DP, qui utilise des variables de phase dynamique plutôt que des variables temporelles instantanées. Ce modèle tient compte des harmoniques pour présenter une simulation précise des événements déséquilibrés.

De plus, cette thèse explore l'approche DP pour la simulation des Perturbations Géomagnétiques (GMD). La simulation utilise l'harmonique DC pour présenter l'effet de GMD dans le réseau. Un modèle de saturation du transformateur et de la machine synchrone est présenté, qui utilise la fréquence fondamentale et l'harmonique CC pour modéliser GMD.

ABSTRACT

Researchers and engineers extensively utilize the Electromagnetic Transients (EMT) method in studies of power systems. EMT approach allows for detailed modeling. However, the simulation speed is compromised due to the size of the integration time steps.

The dissertation uses the Dynamic Phasor (DP) method to try to accelerate transient simulations of the power systems. The DP method allows using large time steps to accurately simulate power system dynamics within a frequency band centered around the desired frequency.

The thesis presents and improves available simulation methods for power system transients, namely: Phasor Domain (PD), Three-phase Phasor Domain (3pPD), EMT, and DP. Then, the simulation results and simulation timings of the methods are compared for presented practical test cases. New, not previously available, demonstrations and comparisons are made.

Amongst improvements in models, the thesis proposes a new synchronous machine model based on the DP method, which uses dynamic phasor variables rather than instantaneous time-domain variables. This model accounts for harmonics to present an accurate simulation of unbalanced events.

Furthermore, this thesis explores the DP approach for the simulation of Geomagnetic Disturbances (GMDs). The simulation uses the DC harmonic to present the effect of GMD in the network. A saturation model of the transformer and synchronous machine is presented, which uses fundamental frequency and DC harmonic to model GMD.

TABLE OF CONTENTS

LIST OF TABLES

LIST OF FIGURES

LIST OF SYMBOLS AND ABBREVIATIONS

δ	Angle between quadrature axis and terminal voltage
ω_m, ω_r, ω_s	Mechanical, rotor, synchronous angular frequency
ψ_d, ψ_q	Direct and quadrature axis flux
MANA	Modified-augmented-nodal analysis
DP	Dynamic phasor
EMT	Electromagnetic transient
$E_d^{'}$, $E_d^{''}$	Transient and sub-transient emf proportional to quadrature axis flux
$E_q^{'}$, $E_q^{''}$	Transient and sub-transient emf proportional to direct axis flux
E_{fd}	Excitation field voltage
GMD	Geomagnetic disturbance
i_d, i_q, i_0	Direct, quadrature, and zero axis components of stator current
R_a	Stator resistance
TS	Transient stability
PD	Phasor domain
3pPD	three-phase phasor domain
T_m, T_e	Mechanical and electromagnetic torque
$T_{d0}^{'}$, $T_{d0}^{''}$	Transient and sub-transient open-circuit time constants on *d*-axis
$T_{q0}^{'}$, $T_{q0}^{''}$	Transient and sub-transient open-circuit time constants on *q*-axis
v_d, v_q, v_0	Direct, quadrature, and zero axis components of stator voltage
X_d, $X_d^{'}$, $X_d^{''}$	Synchronous, transient, and sub-transient reactance on *d*-axis

X_q, $X_q^{'}$, $X_q^{''}$ Synchronous, transient, and sub-transient reactance on *q*-axis

Chapter 1 INTRODUCTION

1.1 Problem Definition

Power systems are increasingly complex. It is now becoming common practice to simulate large-scale power grids using accurate time-domain (TD) methods. The simulation of transient stability events with electromagnetic transients using the same computing environment is particularly challenging.

Different types of simulation methods exist and fulfill various application objectives. Depending on the simulation speed or precision requirements, a user will choose a specific simulation method. Transient simulation methods are divided into two main categories: electromagnetic transient (EMT)-type and Transient Stability (TS)-type. The EMT approach is circuit-based and detailed. It is a wideband approach suitable for the simulation of both electromagnetic and electromechanical transients. The TS approach is used for slower electromechanical transients and encounters significant limitations for faster transients.

The EMT or TD is an accurate, but it is computationally much more intensive than the TS approach. In recent years, the Dynamic Phasors (DP) have been introduced [1] to deliver an accuracy navigator approach. This means that larger numerical integration time-steps can be used to accelerate EMT computations with sufficient accuracy for fast transients while maintaining the capability to simulate faster transients when using smaller time-steps. The main hypothesis is that such large time-steps cannot be used in the EMT mode.

Reference [2] develops a DP model for imbalanced distribution systems containing single-phase photovoltaic (PV), three-phase induction machine load, three-phase power factor correction capacitor (PFC), and loads. The DP approach is utilised to construct inverter-based microgrids and investigate the transient response under imbalanced conditions in [3]. Reference [4] proposes a frequency-based analytical approach for dynamic analysing of unbalanced three-phase systems in the presence of harmonic distortion in the sequence domain, demonstrating that the classical symmetrical components proposed by Fortescue are inapplicable under non-sinusoidal periodic conditions. In [5-7], the modular multilevel converter (MMC) models of the DP method are introduced. On the long time scale, reference [5] develops a reduced-order DP model of MMC that is utilised for power system low-frequency oscillation analysis. Reference [6] presents a DP model

of a half-bridge MMC based on variables in the stationary *abc* frame. A new DP model of an MMC with extended frequency range is available in [7] for an EMT simulator. Under unbalanced grid situations, [8] proposes a dynamic-phasor-based small-signal model for the modular multilevel converter technology. A DP-based model for line-commutated-converters is developed in [9]. To analyse the sub-synchronous resonance, reference [10] utilises a DP model of the thyristor-controlled series capacitor. Reference [11] presents a multiscale induction machine model using the DP method. A generalised state-space averaging model for a three-phase dual active bridge converter based on the DP concept is proposed in [12]. Reference [13] utilised a variable frequency for the DP principle to improve the method's usability to multi-source, multi-frequency systems, as well as systems with time-varying frequencies. Based on the DP concept, [13] presents a new Type 3 wind farm modelling method. It contains not just 60-Hz frequencies, but also significant frequencies like 36 Hz that are present in the system due to sub-synchronous control interactions. To represent the desired fault behaviour, only the most relevant DPs are chosen, resulting in enhanced computation efficiency.

In order to simulate inrush dynamics, [14] proposes a DP basis model of transformer saturation and uses iterative solver. A DP base estimate model for phasor measurement units is presented in [15]. Reference [16] uses the DP technique to propose a synchronous machine model for the modelling of low frequency system dynamics. The DP is employed to study the effects of passive phase imbalance schemes on a turbine-generator system's torsional modes [17]. For current differential protection of transmission-line, reference [18] uses the DP concept. The DP method is used in [19] to simulate unbalanced faults containing a three-phase synchronous generator connected to a transmission line with an open end. An average-value model of a line commutated converter-based high voltage DC system utilising DP is shown in Reference [20]. The method offers an efficient model of DC dynamics, the converter's low frequency, as well as the ac system.

A new modelling technique for inverter-dominated microgrids utilising DP is provided in [21] in order to preserve simulation compromise for inverter-dominated microgrids. According to the paper, the suggested DP model is capable of properly predicting the system's stability margins, but the reduced-order small signal model fails. A three-phase DP model of high-voltage direct current systems is suggested, with a focus on the converter in [22]. For both symmetrical and asymmetrical operating situations, the suggested model increases simulation speed of the converter's dynamic

characteristics. Under harmonic circumstances, reference [23] acquires the modelling and analysis of inverter-based micro grids. For droop-controlled distributed generators, diodes rectifiers as nonlinear loads, and resistance loads, the DP model of fundamental frequency and harmonics is developed.

Some studies compared the accuracy and computation time of TD and DP methods [7, 9, 11, 14, 24-26]. Reference [24] compares TD and DP methods and reports that the DP method is ten times faster than EMT. The [14] simulates the simple IEEE 4-node test feeder by TD and DP methods. The TD method with PSCAD software using a time-step of 50μs and the DP method with GridLAB-D using a time-step of 500μs are simulated and show that DP is about 17 times faster than the TD method. Reference [7] illustrates that for 400 identical submodules per arm in MMC, the DP model is approximately eight times faster than the detailed equivalent model with the same simulation time-step. The DP-based approach is presented in [27] to accelerate EMT-type studies of modelling the induction machine dynamics. It was discovered that while modelling dynamics with frequency spectra near to the fundamental frequency, the DP-based model is more than 70 times faster than the EMT-type model. To demonstrate time efficiency of DP based model, the article did not utilise the same time.

However, the reported efficiency comparisons are not fair. A significant amount of literature is presenting non-practical material for delivering unsupported conclusions. In some cases, the methods do not use the same simulation time-step [7, 14]. The test cases are not simulated using the same platform for all assessed methods [14, 26]. Accuracy is compared only qualitatively [24, 25]. Also, [7] uses a simplified MMC model, which decreases accuracy for faster transient simulations and increases computational time. A fair and systematic comparison of simulation methods is not currently available in the literature.

During transients, the unsymmetrical components cause harmonics in the synchronous machine (SM). The even and odd harmonics on the bus side cause odd and even harmonics in the SM, respectively [24, 26, 28, 29]. Therefore, the DP model using only fundamental frequency is not able to deliver accurate results. A model of SM using harmonics is necessary to improve the DP model.

The DP method has been mostly used for linear circuits. Extending to account for nonlinearities is feasible but remains challenging for computational performance. It will be demonstrated in this thesis that contrary to common belief, the DP method encounters several limitations when compares to the EMT approach.

To search practical applications of DP, in this thesis, the testing of the DP method is extended into the simulation of geomagnetic disturbances. Such disturbances are studied for large networks and need to run for a long interval. The simulations should be accurate and efficient. The EMT method has the desired properties but has computational performance limitations. The DP method must be adapted for simulating GMD events. A nonlinear saturation model of transformers for DP is developed to simulate GMD.

The following section presents the fundamental theories related to TD, DP, and PD methods. As shown below, the PD method is referred to as a phasor-domain method because it solves its network equations only in the phasor domain.

1.1.1 Time domain method

The TD (or EMT) method uses the actual TD relation of power system elements. For example, the differential equation of inductor is:

$$v_L(t) = L\frac{di_L(t)}{dt} \tag{1.1}$$

where t, v_L, i_L, and L are time, voltage, current, and inductance, respectively.

Note that the lower letters represent time domain quantities, upper letters represent Fourier series coefficient for the dynamic phasor quantities, and upper bold letters represent Fourier series coefficient for the classic phasor quantities.

The simulators do not directly use ordinary differential equation (ODE) in the calculations. The numerical integration rules are employed to discretize ODEs. The Trapezoidal, backward Euler, forward Euler, and Gear's second-order methods are mostly used in the EMT simulators. The Trapezoidal rule has low distortion and numerical stability characteristics.

The discretized form of the (1.1) using Trapezoidal rule is:

$$i_{L_n} = i_{L_{n-1}} + \frac{\Delta t}{2L}\left(v_{L_n} + v_{L_{n-1}}\right) \tag{1.2}$$

The subscript n means the variable value at the *n*-th time-point ($x\left(t_n\right) = x_n$). The distance between the time-points is the numerical integration time-step (Δt). (1.2) can be rewritten as below to obtain Norton equivalent model.

$$i_{L_n} = \frac{v_{L_n}}{Z_L} + i_{hL_{n-1}} \tag{1.3}$$

where Z_L is the TD equivalent resistance and $i_{hL_{n-1}}$ is the TD history term of the numerical solution.

$$Z_L = \frac{2L}{\Delta t} \tag{1.4}$$

$$i_{hL_{n-1}} = i_{L_{n-1}} + \frac{\Delta t}{2L} v_{L_{n-1}} \tag{1.5}$$

The equivalent impedance depends on the size of Δt and is constant. The history term depends on voltage and current variables of the component in the previous time-step.

A discontinuity in the system like a short-circuit ($v_n = 0$) causes numerical oscillations for an inductor using Trapezoidal rule. In this case, the current at the first moment of short-circuit is equal to history term ($i_n = i_{n-1} + \frac{v_{n-1}}{Z}$). At the next time step, the current is equal to negative value of the current at the previous time step ($i_{n+1} = -i_n$). Therefore, the current after a short-circuit oscillates between a positive and a negative value. In case of having a resistance in the circuit, the numerical oscillations damps, and the damping time depends on the time constant (L / R) of the circuit.

After a system discontinuity, the EMTP approach for eliminating numerical oscillations is to use two-halves time steps of the backward Euler technique. For backward Euler, the equivalent impedance is equal to (1.4) where the time step of backward Euler is half of Trapezoidal rule time step. The equivalent history term of backward Euler for the inductor is:

$$i_{h_{n-1}} = i_{n-1} \tag{1.6}$$

By using the backward Euler, the current of an inductance after a short-circuit is constant.

A TD inductor and the Norton equivalent model using Trapezoidal rule can be shown as:

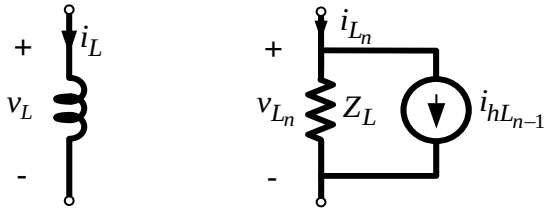

a) b)

Figure 1.1 a) TD relation of inductance, b) Equivalent circuit

The simulators based on the TD method utilize nodal-type analysis approach. The nodal analysis determines the unknown nodal voltages based on the injected current at each node. The nodal analysis is described in the [30, 31]:

$$\mathbf{Yv} = \mathbf{i} \tag{1.7}$$

where $\mathbf{Y}$, $\mathbf{v}$, and $\mathbf{i}$ are the nodal admittance matrix, vector of unknown voltages, and vector of current injected currents. The injected currents are current sources combined with history currents for the Trapezoidal method. The nodal analysis is not able to model ungrounded voltage sources, which is solved by the modified-nodal analysis [32]. The software using nodal analysis model a close switch by a very small resistance and model an open switch by a very large resistance. Moreover, a partial resistance is used to model an ideal transformer in the admittance matrix. As a result, the resistance may cause matrix conditioning problems. The modified-augmented nodal analysis (MANA) is proposed in reference [30] to extend the network representing equations by adding switches, transformers, current sources, and voltage sources. MANA avoids many theoretical complications by providing a systematic method for deriving the Jacobian matrix terms. The formulation of MANA is:

$$\underbrace{\begin{bmatrix} \mathbf{Y}_n & \mathbf{V}_c & \mathbf{D}_c & \mathbf{S}_c \\ \mathbf{V}_r & \mathbf{V}_d & \mathbf{D}_{VD} & \mathbf{S}_{VS} \\ \mathbf{D}_r & \mathbf{D}_{DV} & \mathbf{D}_d & \mathbf{S}_{DS} \\ \mathbf{S}_r & \mathbf{S}_{SV} & \mathbf{S}_{SD} & \mathbf{S}_d \end{bmatrix}}_{\mathbf{A}_n} \underbrace{\begin{bmatrix} \mathbf{v}_n \\ \mathbf{i}_V \\ \mathbf{i}_D \\ \mathbf{i}_S \end{bmatrix}}_{\mathbf{x}_n} = \underbrace{\begin{bmatrix} \mathbf{i}_n \\ \mathbf{v}_b \\ \mathbf{d}_b \\ \mathbf{s}_b \end{bmatrix}}_{\mathbf{b}_n} \tag{1.8}$$

where $\mathbf{A}_n$ is the augmented nodal admittance matrix and includes sub-matrices describing different elements by additional equations. $\mathbf{x}_n$ and $\mathbf{b}_n$ are respectively the unknown and known vectors.

1.1.2 Dynamic phasor method

The DP method has been developed recently and falls into the category of EMT-type methods and phasor-domain methods. It combines phasor coefficients with time dependent variables which enables DP method to simulate both electromagnetic and electromechanical transients efficiently. Contrary to the TS approach, the DP method can simulate electromagnetic transients. It is typically and in the vast majority of publications used for linear circuits, but it is possible to extend it to include nonlinear components.

The DP method approximates the TD waveform $x(\tau)$ in the interval $\tau \in (t-\tau, t]$ by a Fourier series representation as:

$$x(t) = \sum_{k=-\infty}^{\infty} \mathrm{X}_k(t) e^{jk\omega_s t} \tag{1.9}$$

where T is period, k is the number of Fourier coefficient, $\omega_s = 2\pi / T$, and $\mathrm{X}_k(t)$ is the k-th time-varying Fourier coefficient, which is given by:

$$\mathrm{X}_k = x\big|_k \tag{1.10}$$

where $x\big|_k$ means calculate Fourier of function x by k-th harmonic, which is:

$$x\big|_k = \frac{1}{T} \int_{t-T}^{t} x(\tau) e^{-jk\omega_s \tau} d\tau \tag{1.11}$$

The following properties of dynamic phasors are important in developing the model:

1) The derivative of the *k*-th coefficient is given by:

$$\left.\frac{dx}{dt}\right|_k = \frac{d\mathrm{X}_k}{dt} + jk\omega_s \mathrm{X}_k \tag{1.12}$$

2) The product of two TD variables is equal to a discrete time convolution of the two dynamic phasor sets of variables given by:

$$\left.xy\right|_k = \sum_l \mathrm{X}_l \mathrm{Y}_{k-l} \tag{1.13}$$

3) The negative *k*-th component is equal to conjugation of *k*-th component:

$$\mathrm{X}_{-k} = \mathrm{X}_k^{\,*} \tag{1.14}$$

Using the properties of dynamic phasors, the DP relation of voltage and current for an inductance is:

$$\mathrm{V}_{L_k}(t) = L\frac{d\mathrm{I}_{L_k}(t)}{dt} + jk\omega_s L\mathrm{I}_{L_k}(t) \tag{1.15}$$

where V_k and I_k are voltage and current phasors for the *k*-th Fourier coefficient, respectively. Using the Trapezoidal rule, the (1.15) is discretized as:

$$\mathrm{I}_{L_{k,n}} = \frac{\frac{2}{\Delta t} - jk\omega_s}{\frac{2}{\Delta t} + jk\omega_s}\mathrm{I}_{L_{k,n-1}} + \frac{\mathrm{V}_{L_{k,n}} + \mathrm{V}_{L_{k,n-1}}}{\left(\frac{2}{\Delta t} + jk\omega_s\right)L} \tag{1.16}$$

The (1.16) can be rewritten as below to obtain Norton equivalent model.

$$\mathrm{I}_{L_{k,n}} = \frac{\mathrm{V}_{L_{k,n}}}{Z_{L_k}} + \mathrm{I}_{hL_{k,n-1}} \tag{1.17}$$

where Z_{L_k} is the DP equivalent impedance and $\mathrm{I}_{h_{k,n-1}}$ is the DP history term.

$$\mathrm{Z}_{L_k} = \left(\frac{2}{\Delta t} + jk\omega_s\right)L \tag{1.18}$$

$$I_{hL_{k,n}} = \frac{V_{L_{k,n-1}} + Z_{L_k}^{*} I_{L_{k,n-1}}}{Z_{L_k}} \tag{1.19}$$

The equivalent impedance depends on the size of Δt and is constant. The history term depends on voltage and current of the component in the previous time-step.

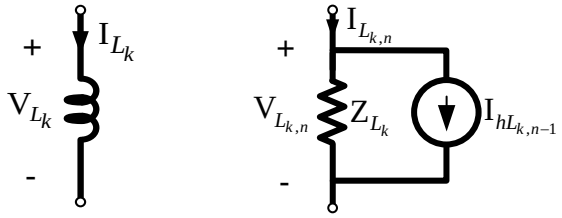

a) b)

Figure 1.2 a) Dynamic phasor inductance, b) Equivalent circuit

The DP contains the numerical ability to navigate between EMT-type and TS-type methods by increasing/reducing numerical integration time-step. In case of decreasing the time-step, the real part becomes dominant and DP acts like a TD method. Also, in case of increasing the time-step, the imaginary part becomes dominant and DP acts like a pure phasor-domain method.

1.1.3 Phasor domain method

Electromechanical transient is the interplay between the mechanical spinning machines' stored energy and the electromagnetic energy stored in the system's inductors and capacitors. Electromechanical transients are simulated using TS-type algorithms. The basic goal of TS-type approaches is to model electromechanical transients. To simplify the modeling, several assumptions are utilized. One assumption is to treat the system in quasi-steady state (QSS), ignoring inductors and capacitors' electromagnetic transients. Moreover, the TS-type examines just the fundamental frequency of the system, ignoring all other harmonics.

The classic TS approach used in this thesis is termed as phasor-domain (PD). The classic PD technique assumes that the three phases are balanced and ignores negative and zero symmetrical components, relying only on a positive sequence model of the system. The sequential components

are introduced to the DP technique to mimic unbalanced events and improve it. The modified DP approach is referred to as three-phase Phasor Domain (3pPD).

The TS-type programs ignore the electromagnetic transient, therefore the derivative equation of inductors and capacitors is:

$$\frac{dx}{dt} = j\omega_s \mathbf{X} \tag{1.20}$$

To increase accuracy of the simulation, the reference [33] uses variable frequency according to rotor speed of SMs during a transient.

Using equation (1.20), the TS relation of voltage and current of an inductance is:

$$\mathbf{V}_{L_n} = \mathbf{Z}_L \mathbf{I}_{L_n} \tag{1.21}$$

where $\mathbf{V}_{L_n}$ and $\mathbf{I}_{L_n}$ are voltage and current of TS-type phasors, respectively. The equivalent impedance, $\mathbf{Z}_L$, is:

$$\mathbf{Z}_L = j\omega_s \mathrm{L} \tag{1.22}$$

Unlike EMT-type methods, the PD models inductors independently from simulation time-step and without history term.

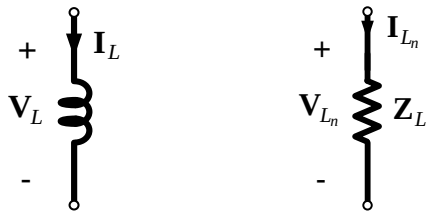

a) b)

Figure 1.3 a) Transient stability inductance, b) Equivalent circuit

1.2 Contributions

The main objective of this thesis is to study and improve the DP approach for objectively verifying its so-called advantages over the EMT approach. The demonstrations and analysis are conducted using objective methods and realistic practical networks.

The contributions are as follows:

1. Improvements to the DP synchronous generator model with controllers to account for harmonics with comparisons to existing models.
2. Presentation of a 3-phase phasor domain method.
3. Comprehensive comparisons of DP approach with TD and phasor-domain methods. A practical test case is used to compare accuracy and performance.
4. Inclusion of transformer magnetization into DP solution.
5. Application of the DP method to study geomagnetic disturbances by including transformation magnetization.

1.3 Thesis Structure

Chapter 2 provides a thorough overview of the available approaches, emphasizing the synchronous generator model. In Chapter 3, the dissertation shows the necessity of modeling harmonics in the synchronous machine and its controllers. The dissertation proposes a new synchronous machine model based on the DP method, which employs harmonics to presents an accurate simulation of unbalanced events. Furthermore in Chapter 4, the dissertation presents a DP model for simulation of Geomagnetic Disturbance (GMD). The simulation uses DC harmonic to present the effect of GMD in the network. A saturation model of the transformer is presented which uses the fundamental frequency and the DC harmonic in order to model GMD.

Chapter 2 SIMULATION METHODS

To simulate power systems, all elements of the network must be modeled according to the chosen solution method. This section presents the modeling of synchronous generator or SM which impacts significantly on simulation of large power grids.

2.1 TD model of synchronous machine

The following assumptions are made in this section to develop SM model:

(a) The stator windings are sinusoidally distributed along the air-gap as far as the mutual effects with the rotor are concerned.

(b) The stator slots cause no appreciable variation of the rotor inductances with rotor position.

(c) Magnetic hysteresis is negligible.

(d) Magnetic saturation effects are negligible.

Ignoring magnetic saturation allows for representing the circuits as linear; hence, the two connected circuits can be superposed.

Figure 2.1 shows the circuits of a synchronous machine. The stator circuits consist of three-phase armature windings carrying alternating currents. The rotor circuits comprise field and damper windings. The field winding is connected to a source of direct current. For purposes of analysis, the currents in the damper windings can be assumed to flow in two sets of closed circuits: one set whose flux is in line with that of the field along the *d*-axis and the other set whose flux is at right angles to the field axis or along the *q*-axis. The model of synchronous machine has one field and one damper circuit on *d*-axis and two damper circuits on *q*-axis.

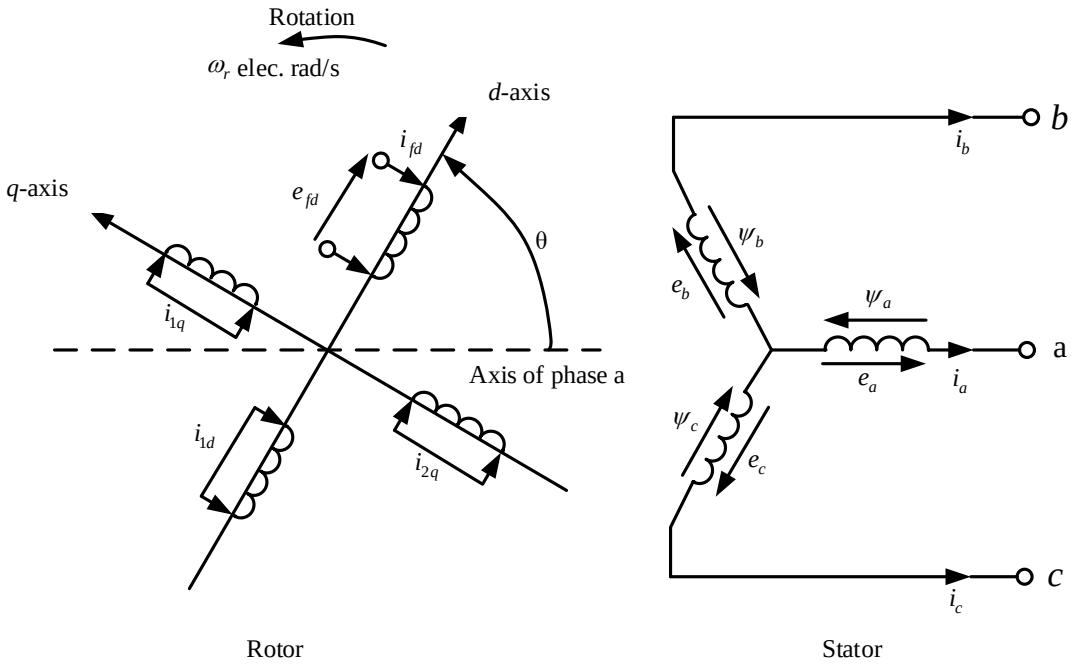

Figure 2.1 Stator and rotor circuit of synchronous machine [34]

where *a*, *b*, *c* are phases of stator windings. fd is the field circuit and $1d$ is damping circuits on *d*-axis. $1q$ and $2q$ are damping circuits on *q*-axis. θ is the angle *d*-axis leads the winding of phase a magnetic axis, and ω_r is the rotor angular velocity. The angle θ continuously increases proportionaly to the rotor angular velocity ω_r. The relationship between θ, ω_r and time t is:

$$\theta = \omega_r t + \theta_0 \tag{2.1}$$

where θ_0 is the initial value of θ.

According to Figure 2.1, three phase voltages of stator are:

$$\begin{bmatrix} v_a \\ v_b \\ v_c \end{bmatrix} = -\begin{bmatrix} R_a & 0 & 0 \\ 0 & R_a & 0 \\ 0 & 0 & R_a \end{bmatrix}\begin{bmatrix} i_a \\ i_b \\ i_c \end{bmatrix} + \frac{d}{dt}\begin{bmatrix} \psi_a \\ \psi_b \\ \psi_c \end{bmatrix} \tag{2.2}$$

where i, v, ψ are instantaneous current, voltage, magnetic flux. R_a is armature resistance.

Also, according to Figure 2.1, the voltage relation of rotor windings is:

$$\begin{bmatrix} e_{fd} \\ 0 \\ 0 \\ 0 \end{bmatrix} = \frac{d}{dt}\begin{bmatrix} \psi_{fd} \\ \psi_{1d} \\ \psi_{1q} \\ \psi_{2q} \end{bmatrix} + \begin{bmatrix} R_{fd} & 0 & 0 & 0 \\ 0 & R_{1d} & 0 & 0 \\ 0 & 0 & R_{1q} & 0 \\ 0 & 0 & 0 & R_{2q} \end{bmatrix}\begin{bmatrix} i_{fd} \\ i_{1d} \\ i_{1q} \\ i_{2q} \end{bmatrix} \tag{2.3}$$

In equation (2.3), e_{fd} is field voltage on *d*-axis.

Considering mutual inductance between stator and rotor windings, magnetic fluxes on stator windings are:

$$\begin{bmatrix} \psi_a \\ \psi_b \\ \psi_c \end{bmatrix} = -\begin{bmatrix} \tilde{L}_{aa} & \tilde{L}_{ab} & \tilde{L}_{ac} \\ \tilde{L}_{ba} & \tilde{L}_{bb} & \tilde{L}_{bc} \\ \tilde{L}_{ca} & \tilde{L}_{cb} & \tilde{L}_{cc} \end{bmatrix}\begin{bmatrix} i_a \\ i_b \\ i_c \end{bmatrix} + \begin{bmatrix} \tilde{L}_{afd} & \tilde{L}_{a1d} & \tilde{L}_{a1q} & \tilde{L}_{a2q} \\ \tilde{L}_{bfd} & \tilde{L}_{b1d} & \tilde{L}_{b1q} & \tilde{L}_{b2q} \\ \tilde{L}_{cfd} & \tilde{L}_{c1d} & \tilde{L}_{c1q} & \tilde{L}_{c2q} \end{bmatrix}\begin{bmatrix} i_{fd} \\ i_{1d} \\ i_{1q} \\ i_{2q} \end{bmatrix} \tag{2.4}$$

In equation (2.4), $\tilde{L}_{aa}$, $\tilde{L}_{bb}$, and $\tilde{L}_{cc}$ are the self-inductance of stator windings. The tilde (~) is used to demonstrate that the inductances are variable. $\tilde{L}_{ab}$, $\tilde{L}_{bc}$, and $\tilde{L}_{ca}$ are the mutual inductance between stator windings. $\tilde{L}_{afd}$, $\tilde{L}_{a1d}$, $\tilde{L}_{a1q}$, and $\tilde{L}_{2q}$ are the mutual inductance between stator and rotor windings. The mutual inductances between two windings are equal. For instance, $\tilde{L}_{ab}$ is equal to $\tilde{L}_{bc}$.

Since the *d*- and *q*- axes are perpendicular to each other, there is no mutual flux between them. Considering mutual inductance between stator and rotor *d*-axis windings, magnetic fluxes on rotor *d*-axis windings are:

$$\begin{bmatrix} \psi_{fd} \\ \psi_{1d} \end{bmatrix} = -\begin{bmatrix} \tilde{L}_{fda} & \tilde{L}_{fdb} & \tilde{L}_{fdc} \\ \tilde{L}_{1da} & \tilde{L}_{1db} & \tilde{L}_{1dc} \end{bmatrix}\begin{bmatrix} i_a \\ i_b \\ i_c \end{bmatrix} + \begin{bmatrix} L_{fdfd} & L_{fd1d} \\ L_{1dfd} & L_{1d1d} \end{bmatrix}\begin{bmatrix} i_{fd} \\ i_{1d} \end{bmatrix} \tag{2.5}$$

where L_{fdfd} and L_{1d1d} are the self-inductance of rotor *d*-axis windings. L_{fd1d} is the mutual inductance between two circuit of rotor *d*-axis windings. The mutual inductances between two windings are equal, therefore, L_{fd1d} is equal to L_{1dfd} and $\tilde{L}_{fda}$ is equal to $\tilde{L}_{afd}$.

Considering mutual inductance between stator and rotor *q*-axis windings, magnetic fluxes on rotor *q*-axis windings are:

$$\begin{bmatrix} \psi_{1q} \\ \psi_{2q} \end{bmatrix} = -\begin{bmatrix} \tilde{L}_{1qa} & \tilde{L}_{1qb} & \tilde{L}_{1qc} \\ \tilde{L}_{2qa} & \tilde{L}_{2qb} & \tilde{L}_{2qc} \end{bmatrix} \begin{bmatrix} i_a \\ i_b \\ i_c \end{bmatrix} + \begin{bmatrix} L_{1q1q} & L_{1q2q} \\ L_{2q1q} & L_{2q2q} \end{bmatrix} \begin{bmatrix} i_{1q} \\ i_{2q} \end{bmatrix} \tag{2.6}$$

where L_{1q1q}, and L_{2q2q} are the self-inductance of rotor *q*-axis windings. L_{1q2q} is the mutual inductance between two circuit of rotor *q*-axis windings. The mutual inductances between two windings are equal, therefore, L_{1q2q} is equal to L_{2q1q} and $\tilde{L}_{1qa}$ is equal to $\tilde{L}_{a1q}$.

The stator self inductances are:

$$\tilde{L}_{aa} = L_{aa0} + L_{aa2}\cos(2\theta) \tag{2.7}$$

$$\tilde{L}_{bb} = L_{aa0} + L_{aa2}\cos\left(2\theta + \frac{2\pi}{3}\right) \tag{2.8}$$

$$\tilde{L}_{cc} = L_{aa0} + L_{aa2}\cos\left(2\theta - \frac{2\pi}{3}\right) \tag{2.9}$$

where L_{aa0} is the constant inductance, and L_{aa2} is the magnitude of variable inductance.

The stator self inductances are:

$$\tilde{L}_{ab} = \tilde{L}_{ba} = -L_{ab0} - L_{ab2}\cos\left(2\theta + \frac{\pi}{3}\right) \tag{2.10}$$

$$\tilde{L}_{bc} = \tilde{L}_{cb} = -L_{ab0} - L_{ab2}\cos(2\theta + \pi) \tag{2.11}$$

$$\tilde{L}_{ca} = \tilde{L}_{ac} = -L_{ab0} - L_{ab2}\cos\left(2\theta - \frac{\pi}{3}\right) \tag{2.12}$$

the same variation in permeance produces the second harmonic terms in self and mutual inductances, therefore $\tilde{L}_{ab}$ is nearly equal to $\tilde{L}_{ba}$.

Because the second harmonic terms in self and mutual inductances are produced by the same variation in permeance [34], L_{ab2} is almost equivalent to L_{aa2}.

The rotor mutual inductances are:

$$\tilde{L}_{afd} = L_{afd}\cos(\theta) \tag{2.13}$$

$$\tilde{L}_{a1d} = L_{a1d}\cos(\theta) \tag{2.14}$$

$$\tilde{L}_{a1q} = L_{a1q}\cos\left(\theta + \frac{\pi}{2}\right) \tag{2.15}$$

$$\tilde{L}_{a2q} = L_{a2q}\cos\left(\theta + \frac{\pi}{2}\right) \tag{2.16}$$

In this SM model, all stator quantities from phase *a*, *b*, and *c* are transformed into a frame reference rotating with the rotor. The following equation expresses relation *dq0* frame and *abc* frame.

$$x_{dq0} = T(\theta)\, x_{abc} \tag{2.17}$$

where the transformation matrix T is:

$$T(\theta) = \sqrt{\frac{2}{3}}\begin{bmatrix} \cos(\theta) & \cos\left(\theta - \frac{2\pi}{3}\right) & \cos\left(\theta + \frac{2\pi}{3}\right) \\ -\sin(\theta) & -\sin\left(\theta - \frac{2\pi}{3}\right) & -\sin\left(\theta + \frac{2\pi}{3}\right) \\ \frac{1}{2} & \frac{1}{2} & \frac{1}{2} \end{bmatrix} \tag{2.18}$$

where θ is defined in equation (2.1). Subscripts *a*, *b*, and *c* are the phases of the three-phase system. Subscripts *d*, *q*, and 0 are the components of *dq*0 frame.

The inverse transformation of (2.18) is:

$$T^{-1}(\theta) = \sqrt{\frac{2}{3}}\begin{bmatrix} \cos(\theta) & -\sin(\theta) & 1 \\ \cos\left(\theta - \frac{2\pi}{3}\right) & -\sin\left(\theta - \frac{2\pi}{3}\right) & 1 \\ \cos\left(\theta + \frac{2\pi}{3}\right) & -\sin\left(\theta + \frac{2\pi}{3}\right) & 1 \end{bmatrix} \tag{2.19}$$

Equations (2.7)-(2.16) are substituted in equation (2.4), and then the transformation of (2.18) is applied, yielding:

$$\begin{bmatrix}\psi_d\\ \psi_q\\ \psi_0\end{bmatrix}=-\begin{bmatrix}L_{aa0}+L_{ab0}+\frac{3}{2}L_{aa2} & 0 & 0\\ 0 & L_{aa0}+L_{ab0}-\frac{3}{2}L_{aa2} & 0\\ 0 & 0 & L_{aa0}-2L_{ab0}\end{bmatrix}\begin{bmatrix}i_d\\ i_q\\ i_0\end{bmatrix}+\begin{bmatrix}L_{afd} & L_{a1d} & 0 & 0\\ 0 & 0 & L_{a1q} & L_{a2q}\\ 0 & 0 & 0 & 0\end{bmatrix}\begin{bmatrix}i_{fd}\\ i_{1d}\\ i_{1q}\\ i_{2q}\end{bmatrix} \tag{2.20}$$

Equations (2.7)-(2.16) are substituted in (2.5), and then the transformation of (2.18) is applied, yielding:

$$\begin{bmatrix}\psi_{fd}\\ \psi_{1d}\end{bmatrix}=-\begin{bmatrix}L_{afd} & 0 & 0\\ L_{a1d} & 0 & 0\end{bmatrix}\begin{bmatrix}i_d\\ i_q\\ i_0\end{bmatrix}+\begin{bmatrix}L_{fdfd} & L_{fd1d}\\ L_{1dfd} & L_{1d1d}\end{bmatrix}\begin{bmatrix}i_{fd}\\ i_{1d}\end{bmatrix} \tag{2.21}$$

Equations (2.7)-(2.16) are substituted in equation (2.6), and then the transformation of equation (2.18) is applied, yielding:

$$\begin{bmatrix}\psi_{1q}\\ \psi_{2q}\end{bmatrix}=-\begin{bmatrix}0 & L_{a1q} & 0\\ 0 & L_{a2q} & 0\end{bmatrix}\begin{bmatrix}i_d\\ i_q\\ i_0\end{bmatrix}+\begin{bmatrix}L_{1q1q} & L_{1q2q}\\ L_{2q1q} & L_{2q2q}\end{bmatrix}\begin{bmatrix}i_{1q}\\ i_{2q}\end{bmatrix} \tag{2.22}$$

Rearranging equations (2.20), (2.21), and (2.22) then separating *d*-, *q*-, and 0- axes gives:

$$\begin{bmatrix}\psi_d\\ \psi_{fd}\\ \psi_{1d}\end{bmatrix}=\begin{bmatrix}L_{aa0}+L_{ab0}+\frac{3}{2}L_{aa2} & L_{afd} & L_{a1d}\\ L_{afd} & L_{fdfd} & L_{fd1d}\\ L_{a1d} & L_{fd1d} & L_{1d1d}\end{bmatrix}\begin{bmatrix}-i_d\\ i_{fd}\\ i_{1d}\end{bmatrix} \tag{2.23}$$

$$\begin{bmatrix} \psi_q \\ \psi_{1q} \\ \psi_{2q} \end{bmatrix} = \begin{bmatrix} L_{aa0} + L_{ab0} - \frac{3}{2} L_{aa2} & L_{a1q} & L_{a2q} \\ L_{a1q} & L_{1q1q} & L_{1q2q} \\ L_{a2q} & L_{1q2q} & L_{2q2q} \end{bmatrix} \begin{bmatrix} -i_q \\ i_{1q} \\ i_{2q} \end{bmatrix} \tag{2.24}$$

$$\psi_0 = -\left(L_{aa0} - 2L_{ab0}\right) i_0 \tag{2.25}$$

The total flux linkages related to i_d, i_q, and i_0 are represented by the stator self inductances L_d, L_q, and L_0.

$$L_d = L_{aa0} + L_{ab0} + \frac{3}{2} L_{aa2} \tag{2.26}$$

$$L_q = L_{aa0} + L_{ab0} - \frac{3}{2} L_{aa2} \tag{2.27}$$

$$L_0 = L_{aa0} - 2L_{ab0} \tag{2.28}$$

The leakage inductance due to flux that does not link any rotor circuit and the mutual inductance due to flux that links the rotor circuits are the two portions of the stator self inductances. In the *dq*0 axes, the stator leakage inductances are approximately equal [34]. The stator self inductances are represented as:

$$L_d = L_l + L_{ad} \tag{2.29}$$

$$L_q = L_l + L_{aq} \tag{2.30}$$

$$L_0 = L_l + 3L_n \tag{2.31}$$

where L_l is the stator leakage inductances, L_{ad} and L_{aq} are the mutual inductance due to flux links the rotor circuits on *d*- and *q*- axes.

The per unit approach is used in this part to simplify mathematical equations and make the equivalent circuits of the SM model easier to comprehend. The stator base quantities are chosen arbitrary, and the rotor base values are determined in relation to the stator base quantities [34].

$$i_{d_{base}} = i_{q_{base}} = i_{0_{base}} = i_{s_{base}} \tag{2.32}$$

$$\psi_{d_{base}} = \psi_{q_{base}} = \psi_{0_{base}} = \psi_{s_{base}} = \frac{e_{s_{base}}}{\omega_s} = \frac{S_{base}}{\omega_s i_{base}} \tag{2.33}$$

$$L_{d_{base}} = L_{q_{base}} = L_{0_{base}} = L_{s_{base}} = \frac{\psi_{s_{base}}}{i_{s_{base}}} \tag{2.34}$$

where subscript *base* means the base quantity of the variable, $i_{s_{base}}$ is the stator nominal current, $e_{s_{base}}$ is stator line to neutral peak nominal voltage, and S_{base} is single phase nominal power.

The following are the rotor base values in relation to the stator base values:

$$i_{fd_{base}} = \frac{L_{ad}}{L_{afd}} i_{s_{base}} \tag{2.35}$$

$$i_{1d_{base}} = \frac{L_{ad}}{L_{a1d}} i_{s_{base}} \tag{2.36}$$

$$\psi_{fd_{base}} = \frac{L_{afd}}{L_{ad}} \psi_{s_{base}} \tag{2.37}$$

$$\psi_{1d_{base}} = \frac{L_{a1d}}{L_{ad}} \psi_{s_{base}} \tag{2.38}$$

$$L_{fdfd_{base}} = \left(\frac{L_{afd}}{L_{ad}} \right)^2 L_{base} \tag{2.39}$$

$$L_{1d1d_{base}} = \left(\frac{L_{a1d}}{L_{ad}} \right)^2 L_{base} \tag{2.40}$$

$$i_{1q_{base}} = \frac{L_{aq}}{L_{a1q}} i_{s_{base}} \tag{2.41}$$

$$i_{2q_{base}} = \frac{L_{aq}}{L_{a2q}} i_{s_{base}} \tag{2.42}$$

$$\psi_{1q_{base}} = \frac{L_{a1q}}{L_{aq}} \psi_{s_{base}} \tag{2.43}$$

$$\psi_{2q_{base}} = \frac{L_{a2q}}{L_{aq}} \psi_{s_{base}} \tag{2.44}$$

$$L_{1q1q_{base}} = \left(\frac{L_{a1q}}{L_{aq}} \right)^2 L_{base} \tag{2.45}$$

$$L_{2q2q_{base}} = \left(\frac{L_{a2q}}{L_{aq}} \right)^2 L_{base} \tag{2.46}$$

A superbar is used to identify per unit quantities and demonstrate their relationships to the actual values. Using the base values defined in equations (2.32)-(2.46), the per unit inductance of equations (2.23), (2.24), and (2.25) are:

$$\begin{bmatrix} \bar{\psi}_d \\ \bar{\psi}_{fd} \\ \bar{\psi}_{1d} \end{bmatrix} = \begin{bmatrix} \bar{L}_d & \bar{L}_{ad} & \bar{L}_{ad} \\ \bar{L}_{ad} & \bar{L}_{fdfd} & c_d \bar{L}_{ad} \\ \bar{L}_{ad} & c_d \bar{L}_{ad} & L_{1d1d} \end{bmatrix} \begin{bmatrix} -\bar{i}_d \\ \bar{i}_{fd} \\ \bar{i}_{1d} \end{bmatrix} \tag{2.47}$$

$$\begin{bmatrix} \bar{\psi}_q \\ \bar{\psi}_{1q} \\ \bar{\psi}_{2q} \end{bmatrix} = \begin{bmatrix} \bar{L}_q & \bar{L}_{aq} & \bar{L}_{aq} \\ \bar{L}_{aq} & \bar{L}_{1q1q} & c_q \bar{L}_{aq} \\ \bar{L}_{aq} & c_q \bar{L}_{aq} & \bar{L}_{2q2q} \end{bmatrix} \begin{bmatrix} -\bar{i}_q \\ \bar{i}_{1q} \\ \bar{i}_{2q} \end{bmatrix} \tag{2.48}$$

$$\bar{\psi}_0 = -\bar{L}_0 \bar{i}_0 \tag{2.49}$$

In equations (2.47), parameters c_d and c_q are:

$$c_d = \frac{L_{ad} L_{fd1d}}{L_{afd} L_{a1d}} \tag{2.50}$$

$$c_q = \frac{L_{aq} L_{1q2q}}{L_{a1q} L_{a2q}} \tag{2.51}$$

Reference [35] demonstrated the importance of parameters c_d and c_q. To simplify equations (2.47) and (2.48), the following assumptions are used [36, 37]:

$$c_d \approx 1, \text{ and } c_q \approx 1 \tag{2.52}$$

Also, the following parameters are defined:

$$\bar{L}_{fd} = \bar{L}_{fdfd} - \bar{L}_{ad} \tag{2.53}$$

$$\bar{L}_{1d} = \bar{L}_{1d1d} - \bar{L}_{ad} \tag{2.54}$$

$$\bar{L}_{1q} = \bar{L}_{1q1q} - \bar{L}_{aq} \tag{2.55}$$

$$\bar{L}_{2q} = \bar{L}_{2q2q} - \bar{L}_{aq} \tag{2.56}$$

Using defined parameters in equations (2.53)-(2.56),the per unit flux equations (2.47), (2.48), and (2.49) are represented as:

$$\begin{bmatrix} \bar{\psi}_d \\ \bar{\psi}_{fd} \\ \bar{\psi}_{1d} \end{bmatrix} = \begin{bmatrix} \bar{L}_l + \bar{L}_{ad} & \bar{L}_{ad} & \bar{L}_{ad} \\ \bar{L}_{ad} & \bar{L}_{fd} + \bar{L}_{ad} & \bar{L}_{ad} \\ \bar{L}_{ad} & \bar{L}_{ad} & \bar{L}_{1d} + \bar{L}_{ad} \end{bmatrix} \begin{bmatrix} -\bar{i}_d \\ \bar{i}_{fd} \\ \bar{i}_{1d} \end{bmatrix} \tag{2.57}$$

$$\begin{bmatrix} \bar{\psi}_q \\ \bar{\psi}_{1q} \\ \bar{\psi}_{2q} \end{bmatrix} = \begin{bmatrix} \bar{L}_l + \bar{L}_{aq} & \bar{L}_{aq} & \bar{L}_{aq} \\ \bar{L}_{aq} & \bar{L}_{1q} + \bar{L}_{aq} & \bar{L}_{aq} \\ \bar{L}_{aq} & \bar{L}_{aq} & \bar{L}_{2q} + \bar{L}_{aq} \end{bmatrix} \begin{bmatrix} -\bar{i}_q \\ \bar{i}_{1q} \\ \bar{i}_{2q} \end{bmatrix} \tag{2.58}$$

$$\bar{\psi}_0 = -\left(\bar{L}_l + 3\bar{L}_n\right)\bar{i}_0 \tag{2.59}$$

Applying the transformer of (2.17) in (2.2), the stator voltage equations in the *dq*0 frame are:

$$\begin{bmatrix} v_d \\ v_q \\ v_0 \end{bmatrix} = -\begin{bmatrix} R_a & 0 & 0 \\ 0 & R_a & 0 \\ 0 & 0 & R_a \end{bmatrix} \begin{bmatrix} i_d \\ i_q \\ i_0 \end{bmatrix} + T(\theta)\frac{d}{dt}\left(T^{-1}(\theta) \begin{bmatrix} \psi_d \\ \psi_q \\ \psi_0 \end{bmatrix} \right) \tag{2.60}$$

Therefore,

$$\begin{bmatrix} v_d \\ v_q \\ v_0 \end{bmatrix} = -\begin{bmatrix} R_a & 0 & 0 \\ 0 & R_a & 0 \\ 0 & 0 & R_a \end{bmatrix}\begin{bmatrix} i_d \\ i_q \\ i_0 \end{bmatrix} + \begin{bmatrix} p & -\omega_r & 0 \\ \omega_r & p & 0 \\ 0 & 0 & p \end{bmatrix}\begin{bmatrix} \psi_d \\ \psi_q \\ \psi_0 \end{bmatrix} \tag{2.61}$$

where generator states, v_d, v_q, v_0, i_d, i_q and i_0 are stator voltage and current on *dq*0 axes. ψ_d, ψ_q, and ψ_0 are flux on *dq*0 axes.

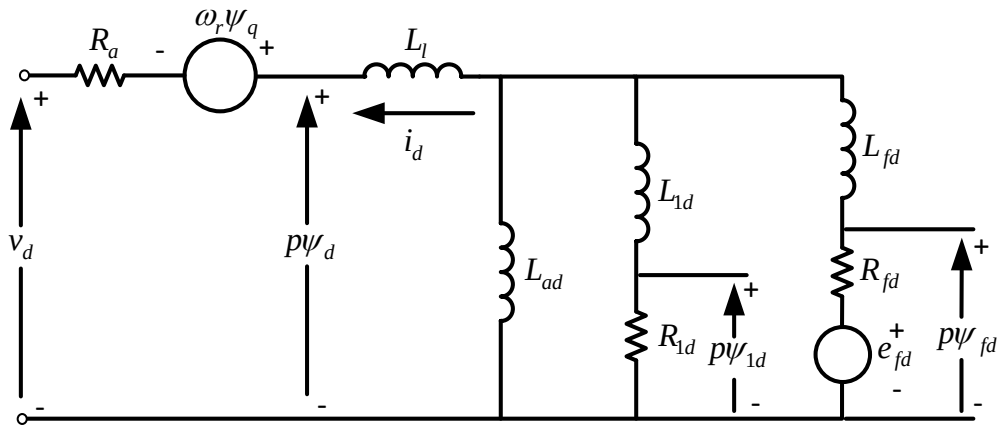

a) *d*-axis equivalent circuit

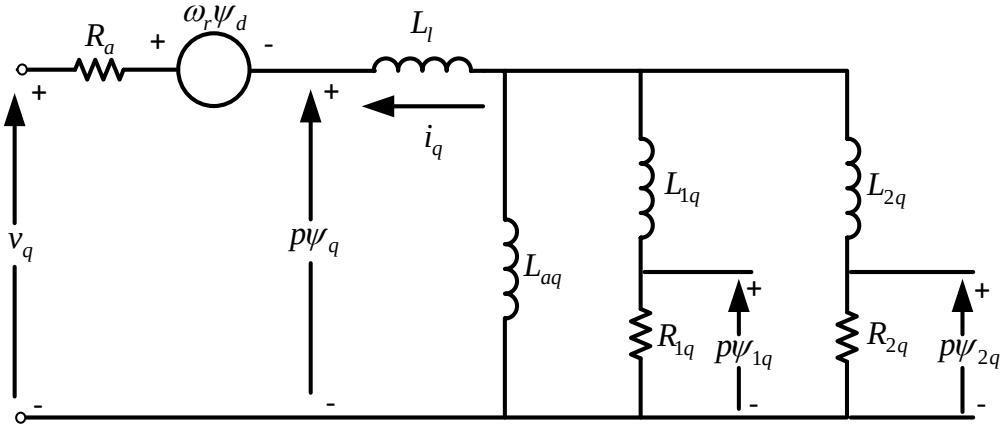

b) *q*-axis equivalent circuit

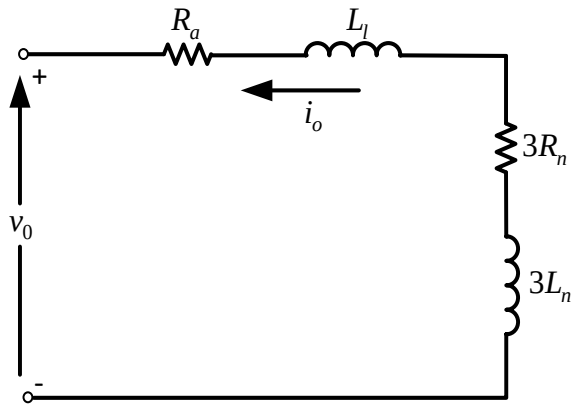

c) 0-axis equivalent circuit

Figure 2.2 *dq*0-axes equivalent circuits

Figure 2.2 shows the equivalent circuits of SM in *dq*0 frame, which represents equations (2.57), (2.58), (2.59), and (2.61).

To find the per unit form of (2.61), the per unit of derivative term is required.

$$\bar{p} = \frac{d}{d\bar{t}} = \frac{1}{\omega_s}\frac{d}{dt} = \frac{1}{\omega_s}p \tag{2.62}$$

where $\bar{p}$ is per unit derivative and $\bar{t}$ is the per unit time. The time base value is the time it takes for the rotor to rotate at the synchronous speed for one electrical radian [34].

Therefore, the per unit form of (2.61) is:

$$\begin{aligned}\begin{bmatrix}\bar{v}_d\\ \bar{v}_q\\ \bar{v}_0\end{bmatrix} &= -\begin{bmatrix}\bar{R}_a & 0 & 0\\ 0 & \bar{R}_a & 0\\ 0 & 0 & \bar{R}_a\end{bmatrix}\begin{bmatrix}\bar{i}_d\\ \bar{i}_q\\ \bar{i}_0\end{bmatrix} + \frac{1}{\omega_s}\begin{bmatrix}p & -\omega_r & 0\\ \omega_r & p & 0\\ 0 & 0 & p\end{bmatrix}\begin{bmatrix}\bar{\psi}_d\\ \bar{\psi}_q\\ \bar{\psi}_0\end{bmatrix}\\ &= -\begin{bmatrix}\bar{R}_a & 0 & 0\\ 0 & \bar{R}_a & 0\\ 0 & 0 & \bar{R}_a\end{bmatrix}\begin{bmatrix}\bar{i}_d\\ \bar{i}_q\\ \bar{i}_0\end{bmatrix} + \begin{bmatrix}\bar{p} & -\bar{\omega}_r & 0\\ \bar{\omega}_r & \bar{p} & 0\\ 0 & 0 & \bar{p}\end{bmatrix}\begin{bmatrix}\bar{\psi}_d\\ \bar{\psi}_q\\ \bar{\psi}_0\end{bmatrix}\end{aligned} \tag{2.63}$$

Hereafter, the SM equations are presented in the per-unit form. The superbar, which distinguishes per unit variables, is removed from the notation.

The aim is to find stator voltages based on the stator currents and rotor transient and sub-transient quantities. The rotor currents are obtained by rewriting equations (2.57) and (2.58) depending on the rotor flux.

$$\begin{bmatrix} -L_l i_d \\ L_{1d} i_{1d} \\ L_{fd} i_{fd} \end{bmatrix} = \frac{1}{\frac{1}{L_l}+\frac{1}{L_{ad}}+\frac{1}{L_{1d}}+\frac{1}{L_{fd}}} \begin{bmatrix} \frac{1}{L_{ad}}+\frac{1}{L_{1d}}+\frac{1}{L_{fd}} & -\frac{1}{L_{1d}} & -\frac{1}{L_{fd}} \\ -\frac{1}{L_l} & \frac{1}{L_l}+\frac{1}{L_{ad}}+\frac{1}{L_{fd}} & -\frac{1}{L_{fd}} \\ -\frac{1}{L_l} & -\frac{1}{L_{1d}} & \frac{1}{L_l}+\frac{1}{L_{ad}}+\frac{1}{L_{1d}} \end{bmatrix} \begin{bmatrix} \psi_d \\ \psi_{1d} \\ \psi_{fd} \end{bmatrix} \quad (2.64)$$

$$\begin{bmatrix} -L_l i_q \\ L_{1q} i_{1q} \\ L_{2q} i_{2q} \end{bmatrix} = \frac{1}{\frac{1}{L_l}+\frac{1}{L_{aq}}+\frac{1}{L_{1q}}+\frac{1}{L_{2q}}} \begin{bmatrix} \frac{1}{L_{aq}}+\frac{1}{L_{1q}}+\frac{1}{L_{2q}} & -\frac{1}{L_{1q}} & -\frac{1}{L_{2q}} \\ -\frac{1}{L_l} & \frac{1}{L_l}+\frac{1}{L_{aq}}+\frac{1}{L_{2q}} & -\frac{1}{L_{2q}} \\ -\frac{1}{L_l} & -\frac{1}{L_{1q}} & \frac{1}{L_l}+\frac{1}{L_{aq}}+\frac{1}{L_{1q}} \end{bmatrix} \begin{bmatrix} \psi_q \\ \psi_{1q} \\ \psi_{2q} \end{bmatrix} \quad (2.65)$$

The first cycles of a transient in the system after a disturbance have higher frequency oscillations than the rest cycles. Due to the existence of resistors (or dampers) in the systems, the frequency of the oscillations reduces. The transient behaviour of the SM depends on the number of damper circuits. In a SM having two dampers, the fast oscillations are known as sub-transient, and lower frequency oscillations are known as transient. To model machine sub-transient, the whole circuit is considered. Then, during low frequency oscillations, the damper with lower time constant can be neglected.

The sub-transient emf proportional to *d*-axis flux, $E_q^{''}$, is defined as the sub-transient flux on *d*-axis when the circuit is open, and the flux is propotional to sub-transient emf on the *q*-axis. Therefore, $E_q^{''}$ is the flux on the *d*-axis when the circuit is open.

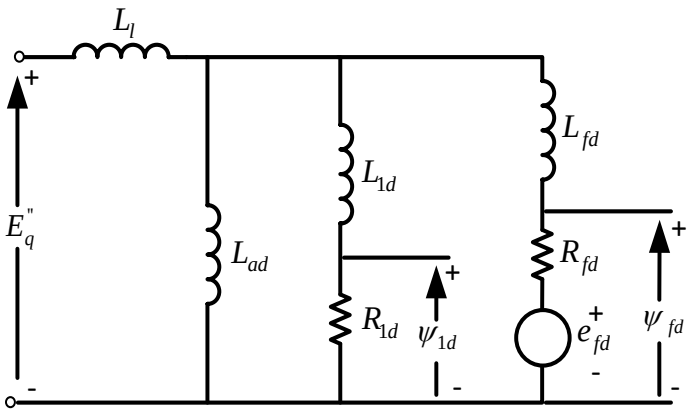

Figure 2.3 Equivalent circuit of sub-transient emf proportional to *d*-axis flux

According to Figure 2.3, the sub-transient emf proportional to *d*-axis flux is:

$$E_q'' = \frac{1}{\frac{1}{L_{ad}} + \frac{1}{L_{1d}} + \frac{1}{L_{fd}}} \left(\frac{\psi_{fd}}{L_{fd}} + \frac{\psi_{1d}}{L_{1d}} \right) \tag{2.66}$$

As illustrated in Figure 2.3, sub-transient inductance is the equivalent inductance on the *d*-axis with the field voltage and damper circuits.

$$L_d'' = L_l + \frac{1}{\frac{1}{L_{ad}} + \frac{1}{L_{1d}} + \frac{1}{L_{fd}}} \tag{2.67}$$

The relation of the current on the *d*-axis, i_d, in equation (2.64) can be written as:

$$-\left(\frac{1}{L_l} + \frac{1}{L_{ad}} + \frac{1}{L_{1d}} + \frac{1}{L_{fd}} \right) L_l i_d = \left(\frac{1}{L_{ad}} + \frac{1}{L_{1d}} + \frac{1}{L_{fd}} \right) \psi_d - \frac{1}{L_{1d}} \psi_{1d} - \frac{1}{L_{fd}} \psi_{fd} \tag{2.68}$$

And equation (2.68) is rearranged as:

$$\frac{\frac{1}{L_{1d}} \psi_{1d} + \frac{1}{L_{fd}} \psi_{fd}}{\frac{1}{L_{ad}} + \frac{1}{L_{1d}} + \frac{1}{L_{fd}}} = \psi_d + \left(L_l + \frac{1}{\frac{1}{L_{ad}} + \frac{1}{L_{1d}} + \frac{1}{L_{fd}}} \right) i_d \tag{2.69}$$

Replacing equations (2.66) and (2.67) in equation (2.69) gives:

$$E_q^{''} = \psi_d + L_d^{''} i_d \tag{2.70}$$

The sub-transient emf proportional to *q*-axis flux, $E_d^{''}$, is defined as the sub-transient flux on *q*-axis when the circuit is open, and the flux is propotional to sub-transient emf on the *d*-axis. Therefore, $E_d^{''}$ is the flux on the *d*-axis when the circuit is open.

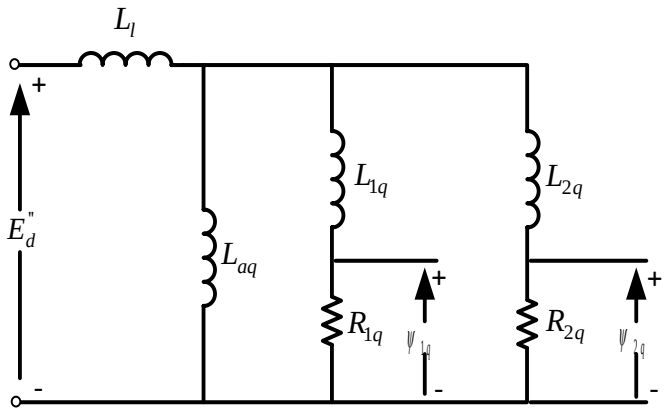

Figure 2.4 Equivalent circuit of sub-transient emf proportional to *q*-axis flux

According to Figure 2.4, the sub-transient emf proportional to *q*-axis flux is:

$$E_d^{''} = -\frac{1}{\frac{1}{L_{aq}} + \frac{1}{L_{1q}} + \frac{1}{L_{2q}}} \left(\frac{\psi_{1q}}{L_{1q}} + \frac{\psi_{2q}}{L_{2q}} \right) \tag{2.71}$$

As illustrated in Figure 2.4, sub-transient inductance is the equivalent inductance on the *q*-axis with the two circuits.

$$L_q^{''} = L_l + \frac{1}{\frac{1}{L_{aq}} + \frac{1}{L_{1q}} + \frac{1}{L_{2q}}} \tag{2.72}$$

The relation of the current on the *q*-axis, i_q, in equation (2.65) can be written as:

$$-L_l \left(\frac{1}{L_l} + \frac{1}{L_{aq}} + \frac{1}{L_{1q}} + \frac{1}{L_{2q}} \right) i_q = \left(\frac{1}{L_{aq}} + \frac{1}{L_{1q}} + \frac{1}{L_{2q}} \right) \psi_q - \frac{1}{L_{1q}} \psi_{1q} - \frac{1}{L_{2q}} \psi_{2q} \tag{2.73}$$

And equation (2.73) is rearranged as:

$$\frac{\frac{1}{L_{1q}}\psi_{1q}+\frac{1}{L_{2q}}\psi_{2q}}{\frac{1}{L_{aq}}+\frac{1}{L_{1q}}+\frac{1}{L_{2q}}}=\psi_q+\left(L_l+\frac{1}{\frac{1}{L_{aq}}+\frac{1}{L_{1q}}+\frac{1}{L_{2q}}}\right)i_q \tag{2.74}$$

Replacing equations (2.71) and (2.72) in equation (2.74) gives:

$$E_d^{''}=-\left(\psi_q+L_q^{''}i_q\right) \tag{2.75}$$

The transient emf proportional to *d*-axis flux, $E_q^{'}$, is defined as the transient flux on *d*-axis when the circuit is open, and the flux is propotional to the transient emf on the *q*-axis. Therefore, $E_q^{'}$ is the flux on the *d*-axis when the circuit is open.

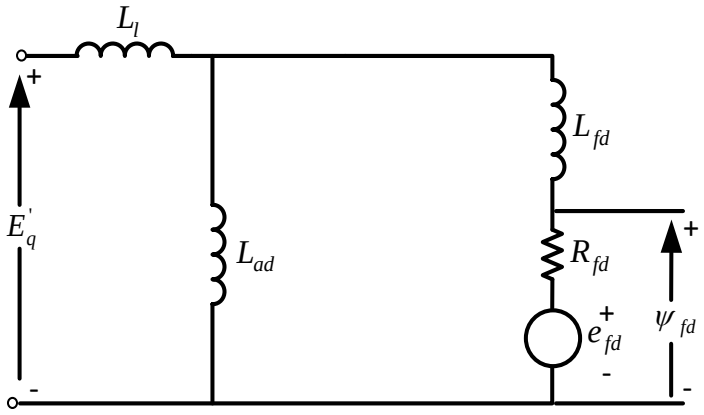

Figure 2.5 Equivalent circuit of transient emf proportional to *d*-axis flux

According to Figure 2.5, the transient emf proportional to the *d*-axis flux is:

$$E_q^{'}=\frac{L_{ad}}{L_{ad}+L_{fd}}\psi_{fd} \tag{2.76}$$

As illustrated in Figure 2.5, transient inductance is the equivalent inductance on the *d*-axis with the field voltage.

$$L_d^{'} = L_l + \frac{1}{\frac{1}{L_{ad}} + \frac{1}{L_{fd}}} \tag{2.77}$$

The transient emf proportional to *q*-axis flux, $E_d^{'}$, is defined as the transient flux on *q*-axis when the circuit is open, and the flux is propotional to the transient emf on the *d*-axis. Therefore, $E_d^{'}$ is the flux on the *d*-axis when the circuit is open.

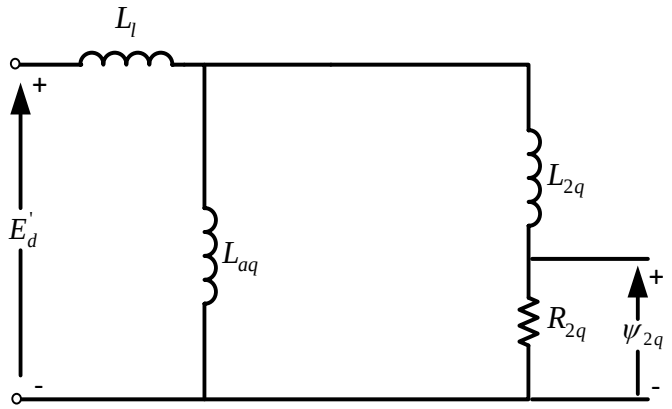

Figure 2.6 Equivalent circuit of transient emf proportional to *q*-axis flux

According to Figure 2.6, the transient emf proportional to *q*-axis flux is:

$$E_d^{'} = -\frac{L_{aq}}{L_{aq} + L_{2q}} \psi_{2q} \tag{2.78}$$

As illustrated in Figure 2.6, transient inductance is the equivalent inductance on the *q*-axis with the first damper.

$$L_q^{'} = L_l + \frac{1}{\frac{1}{L_{aq}} + \frac{1}{L_{2q}}} \tag{2.79}$$

Transient time constant is the total equivalent time constant on each axis considering the first damper. The transient open-circuit time constant on *d*-axis is calculated based on circuit shown in Figure 2.5.

$$T_{d0}^{'} = \frac{L_{ad} + L_{fd}}{R_{fd}} \tag{2.80}$$

The transient open circuit time constant on *q*-axis is calculated based on circuit shown in Figure 2.6.

$$T_{q0}^{'} = \frac{L_{ad} + L_{2q}}{R_{2q}} \tag{2.81}$$

Sub-transient time constant is the total equivalent time constant on each axis considering the two dampers. The sub-transient open-circuit time constant on *d*-axis is calculated based on circuit shown in Figure 2.3.

$$T_{d0}^{''} = \frac{1}{R_{1d}} \left(L_{1d} + \frac{1}{\frac{1}{L_{ad}} + \frac{1}{L_{fd}}} \right) \tag{2.82}$$

The sub-transient open-circuit time constant on *q*-axis is calculated based on circuit shown in Figure 2.4.

$$T_{q0}^{''} = \frac{1}{R_{1q}} \left(L_{1q} + \frac{1}{\frac{1}{L_{aq}} + \frac{1}{L_{2q}}} \right) \tag{2.83}$$

where L_d, $L_d^{'}$, $L_d^{''}$, L_q, $L_q^{'}$, and $L_q^{''}$ are synchronous, transient, and sub-transient inductance on the *d* and *q* axes. $T_{d0}^{'}$, $T_{d0}^{''}$, $T_{q0}^{'}$, and $T_{q0}^{''}$ are transient and sub-transient open circuit time constants on the *d*- and *q*- axes.

Equations (2.64) and (2.65) are rearranged after replacing the stated parameters:

$$\begin{bmatrix} i_{1d} \\ i_{fd} \end{bmatrix} = \frac{1}{L_d^{'} - L_l} \begin{bmatrix} L_d^{'} - L_d^{''} & 1 & -1 \\ \dfrac{\left(L_d - L_d^{'}\right)\left(L_d^{''} - L_l\right)}{L_d - L_l} & -\dfrac{L_d - L_d^{'}}{L_d - L_l} & 1 \end{bmatrix} \begin{bmatrix} i_d \\ E_q^{''} \\ E_q^{'} \end{bmatrix} \tag{2.84}$$

$$\begin{bmatrix} i_{1q} \\ i_{2q} \end{bmatrix} = \frac{1}{L_q^{'} - L_l} \begin{bmatrix} L_q^{'} - L_q^{''} & -1 & 1 \\ \dfrac{\left(L_q - L_q^{'}\right)\left(L_q^{''} - L_l\right)}{L_q - L_l} & \dfrac{L_q - L_q^{'}}{L_q - L_l} & -1 \end{bmatrix} \begin{bmatrix} i_q \\ E_d^{''} \\ E_d^{'} \end{bmatrix} \tag{2.85}$$

The field voltage on *d*-axis flux, E_{fd}, is defined as the emf on the *d*-axis flux caused by the field current. Therefore, E_{fd} is the emf flux on the *d*-axis flux when the i_d, i_{1d},and ψ_q are dismissed:

$$E_{fd} = \frac{L_{ad}}{R_{fd}} e_{fd} \tag{2.86}$$

In the following equations the per unit inductance are replaced by per unit reactance. The per unit reactance is:

$$\bar{X} = \frac{X}{X_{base}} = \frac{L}{L_{base}} = \bar{L} \tag{2.87}$$

Using equation (2.61) and defined flux in equation (2.70) and (2.75), the stator voltage on *d*- and *q*- axes are:

$$v_d = -X_d^{''} \frac{di_d}{dt} + \frac{dE_q^{''}}{dt} + \omega_r \left(X_q^{''} i_q + E_d^{''}\right) - R_a i_d \tag{2.88}$$

$$v_q = -X_q^{''} \frac{di_q}{dt} - \frac{dE_d^{''}}{dt} - \omega_r \left(X_d^{''} i_d - E_q^{''}\right) - R_a i_q \tag{2.89}$$

Using equation (2.61) and the flux relation in equations (2.59), the stator voltage on 0-axis is:

$$v_0 = -\left(X_l + 3X_n\right)\frac{di_0}{dt} - \left(R_a + 3R_n\right) i_0 \tag{2.90}$$

where R_n and X_n are respectively resistance and reactance connected to the neutral of machine.

Replacing equation (2.84) and (2.85) in equation (2.3) gives:

$$\frac{dE_q^{'}}{dt}=\frac{1}{T_{d0}^{'}}\left[E_{fd}-\frac{X_d-X_l}{X_d^{'}-X_l}E_q^{'}+\frac{X_d-X_d^{'}}{X_d^{'}-X_l}E_q^{''}-\frac{\left(X_d-X_d^{'}\right)\left(X_d^{''}-X_l\right)}{X_d^{'}-X_l}i_d\right] \tag{2.91}$$

$$\frac{dE_d^{'}}{dt}=\frac{1}{T_{q0}^{'}}\left[-\frac{X_q-X_l}{X_q^{'}-X_l}E_d^{'}+\frac{X_q-X_q^{'}}{X_q^{'}-X_l}E_d^{''}+\frac{\left(X_q-X_q^{'}\right)\left(X_q^{''}-X_l\right)}{X_q^{'}-X_l}i_q\right] \tag{2.92}$$

$$\frac{dE_q^{''}}{dt}=\frac{1}{T_{do}^{''}}\left[-E_q^{''}+E_q^{'}-\left(X_d^{'}-X_d^{''}\right)i_d\right]+\frac{X_d^{''}-X_l}{X_d^{'}-X_l}\frac{dE_q^{'}}{dt} \tag{2.93}$$

$$\frac{dE_d^{''}}{dt}=\frac{1}{T_{qo}^{''}}\left[-E_d^{''}+E_d^{'}+\left(X_q^{'}-X_q^{''}\right)i_q\right]+\frac{X_q^{''}-X_l}{X_q^{'}-X_l}\frac{dE_d^{'}}{dt} \tag{2.94}$$

The SM terminal power is:

$$p_t=v_a i_a+v_b i_b+v_c i_c=v_{abc}^T i_{abc} \tag{2.95}$$

Then using the inverse of Park's transform in equation (2.19), the equation (2.95) is written as:

$$\begin{aligned}p_t&=\left(T^{-1}v_{dq0}\right)^T T^{-1}i_{dq0}\\&=v_{dq0}^T\left(T^{-1}\right)^T T^{-1}i_{dq0}\end{aligned} \tag{2.96}$$

where the product of two matrices is:

$$\left(T^{-1}\right)^T T^{-1}=\begin{bmatrix}1&0&0\\0&1&0\\0&0&2\end{bmatrix} \tag{2.97}$$

Therefore, the SM terminal power in $dq0$ axes is

$$p_t=v_d i_d+v_q i_q+2v_0 i_0 \tag{2.98}$$

Replacing equation (2.61) in equation (2.98) gives:

$$p_t=-R_a\left(i_d^2+i_q^2+2i_0^2\right)+\left(\psi_d i_q-\psi_q i_d\right)\omega_r+\left(i_d\frac{d\psi_d}{dt}+i_q\frac{d\psi_q}{dt}+2i_0\frac{d\psi_0}{dt}\right) \tag{2.99}$$

The out power of SM can be separated by three terms, the armature resistance loss:

$$P_{loss} = -R_a \left(i_d^2 + i_q^2 + 2i_0^2 \right) \tag{2.100}$$

Electromagnetic power (also known as air-gap power):

$$P_e = \left(\psi_d i_q - \psi_q i_d \right) \omega_r \tag{2.101}$$

and rate of armature magnetic energy change:

$$i_d \frac{d\psi_d}{dt} + i_q \frac{d\psi_q}{dt} + 2i_0 \frac{d\psi_0}{dt} \tag{2.102}$$

Electromagnetic torque is calculated by dividing the electromagnetic power (equation (2.101)) by the mechanical rotor angular velocity (ω_m). The relationship of per unit mechanical and electrical rotor angular velocity is:

$$\bar{\omega}_r = \frac{\omega_r}{\omega_s} = \frac{\frac{p_f}{2}\omega_m}{\frac{p_f}{2}\omega_s} = \bar{\omega}_m \tag{2.103}$$

where $\frac{\omega_r}{\omega_m} = \frac{p_f}{2}$ and p_f is pole pair number.

Therefore, the electromagnetic torque in per unit is:

$$T_e = \psi_d i_q - \psi_q i_d \tag{2.104}$$

In equation (2.104), flux on *d*-axis (ψ_d) and flux on *q*-axis (ψ_q) are respectively given by rearranging equations (2.70) and (2.75) as:

$$\psi_d = -X_d^{''} i_d + E_q^{''} \tag{2.105}$$

$$\psi_q = -X_q^{''} i_q - E_d^{''} \tag{2.106}$$

The balance between mechanical and electromagnetic torque cause acceleration or deacceleration in rotor angular speed. The relationship known as Swing equation in per unit is [34]:

$$2H\frac{d\omega_m}{dt}+K_D\left(\omega_m-\omega_s\right)=T_m-\left(\psi_d i_q-\psi_q i_d\right) \tag{2.107}$$

where ω_s, ω_m, and ω_r are synchronous, mechanical and rotor angular speed respectively. T_e and T_m are respectively electromagnetic and mechanical torque. H and K_D are the moment of inertia and the viscous friction coefficient (or damping factor).

A balanced three phase terminal voltages are:

$$\begin{cases} v_a=V_t\cos\left(\theta_a\right) \\ v_b=V_t\cos\left(\theta_a-\dfrac{2\pi}{3}\right) \\ v_c=V_t\cos\left(\theta_a+\dfrac{2\pi}{3}\right) \end{cases} \tag{2.108}$$

where θ_a, the phase of voltage phase "a", is:

$$\theta_a=\omega_s t+\theta_{a_0} \tag{2.109}$$

and θ_{a_0} is the initial phase of voltage phase "a".

Then, the *dq*-axes voltages using Park's transform of equation (2.17) are:

$$\begin{cases} v_d=V_t\cos\left(\theta_a-\theta\right) \\ v_q=V_t\sin\left(\theta_a-\theta\right) \end{cases} \tag{2.110}$$

or:

$$\begin{cases} v_d=V_t\sin\left(\dfrac{\pi}{2}+\theta-\theta_a\right) \\ v_q=V_t\cos\left(\dfrac{\pi}{2}+\theta-\theta_a\right) \end{cases} \tag{2.111}$$

Initially the rotor angular velocity (ω_r) is equal to synchronous angular velocity (ω_s). Therefore, the voltage on the *dq*-axes can be represented as:

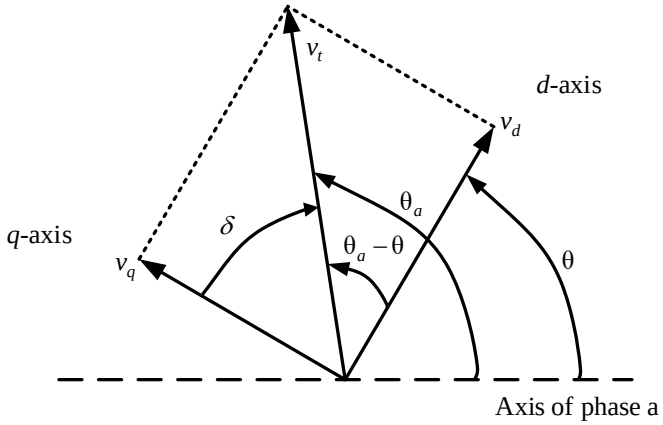

Figure 2.7 Representation of *dq*-axes voltage

In Figure 2.7, δ is the angle between *q*-axis and terminal voltage, and it is defined as:

$$\delta = \frac{\pi}{2} + \theta - \theta_a \tag{2.112}$$

Replacing equations (2.1) and (2.109) in (2.112) gives:

$$\delta = (\omega_r - \omega_s)t + \frac{\pi}{2} + \theta_0 - \theta_{a_0} \tag{2.113}$$

The terminal voltage oscillates with synchronous angular velocity (ω_s) and the *dq*-axes rotate by the rotor angular velocity (ω_r). Therefore, the angular velocity of δ is the relative angular velocity of rotor and synchronous ($\omega_r - \omega_s$).

The derivative of equation (2.113) is:

$$\frac{d\delta}{dt} = \omega_r - \omega_s \tag{2.114}$$

Note that unit of equations (2.112), (2.113), and (2.114) are in radian.

2.1.1 Discretized equations

Power system simulators solve differential equations of the network by numerical methods. Integration rules discretize differential equations and convert them to set of algebraic equations. The tool solves algebraic equations in each time step. This section contains the discretized equations for the time domain model of a synchronous machine using the Trapezoidal rule.

To make (2.91)–(2.94) shorter, the below parameters are defined [38].

$$a_1 = \frac{1}{T'_{d0}} \frac{X_d - X_l}{X'_d - X_l} \tag{2.115}$$

$$a_2 = \frac{1}{T'_{d0}} \frac{X_d - X'_d}{X'_d - X_l} \tag{2.116}$$

$$a_3 = \frac{\left(X_d - X'_d\right)\left(X''_d - X_l\right)}{T'_{d0}\left(X'_d - X_l\right)} \tag{2.117}$$

$$a_4 = \frac{X''_d - X_l}{X'_d - X_l} \tag{2.118}$$

$$b_1 = \frac{1}{T'_{q0}} \frac{X_q - X_l}{X'_q - X_l} \tag{2.119}$$

$$b_2 = \frac{1}{T'_{q0}} \frac{X_q - X'_q}{X'_q - X_l} \tag{2.120}$$

$$b_3 = \frac{\left(X_q - X'_q\right)\left(X''_q - X_l\right)}{T'_{q0}\left(X'_q - X_l\right)} \tag{2.121}$$

$$b_4 = \frac{X''_q - X_l}{X'_q - X_l} \tag{2.122}$$

Rewriting (2.91)–(2.94) gives:

$$\frac{dE_q^{'}(t)}{dt} = -a_1 E_q^{'}(t) + a_2 E_q^{''}(t) - a_3 i_d(t) + \frac{E_{fD}(t)}{T_{d0}^{'}} \tag{2.123}$$

$$\frac{dE_d^{'}(t)}{dt} = -b_1 E_d^{'}(t) + b_2 E_d^{''}(t) + b_3 i_q(t) \tag{2.124}$$

$$\frac{dE_q^{''}(t)}{dt} = a_4 \frac{dE_q^{'}(t)}{dt} + \frac{1}{T_{d0}^{''}}\left[-E_q^{''}(t) + E_q^{'}(t) - \left(x_d^{'} - x_d^{''}\right) i_d(t)\right] \tag{2.125}$$

$$\frac{dE_d^{''}(t)}{dt} = b_4 \frac{dE_d^{'}(t)}{dt} + \frac{1}{T_{q0}^{''}}\left[-E_d^{''}(t) + E_d^{'}(t) + \left(x_q^{'} - x_q^{''}\right) i_q(t)\right] \tag{2.126}$$

The transient emf on *d*-axis, given in (2.123), is discretized as follows :

$$E_{q_n}^{'} = \frac{a_2 E_{q_n}^{''} - a_3 i_{d_n} + E_{hq_{n-1}}^{'}}{\frac{2}{\Delta t} + a_1} \tag{2.127}$$

where the history term is:

$$E_{hq_{n-1}}^{'} = \frac{E_{fD_n}}{T_{d0}^{'}} + \frac{E_{fD_{n-1}}}{T_{d0}^{'}} + \left(\frac{2}{\Delta t} - a_1\right) E_{q_{n-1}}^{'} + a_2 E_{q_{n-1}}^{''} - a_3 i_{d_{n-1}} \tag{2.128}$$

The subscript *n* means the value of variable at the *n*-th time steps ($x\left(t_n\right) = x_n$). The sub-transient emf on *d*-axis, given in (2.125), is discretized as follows:

$$E_{q_n}^{''} = \frac{\left(\frac{2a_4}{\Delta t} + \frac{1}{T_{d0}^{''}}\right) E_{q_n}^{'} - \frac{1}{T_{d0}^{''}}\left(x_d^{'} - x_d^{''}\right) i_{d_n} + E_{hq_{n-1}}^{''}}{\frac{2}{\Delta t} + \frac{1}{T_{d0}^{''}}} \tag{2.129}$$

where the history term is:

$$E_{hq_{n-1}}^{''} = -\left(\frac{2a_4}{\Delta t} - \frac{1}{T_{d0}^{''}}\right) E_{q_{n-1}}^{'} + \left(\frac{2}{\Delta t} - \frac{1}{T_{d0}^{''}}\right) E_{q_{n-1}}^{''} - \frac{1}{T_{d0}^{''}}\left(x_d^{'} - x_d^{''}\right) i_{d_{n-1}} \tag{2.130}$$

The transient and the sub-transient emfs on the *d*-axis as a function of input current and history term are found by rearranging equations (2.127) and (2.129):

$$E'_{q_n} = \frac{\frac{-1}{T''_{d0}}\left(x'_d - x''_d\right)a_2 + \left(\frac{2}{\Delta t} + \frac{1}{T''_{d0}}\right)a_3}{\left(\frac{2}{\Delta t} + \frac{1}{T''_{d0}}\right)\left(\frac{2}{\Delta t} + a_1\right) - \left(\frac{2a_4}{\Delta t} + \frac{1}{T''_{d0}}\right)a_2} i_{d_n} + \frac{\left(\frac{2}{\Delta t} + \frac{1}{T''_{d0}}\right)E'_{hq_{n-1}} + a_2 E''_{hq_{n-1}}}{\left(\frac{2}{\Delta t} + \frac{1}{T''_{d0}}\right)\left(\frac{2}{\Delta t} + a_1\right) - \left(\frac{2a_4}{\Delta t} + \frac{1}{T''_{d0}}\right)a_2} \tag{2.131}$$

$$E''_{q_n} = \frac{\frac{-1}{T''_{d0}}\left(x'_d - x''_d\right)\left(\frac{2}{\Delta t} + a_1\right) + \left(\frac{2a_4}{\Delta t} + \frac{1}{T''_{d0}}\right)a_3}{\left(\frac{2}{\Delta t} + \frac{1}{T''_{d0}}\right)\left(\frac{2}{\Delta t} + a_1\right) - \left(\frac{2a_4}{\Delta t} + \frac{1}{T''_{d0}}\right)a_2} i_{d_n} + \frac{\left(\frac{2a_4}{\Delta t} + \frac{1}{T''_{d0}}\right)E'_{hq_{n-1}} + \left(\frac{2}{\Delta t} + a_1\right)E''_{hq_{n-1}}}{\left(\frac{2}{\Delta t} + \frac{1}{T''_{d0}}\right)\left(\frac{2}{\Delta t} + a_1\right) - \left(\frac{2a_4}{\Delta t} + \frac{1}{T''_{d0}}\right)a_2} \tag{2.132}$$

The transient emf on *q*-axis, given in (2.124), is discretized as follows:

$$E'_{d_n} = \frac{b_2 E''_{d_n} + b_3 i_{q_n} + E'_{d_{n-1}}}{\frac{2}{\Delta t} + b_1} \tag{2.133}$$

where the history term is:

$$E'_{d_{n-1}} = \left(\frac{2}{\Delta t} - b_1\right)E'_{d_{n-1}} + b_2 E''_{d_{n-1}} + b_3 i_{q_{n-1}} \tag{2.134}$$

The sub-transient emf on *q*-axis, given in (2.126), is discretized as follows:

$$E''_{d_n} = \frac{\left(\frac{2b_4}{\Delta t} + \frac{1}{T''_{q0}}\right) E'_{d_n} + \frac{1}{T''_{q0}}\left(x'_q - x''_q\right) i_{q_n} + E''_{hd_{n-1}}}{\frac{2}{\Delta t} + \frac{1}{T''_{q0}}} \tag{2.135}$$

where the history term is:

$$E''_{hd_{n-1}} = \left(\frac{2}{\Delta t} - \frac{1}{T''_{q0}}\right) E''_{d_{n-1}} - \left(\frac{2b_4}{\Delta t} - \frac{1}{T''_{q0}}\right) E'_{d_{n-1}} + \frac{1}{T''_{q0}}\left(x'_q - x''_q\right) i_{q_{n-1}} \tag{2.136}$$

The transient and the sub-transient emfs on the *q*-axis as a function of input current and history term are found by rearranging equations (2.133) and (2.135):

$$\begin{aligned} E'_{d_n} &= \frac{\left(\frac{2}{\Delta t} + \frac{1}{T''_{q0}}\right) b_3 + \frac{1}{T''_{q0}}\left(x'_q - x''_q\right) b_2}{\left(\frac{2}{\Delta t} + \frac{1}{T''_{q0}}\right)\left(\frac{2}{\Delta t} + b_1\right) - \left(\frac{2b_4}{\Delta t} + \frac{1}{T''_{q0}}\right) b_2} i_{q_n} \\ &+ \frac{\left(\frac{2}{\Delta t} + \frac{1}{T''_{q0}}\right) E'_{hd_{n-1}} + b_2 E''_{d_{n-1}}}{\left(\frac{2}{\Delta t} + \frac{1}{T''_{q0}}\right)\left(\frac{2}{\Delta t} + b_1\right) - \left(\frac{2b_4}{\Delta t} + \frac{1}{T''_{q0}}\right) b_2} \end{aligned} \tag{2.137}$$

$$\begin{aligned} E''_{d_n} &= \frac{\left(\frac{2b_4}{\Delta t} + \frac{1}{T''_{q0}}\right) b_3 + \frac{1}{T''_{q0}}\left(x'_q - x''_q\right)\left(\frac{2}{\Delta t} + b_1\right)}{\left(\frac{2}{\Delta t} + \frac{1}{T''_{q0}}\right)\left(\frac{2}{\Delta t} + b_1\right) - \left(\frac{2b_4}{\Delta t} + \frac{1}{T''_{q0}}\right) b_2} i_{q_n} \\ &+ \frac{\left(\frac{2b_4}{\Delta t} + \frac{1}{T''_{q0}}\right) E'_{hd_{n-1}} + \left(\frac{2}{\Delta t} + b_1\right) E''_{hd_{n-1}}}{\left(\frac{2}{\Delta t} + \frac{1}{T''_{q0}}\right)\left(\frac{2}{\Delta t} + b_1\right) - \left(\frac{2b_4}{\Delta t} + \frac{1}{T''_{q0}}\right) b_2} \end{aligned} \tag{2.138}$$

The voltage on *d*-axis, given in (2.88), is discretized as follows:

$$V_{d_n} = -\left(R_s + \frac{2X_d^{"}}{\omega_s \Delta t} \right) i_{d_n} + \frac{2}{\omega_s \Delta t} E_{q_n}^{"} + \frac{\omega_{r,n}}{\omega_s} \left(X_q^{"} i_{q_n} + E_{d_n}^{"} \right) + V_{hd_{n-1}} \tag{2.139}$$

where the history term is:

$$V_{hd_{n-1}} = -V_{d_{n-1}} - \left(R_s - \frac{2X_d^{"}}{\omega_s \Delta t} \right) i_{d_{n-1}} - \frac{2}{\omega_s \Delta t} E_{q_{n-1}}^{"} + \frac{\omega_{r_{n-1}}}{\omega_s} \left(X_q^{"} i_{q_{n-1}} + E_{d_{n-1}}^{"} \right) \tag{2.140}$$

To define the voltage on *d*-axis voltage as a function of input currents, equations (2.132) and (2.138) are replaced in (2.139). Then, the obtained function is rearranged as follow:

$$V_{d_n} = -Z_{dd} i_{d_n} + Z_{dq_n} i_{q_n} + E_{hd_{n-1}} \tag{2.141}$$

where Z_{dd} is:

$$Z_{dd} = R_s + \frac{2X_d^{"}}{\Delta t \omega_s} + \frac{2}{\Delta t \omega_s} \frac{\left(\frac{2a_4}{\Delta t} + \frac{1}{T_{d0}^{"}} \right) a_3 + \frac{1}{T_{d0}^{"}} \left(x_d^{'} - x_d^{"} \right) \left(\frac{2}{\Delta t} + a_1 \right)}{\left(\frac{2}{\Delta t} + \frac{1}{T_{d0}^{"}} \right) \left(\frac{2}{\Delta t} + a_1 \right) - \left(\frac{2a_4}{\Delta t} + \frac{1}{T_{d0}^{"}} \right) a_2} \tag{2.142}$$

and Z_{dq_n} is given by:

$$Z_{dq_n} = \frac{\omega_{r_n}}{\omega_s} \left(X_q^{"} + \frac{\left(\frac{2b_4}{\Delta t} + \frac{1}{T_{q0}^{"}} \right) b_3 + \frac{1}{T_{q0}^{"}} \left(x_q^{'} - x_q^{"} \right) \left(\frac{2}{\Delta t} + b_1 \right)}{\left(\frac{2}{\Delta t} + \frac{1}{T_{q0}^{"}} \right) \left(\frac{2}{\Delta t} + b_1 \right) - \left(\frac{2b_4}{\Delta t} + \frac{1}{T_{q0}^{"}} \right) b_2} \right) \tag{2.143}$$

The Z_{dd} is constant and Z_{dq_n} is a function of rotor speed.

The total history term of *d*-axis voltage in equation (2.141) is:

$$E_{hd_{n-1}} = V_{hd_{n-1}} + \frac{2}{\omega_s \Delta t} \frac{\left(\frac{2a_4}{\Delta t} + \frac{1}{T_{d0}^{"}}\right) E_{hq_{n-1}}^{'} + \left(\frac{2}{\Delta t} + a_1\right) E_{hq_{n-1}}^{"}}{\left(\frac{2}{\Delta t} + \frac{1}{T_{d0}^{"}}\right)\left(\frac{2}{\Delta t} + a_1\right) - \left(\frac{2a_4}{\Delta t} + \frac{1}{T_{d0}^{"}}\right) a_2} + \frac{\omega_{r_{n-1}}}{\omega_s} \frac{\left(\frac{2b_4}{\Delta t} + \frac{1}{T_{q0}^{"}}\right) E_{hd_{n-1}}^{'} + \left(\frac{2}{\Delta t} + b_1\right) E_{hd_{n-1}}^{"}}{\left(\frac{2}{\Delta t} + \frac{1}{T_{q0}^{"}}\right)\left(\frac{2}{\Delta t} + b_1\right) - \left(\frac{2b_4}{\Delta t} + \frac{1}{T_{q0}^{"}}\right) b_2} \tag{2.144}$$

The voltage on *q*-axis, given in (2.89), is discretized as follows:

$$V_{q_n} = -\left(R_s + \frac{2X_q^{"}}{\omega_s \Delta t}\right) i_{q_n} - \frac{2}{\omega_s \Delta t} E_{d_n}^{"} - \frac{\omega_{r_n}}{\omega_s}\left(X_d^{"} i_{d_n} + E_{q_n}^{"}\right) + V_{hq_{n-1}} \tag{2.145}$$

where the history term is:

$$V_{hq_{n-1}} = -V_{q_{n-1}} - \left(R_s + \frac{2X_q^{"}}{\omega_s \Delta t}\right) i_{q_{n-1}} + \frac{2}{\omega_s \Delta t} E_{d_{n-1}}^{"} - \frac{\omega_{r_{n-1}}}{\omega_s}\left(X_d^{"} i_{d_{n-1}} - E_{q_{n-1}}^{"}\right) \tag{2.146}$$

To define the voltage on *q*-axis voltage as a function of input currents, equations (2.132) and (2.138) are replaced in (2.145). Then, the obtained function is rearranged as follow:

$$V_{q_n} = -Z_{qd_n} i_{d_n} - Z_{qq} i_{q_n} + E_{hq_{n-1}} \tag{2.147}$$

where Z_{qq} is given by:

$$Z_{qq} = R_s + \frac{2X_q^{"}}{\Delta t \omega_s} + \frac{2}{\Delta t \omega_s} \frac{\left(\frac{2b_4}{\Delta t} + \frac{1}{T_{q0}^{"}}\right) b_3 + \frac{\left(x_q^{'} - x_q^{"}\right)}{T_{q0}^{"}}\left(\frac{2}{\Delta t} + b_1\right)}{\left(\frac{2}{\Delta t} + \frac{1}{T_{q0}^{"}}\right)\left(\frac{2}{\Delta t} + b_1\right) - \left(\frac{2b_4}{\Delta t} + \frac{1}{T_{q0}^{"}}\right) b_2} \tag{2.148}$$

and Z_{qd_n} is given by:

$$Z_{qd_n} = \frac{\omega_{r_n}}{\omega_s}\left(X_d^{"} + \frac{\left(\frac{2a_4}{\Delta t} + \frac{1}{T_{d0}^{"}}\right)a_3 + \frac{\left(x_d^{'} - x_d^{"}\right)}{T_{d0}^{"}}\left(\frac{2}{\Delta t} + a_1\right)}{\left(\frac{2}{\Delta t} + \frac{1}{T_{d0}^{"}}\right)\left(\frac{2}{\Delta t} + a_1\right) - \left(\frac{2a_4}{\Delta t} + \frac{1}{T_{d0}^{"}}\right)a_2} \right) \tag{2.149}$$

The Z_{qq} is constant and Z_{qd_n} is a function of rotor speed.

The total history term of *q*-axis voltage in equation (2.147) is:

$$\begin{aligned} E_{hq_{n-1}} = V_{hq_{n-1}} &- \frac{2}{\omega_s \Delta t}\frac{\left(\frac{2b_4}{\Delta t} + \frac{1}{T_{q0}^{"}}\right)E_{hd_{n-1}}^{'} + \left(\frac{2}{\Delta t} + b_1\right)E_{hd_{n-1}}^{"}}{\left(\frac{2}{\Delta t} + \frac{1}{T_{q0}^{"}}\right)\left(\frac{2}{\Delta t} + b_1\right) - \left(\frac{2b_4}{\Delta t} + \frac{1}{T_{q0}^{"}}\right)b_2} \\ &+ \frac{\omega_{r_{n-1}}}{\omega_s}\frac{\left(\frac{2a_4}{\Delta t} + \frac{1}{T_{d0}^{"}}\right)E_{hq_{n-1}}^{'} + \left(\frac{2}{\Delta t} + a_1\right)E_{hq_{n-1}}^{"}}{\left(\frac{2}{\Delta t} + \frac{1}{T_{d0}^{"}}\right)\left(\frac{2}{\Delta t} + a_1\right) - \left(\frac{2a_4}{\Delta t} + \frac{1}{T_{d0}^{"}}\right)a_2} \end{aligned} \tag{2.150}$$

The voltage on 0-axis, given in (2.90), is discretized as follows:

$$v_{0_n} = -Z_{00} i_{0_n} + E_{h0_{n-1}} \tag{2.151}$$

where Z_{00} is given by:

$$Z_{00} = \frac{2\left(X_l + 3X_n\right)}{\omega_s \Delta t} + R_a + 3R_n \tag{2.152}$$

and the history term of 0-axis voltage in equation (2.151) is:

$$E_{h0_{n-1}} = -v_{0_{n-1}} + \left(\frac{2\left(X_l + 3X_n\right)}{\omega_s \Delta t} - \left(R_a + 3R_n\right)\right) i_{0_{n-1}} \tag{2.153}$$

The angular speed, given in (2.107), is discretized as follows:

$$\omega_{m_n} = \frac{T_{m_n} - \left(\psi_{d_n} i_{q_n} - \psi_{q_n} i_{d_n}\right)}{\frac{4H}{\omega_s \Delta t} + K_D} + \omega_{hm_{n-1}} \tag{2.154}$$

In (2.154), the history term of mechanical angular speed is:

$$\omega_{hm_{n-1}} = \frac{T_{m_{n-1}} - \left(\psi_{d_{n-1}} i_{q_{n-1}} - \psi_{q_{n-1}} i_{d_{n-1}}\right) + \left(\frac{4H}{\omega_s \Delta t} - k_D\right)\omega_{m_{n-1}} + 2K_D\omega_s}{\frac{4H}{\omega_s \Delta t} + K_D} \tag{2.155}$$

The rotor angle, given in (2.114), is discretized as follows:

$$\delta_n = \frac{P\Delta t}{4}\omega_{m_n} + \delta_{h_{n-1}} \tag{2.156}$$

In (2.156), the history term of rotor angle is:

$$\delta_{h_{n-1}} = \delta_{n-1} + \frac{P\Delta t}{4}\left(\omega_{m_{n-1}} - 2\omega_s\right) \tag{2.157}$$

2.1.2 Norton equivalent circuit of SM

The voltage relation of SM in the *dq0*-frame is expressed as follows using equations (2.141), (2.147), and (2.151):

$$v_{dq0_n} = -Z_{dq0_n} i_{dq0_n} + E_{hdq0_{n-1}} \tag{2.158}$$

where the Z_{dq0_n} matrix is the SM equivalent impedance in *dq0*-frame. It should be noted that the *dq0* impedance is not constant and is a function of rotor speed.

$$Z_{dq0_n} = \begin{bmatrix} Z_{dd} & -Z_{dq_n} & 0 \\ Z_{qd_n} & Z_{qq} & 0 \\ 0 & 0 & Z_{00} \end{bmatrix} \tag{2.159}$$

and $E_{hdq0_{n-1}}$, vector of history term, is:

$$E_{hdq0_{n-1}} = \begin{bmatrix} E_{hd_{n-1}} & E_{hq_{n-1}} & E_{h0_{n-1}} \end{bmatrix}^T \tag{2.160}$$

To add the equivalent SM model to the MANA matrix, the *dq*0 frame model explained in (2.158) needs to transform to the *abc* frame.

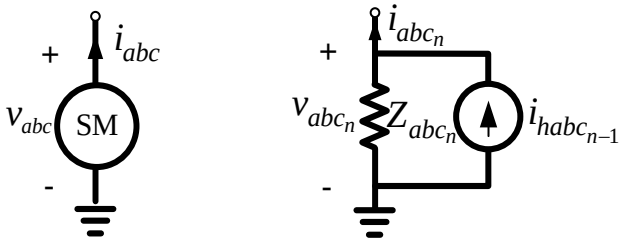

a) b)

Figure 2.8 a) Time domain SM, b) Equivalent circuit

Figure 2.8 shows the TD Norton equivalent circuit by Trapezoidal rule. The equivalent impedance and history terms in the *abc* frame shown in Figure 2.8 are computed as follows:

$$Z_{abc_n} = T^{-1}(\theta_n) Z_{dq0_n} T(\theta_n) \tag{2.161}$$

$$i_{habc_{n-1}} = T^{-1}(\theta_n) Z^{-1}_{dq0_{n-1}} E_{hdq0_{n-1}} \tag{2.162}$$

The equivalent impedance of a linear component, such as an inductor or a capacitor, is constant, and the history term calculated using the Trapezoidal method is dependent on the component's voltage and current in the last time step. The equivalent impedance of SM, on the other hand, is not constant, and the history term is affected by present and prior states. To obtain the proper SM equivalent, the present states are estimated in each time step, and the equivalent model is computed based on the predicted values. Following that, the network equations are solved and the SM's existing states are determined. If the new states have the same values as the predicted value, the prediction is correct. If not, the corresponding model is calculated using the new values. This iterative procedure is continued until the solution converges to a state that is acceptable to the machines.

2.1.3 Simulation steps

The following are the steps in a TD simulation approach:

1. Calculate the three phase Load-flow: to simulate unbalanced network from initial state, a three-phase load flow is used
2. Initialization
    a. Convert the loads to constant impedances: other load models, such as constant power or constant current, are also possible. The focus of this thesis is on the modelling of SM, and the basic load model with constant impedance is employed
    b. Calculate the equivalent circuit of elements by discretized method
    c. Build the admittance submatrix of MANA (equation (1.8)) of the network (exclude the SMs): During the simulation, the impedance of all components except SM remains constant. To avoid having repetitive computation, the constant portion of the admittance submatrix is computed during the initialization phase, and the variable part is added to the admittance submatrix during the simulation
    d. Calculate the history terms for the first time-step based on the load-flow results
3. Dynamic simulation
    a. Calculate the equivalent impedance and the injection current using equations (2.161) and (2.162) for all SMs
    b. Add the equivalent impedance of SMs to admittance submatrix of MANA, add the injection current of SMs to the b_n vector, and solve $A_n x_n = b_n$
    c. Update *dq*0-axes currents (equations (2.141), (2.147), and (2.151)), rotor speed (equation (2.154)), and rotor angle (equation (2.156)) for all SMs
    d. If the angular speed relative error of all SMs is less than the allowed error for two consecutive iterations, the solution is converged, and can proceed to step 3.e. If not, the solution has not converged, and the next iteration should begin at step 3.a.
    e. Calculate the controllers' model for the next time step

f. Predict the rotor speeds of all SMs and determine rotor angles based on the calculated rotor speeds

g. Calculate the history terms of all elements except SMs (the history term of an inductor, for example, as indicated in equation (1.5)), then update the b_n vector and proceed to step 3.a for the next time step

The prediction of variables in step 3.e reduces iteration number. A linear function based on the previous and current variables is used to predict the variables at the initial iteration of the next time step. The function is:

$$x_{n+1}^{(0)} = 2x_n - x_{n-1} \tag{2.163}$$

where $x_{n+1}^{(0)}$ is the predicted value for the next time step, x_n and x_{n-1} are the value of converged solution at the current and previous time step, respectively.

For an iterative solution, the relative error of a variable is:

$$\delta_{x_n^{(j)}} = \left| \frac{x_n^{(j)} - x_n^{(j-1)}}{x_n^{(j)}} \right| \tag{2.164}$$

where $\delta_{x_n^{(j)}}$ represents the relative error of variable *x* at the *n*-th time step for the *j*-th iteration.

2.2 Dynamic phasor model of synchronous machine

The DP model is based on the same premise as the TD model of an SM in the *dq0* frame discussed in the preceding section. To identify the DP model of SM, the approach for computing variables in the *dq0* frame from the *abc* frame for each Fourier coefficient need be determined.

Note that the lower letters represent time domain quantities, upper letters represent Fourier series coefficient for the dynamic phasor quantities.

A three-phase unbalanced current can be presented as:

$$x_{abc} = \mathbf{A}^{-1} x_{pnz} \tag{2.165}$$

where variable x can be the voltage or current of the system. Subscripts *p*, *n*, and *z* are positive, negative, and zero symmetrical components. And the inverse transformation matrix $\mathbf{A}^{-1}$ is:

$$\mathbf{A}^{-1} = \begin{bmatrix} 1 & 1 & 1 \\ e^{-j\frac{2\pi}{3}} & e^{j\frac{2\pi}{3}} & 1 \\ e^{j\frac{2\pi}{3}} & e^{-j\frac{2\pi}{3}} & 1 \end{bmatrix} \tag{2.166}$$

The relationship between currents of *dq*0 frame and symmetrical components is given by combining equations (2.165) and (2.166):

$$\begin{bmatrix} x_d \\ x_q \\ x_0 \end{bmatrix} = \frac{2}{3} \begin{bmatrix} \cos(\theta) & \cos\left(\theta - \frac{2\pi}{3}\right) & \cos\left(\theta + \frac{2\pi}{3}\right) \\ -\sin(\theta) & -\sin\left(\theta - \frac{2\pi}{3}\right) & -\sin\left(\theta + \frac{2\pi}{3}\right) \\ \frac{1}{2} & \frac{1}{2} & \frac{1}{2} \end{bmatrix} \begin{bmatrix} 1 & 1 & 1 \\ e^{-j\frac{2\pi}{3}} & e^{j\frac{2\pi}{3}} & 1 \\ e^{j\frac{2\pi}{3}} & e^{-j\frac{2\pi}{3}} & 1 \end{bmatrix} \begin{bmatrix} x_p \\ x_n \\ x_z \end{bmatrix} \tag{2.167}$$

where $\theta = \omega_s t + \delta - \frac{\pi}{2}$.

The following result is achieved by multiplying and then simplifying the two matrices in equation (2.167):

$$\begin{bmatrix} x_d \\ x_q \\ x_0 \end{bmatrix} = \begin{bmatrix} e^{-j\left(\omega_s t + \delta - \frac{\pi}{2}\right)} & e^{j\left(\omega_s t + \delta - \frac{\pi}{2}\right)} & 0 \\ e^{-j(\omega_s t + \delta)} & e^{j(\omega_s t + \delta)} & 0 \\ 0 & 0 & 1 \end{bmatrix} \begin{bmatrix} x_p \\ x_n \\ x_z \end{bmatrix} \tag{2.168}$$

The symmetrical components based on the first Fourier coefficient is as follows:

$$\begin{bmatrix} x_p \\ x_n \\ x_z \end{bmatrix} = \begin{bmatrix} \mathrm{X}_{p_1} \\ \mathrm{X}_{n_1} \\ \mathrm{X}_{z_1} \end{bmatrix} e^{j\omega_s t} + \begin{bmatrix} \mathrm{X}_{p_{-1}} \\ \mathrm{X}_{n_{-1}} \\ \mathrm{X}_{z_{-1}} \end{bmatrix} e^{-j\omega_s t} \tag{2.169}$$

where X_{p_1}, X_{n_1}, and X_{z_1} are the positive, negative, and zero symmetrical components of the first Fourier coefficient, respectively. $\mathrm{X}_{p_{-1}}$, $\mathrm{X}_{n_{-1}}$, and $\mathrm{X}_{z_{-1}}$ are respectively the positive, negative, and zero symmetrical components of the negative first Fourier coefficient.

When equations (2.168) and (2.169) are added together, the following result is obtained:

$$\begin{bmatrix} x_d \\ x_q \\ x_0 \end{bmatrix} = \begin{bmatrix} e^{-j\left(\delta-\frac{\pi}{2}\right)} & e^{j\left(2\omega_s t+\delta-\frac{\pi}{2}\right)} & 0 \\ e^{-j\delta} & e^{j(2\omega_s t+\delta)} & 0 \\ 0 & 0 & e^{j\omega_s t} \end{bmatrix} \begin{bmatrix} \mathrm{X}_{p_1} \\ \mathrm{X}_{n_1} \\ \mathrm{X}_{z_1} \end{bmatrix} + \begin{bmatrix} e^{-j\left(2\omega_s t+\delta-\frac{\pi}{2}\right)} & e^{j\left(\delta-\frac{\pi}{2}\right)} & 0 \\ e^{-j(2\omega_s t+\delta)} & e^{j\delta} & 0 \\ 0 & 0 & e^{-j\omega_s t} \end{bmatrix} \begin{bmatrix} \mathrm{X}_{p_{-1}} \\ \mathrm{X}_{n_{-1}} \\ \mathrm{X}_{z_{-1}} \end{bmatrix} \tag{2.170}$$

Equation (2.170) shows that in an *abc* frame with a fundamental frequency, the *dq* axes have dc and second harmonic components, whereas the 0-axis has the fundamental frequency component. The components of the two matrices in equation (2.170) that contain the positive and negative second Fourier coefficient are excluded to produce the zero Fourier coefficients of the *d*- and *q*-axes. As a result, the following outcome is obtained:

$$\begin{bmatrix} \mathrm{X}_{d_0} \\ \mathrm{X}_{q_0} \end{bmatrix} = \begin{bmatrix} e^{-j\left(\delta-\frac{\pi}{2}\right)} & e^{j\left(\delta-\frac{\pi}{2}\right)} \\ e^{-j\delta} & e^{j\delta} \end{bmatrix} \begin{bmatrix} \mathrm{X}_{p_1} \\ \mathrm{X}_{n_{-1}} \end{bmatrix} \tag{2.171}$$

According to equation (2.170), the relation between the second Fourier coefficient on *d*- and *q*-axes and sequence components is:

$$\begin{bmatrix} \mathrm{X}_{d_2} \\ \mathrm{X}_{q_2} \end{bmatrix} = e^{j\delta} \begin{bmatrix} e^{-j\frac{\pi}{2}} \\ 1 \end{bmatrix} \mathrm{X}_{n_1} \tag{2.172}$$

and the negative second Fourier coefficient of the *d*- and *q*- axes is:

$$\begin{bmatrix} \mathrm{X}_{d_{-2}} \\ \mathrm{X}_{q_{-2}} \end{bmatrix} = e^{-j\delta} \begin{bmatrix} e^{j\frac{\pi}{2}} \\ 1 \end{bmatrix} \mathrm{X}_{p_{-1}} \tag{2.173}$$

According to equation (2.170), the zero sequence is:

$$x_0 = \mathrm{X}_{z_1} e^{j\omega_s t} + \mathrm{X}_{z_{-1}} e^{-j\omega_s t} \tag{2.174}$$

The following procedure establishes relationships between negative and positive Fourier coefficients of the symmetrical components:

$$\begin{bmatrix} X_{a_k} \\ X_{b_k} \\ X_{c_k} \end{bmatrix} = \begin{bmatrix} 1 & 1 & 1 \\ e^{-j\frac{2\pi}{3}} & e^{j\frac{2\pi}{3}} & 1 \\ e^{j\frac{2\pi}{3}} & e^{-j\frac{2\pi}{3}} & 1 \end{bmatrix} \begin{bmatrix} X_{p_k} \\ X_{n_k} \\ X_{z_k} \end{bmatrix} \tag{2.175}$$

Equation (2.175) is conjugated as:

$$\begin{bmatrix} X_{a_k} \\ X_{b_k} \\ X_{c_k} \end{bmatrix}^* = \begin{bmatrix} 1 & 1 & 1 \\ e^{-j\frac{2\pi}{3}} & e^{j\frac{2\pi}{3}} & 1 \\ e^{j\frac{2\pi}{3}} & e^{-j\frac{2\pi}{3}} & 1 \end{bmatrix}^* \begin{bmatrix} X_{p_k}^* \\ X_{n_k}^* \\ X_{z_k}^* \end{bmatrix} \tag{2.176}$$

Applying the conjugation to the transformation matrix and the applying property of (1.14) on the variables from the *abc* frame, gives:

$$\begin{bmatrix} X_{a_{-k}} \\ X_{b_{-k}} \\ X_{c_{-k}} \end{bmatrix} = \begin{bmatrix} 1 & 1 & 1 \\ e^{j\frac{2\pi}{3}} & e^{-j\frac{2\pi}{3}} & 1 \\ e^{-j\frac{2\pi}{3}} & e^{j\frac{2\pi}{3}} & 1 \end{bmatrix} \begin{bmatrix} X_{p_k}^* \\ X_{n_k}^* \\ X_{z_k}^* \end{bmatrix} \tag{2.177}$$

The following is the result of rearranging equation (2.177):

$$\begin{bmatrix} X_{a_{-k}} \\ X_{b_{-k}} \\ X_{c_{-k}} \end{bmatrix} = \begin{bmatrix} 1 & 1 & 1 \\ e^{-j\frac{2\pi}{3}} & e^{j\frac{2\pi}{3}} & 1 \\ e^{j\frac{2\pi}{3}} & e^{-j\frac{2\pi}{3}} & 1 \end{bmatrix} \begin{bmatrix} X_{n_k}^* \\ X_{p_k}^* \\ X_{z_k}^* \end{bmatrix} \tag{2.178}$$

When equations (2.175) and (2.178) are compared, the following results are obtained:

$$\begin{bmatrix} X_{n_k}^* \\ X_{p_k}^* \\ X_{z_k}^* \end{bmatrix} = \begin{bmatrix} X_{p_{-k}} \\ X_{n_{-k}} \\ X_{z_{-k}} \end{bmatrix} \tag{2.179}$$

According to equation (2.179), the property of equation (1.14) is not valid for Fourier coefficients of symmetrical components. In other word, $\mathrm{X}_{p_{-k}}$ is not equal to $\mathrm{X}_{p_k}{}^{*}$.

Using the relation of equation (2.179), the zero Fourier coefficient of the *d*- and *q*- axis in equation (2.171) can be expressed as follows:

$$\mathrm{X}_{d_0} = \mathrm{X}_{p_1} e^{-j\left(\delta-\frac{\pi}{2}\right)} + \mathrm{X}_{p_1}^{*} e^{j\left(\delta-\frac{\pi}{2}\right)} = \mathrm{X}_{p_1} e^{-j\left(\delta-\frac{\pi}{2}\right)} + \left(\mathrm{X}_{p_1} e^{-j\left(\delta-\frac{\pi}{2}\right)}\right)^{*} \tag{2.180}$$

$$\mathrm{X}_{q_0} = \mathrm{X}_{p_1} e^{-j\delta} + \mathrm{X}_{p_1}^{*} e^{j\delta} = \mathrm{X}_{p_1} e^{-j\delta} + \left(\mathrm{X}_{p_1} e^{-j\delta}\right)^{*} \tag{2.181}$$

or:

$$\mathrm{X}_{d_0} = 2\Re\left(\mathrm{X}_{p_1} e^{-j\left(\delta-\frac{\pi}{2}\right)}\right) \tag{2.182}$$

$$\mathrm{X}_{q_0} = 2\Re\left(\mathrm{X}_{p_1} e^{-j\delta}\right) = 2\Im\left(\mathrm{X}_{p_1} e^{-j\left(\delta-\frac{\pi}{2}\right)}\right) \tag{2.183}$$

where $\Re$ and $\Im$ are the real and imaginary part of the complex number.

The first Fourier coefficient on the 0-axis, according to equation (2.174), is:

$$\mathrm{X}_{0_1} = \mathrm{X}_{z_1} \tag{2.184}$$

According to equations (2.182) and (2.183), the transition from zero Fourier coefficient of the *d*- and *q*- axes to the first Fourier coefficient of positive components is:

$$\mathrm{X}_{p_1} = \frac{1}{2}\left(\mathrm{X}_{d_0} + j\mathrm{X}_{q_0}\right) e^{j\left(\delta-\frac{\pi}{2}\right)} \tag{2.185}$$

According to equation (2.172), the transition from zero Fourier coefficient of the *d*- and *q*- axes to the first Fourier coefficient of negative components is:

$$\mathrm{X}_{n_1} = \frac{1}{2}\left(\mathrm{X}_{d_2} - j\mathrm{X}_{q_2}\right) e^{-j\left(\delta-\frac{\pi}{2}\right)} \tag{2.186}$$

The following conclusions for the representation in *dq0* frame under unbalanced circumstances and fundamental frequency are reached using the preceding discussion.

- Equations (2.182) and (2.183) show that the positive sequence of stator behaves as a zero Fourier coefficient ($k=0$) on the *d*- and *q*- axes
- Equation (2.172) shows that the negative sequence of stator behaves as a second Fourier coefficient ($k=2$) on the *d*- and *q*- axes
- Equation (2.184) shows that the zero sequence of stator behaves as a first Fourier coefficient ($k=1$) on the 0-axis, and equation (2.170) express that zero sequence of the stator does not appear on the *d*- and *q*- axis

The DP model can be obtained form the TD model in section 2.1, as well as the DP properties in section 1.1.2.

The DP relation of the *d*-axis stator voltage is obtained by calculating the zero and second Fourier coefficients from equation (2.88).

$$v_d\big|_{k=0,2} = \left[-\frac{X_d^{"}}{\omega_s}\frac{di_d}{dt} + \frac{1}{\omega_s}\frac{dE_q^{"}}{dt} + \frac{\omega_r}{\omega_s}\left(X_q^{"} i_q + E_d^{"} \right) - R_a i_d \right]\Bigg|_{k=0,2} \tag{2.187}$$

The zero Fourier coefficient of the *d*-axis stator voltage is the zero Fourier coefficient of each term in equation (2.187):

$$v_d\big|_{k=0} = -\frac{X_d^{"}}{\omega_s}\frac{di_d}{dt}\bigg|_{k=0} + \frac{1}{\omega_s}\frac{dE_q^{"}}{dt}\bigg|_{k=0} + \frac{\omega_r}{\omega_s}\left(X_q^{"} i_q + E_d^{"} \right)\bigg|_{k=0} - R_a i_d\big|_{k=0} \tag{2.188}$$

The zero Fourier coefficient of derivate terms, according to the property of DP provided in equation (1.12), are:

$$-\frac{X_d^{"}}{\omega_s}\frac{di_d}{dt}\bigg|_{k=0} = -\frac{X_d^{"}}{\omega_s}\frac{d\mathrm{I}_{d_0}}{dt} \tag{2.189}$$

$$\frac{1}{\omega_s}\frac{dE_q^{"}}{dt}\bigg|_{k=0} = \frac{1}{\omega_s}\frac{d\mathrm{E}_{q_0}^{"}}{dt} \tag{2.190}$$

The zero Fourier coefficient term of product of two TD variables, according to the DP properties in equations (1.13) and (1.14), is:

$$\frac{\omega_r}{\omega_s}\left(X_q^{"}i_q + E_d^{"}\right)\Big|_{k=0} = \frac{\Omega_{r_0}}{\omega_s}\left(X_q^{"}\mathrm{I}_{q_0} + \mathrm{E}_{d_0}^{"}\right) + \frac{\Omega_{r_2}^{\ *}}{\omega_s}\left(X_q^{"}\mathrm{I}_{q_2} + \mathrm{E}_{d_2}^{"}\right) + \frac{\Omega_{r2}}{\omega_s}\left(X_q^{"}\mathrm{I}_{q_2}^{\ *} + \mathrm{E}_{d_2}^{"\ *}\right) \quad (2.191)$$

Therefore, the zero Fourier coefficient of the *d*-axis stator voltage is:

$$\begin{aligned}\mathrm{V}_{d_0} = &-\frac{X_d^{"}}{\omega_s}\frac{d\mathrm{I}_{d_0}}{dt} + \frac{1}{\omega_s}\frac{d\mathrm{E}_{q_0}^{"}}{dt} + \frac{\Omega_{r_0}}{\omega_s}\left(X_q^{"}\mathrm{I}_{q_0} + \mathrm{E}_{d_0}^{"}\right) + \frac{\Omega_{r_2}^{\ *}}{\omega_s}\left(X_q^{"}\mathrm{I}_{q_2} + \mathrm{E}_{d_2}^{"}\right) \\ &+ \frac{\Omega_{r2}}{\omega_s}\left(X_q^{"}\mathrm{I}_{q_2}^{\ *} + \mathrm{E}_{d_2}^{"\ *}\right) - R_a\mathrm{I}_{d_0}\end{aligned} \quad (2.192)$$

The same methodology used to get the zero Fourier coefficient of the d-axis stator voltage, equation (2.192), may be used to compute the other SM equations of the DP model. The second Fourier coefficient of the *d*-axis stator voltage, according to equation (2.187), is:

$$\begin{aligned}\mathrm{V}_{d_2} = &-\frac{X_d^{"}}{\omega_s}\frac{d\mathrm{I}_{d_2}}{dt} - j2X_d^{"}\mathrm{I}_{d_2} + \frac{1}{\omega_s}\frac{d\mathrm{E}_{q_2}^{"}}{dt} + j2\mathrm{E}_{q_2}^{"} + \frac{\Omega_{r_2}}{\omega_s}\left(X_q^{"}\mathrm{I}_{q_0} + \mathrm{E}_{d_0}^{"}\right) \\ &+ \frac{\Omega_{r_0}}{\omega_s}\left(X_q^{"}\mathrm{I}_{q_2} + \mathrm{E}_{d_2}^{"}\right) - R_a\mathrm{I}_{d_2}\end{aligned} \quad (2.193)$$

Equations (2.192) and (2.193), which represent the zero and second Fourier coefficients of the *d*-axis stator voltage, may be summed by the bellow equation.

$$\mathrm{V}_{d_k} = -\frac{X_d^{"}}{\omega_s}\frac{d\mathrm{I}_{d_k}}{dt} - jkX_d^{"}\mathrm{I}_{d_k} + \frac{1}{\omega_s}\frac{d\mathrm{E}_{q_k}^{"}}{dt} + jk\mathrm{E}_{q_k}^{"} + \sum_l \frac{\Omega_{r_{k-l}}}{\omega_s}\left(X_q^{"}\mathrm{I}_{q_l} + \mathrm{E}_{d_l}^{"}\right) - R_a\mathrm{I}_{d_k} \quad (2.194)$$

The DP relation of the *q*-axis stator voltage is obtained by calculating the Fourier coefficients from equation (2.89).

$$\mathrm{V}_{q_k} = -\frac{X_q^{"}}{\omega_s}\frac{d\mathrm{I}_{q_k}}{dt} - jkX_q^{"}\mathrm{I}_{q_k} - \frac{1}{\omega_s}\frac{d\mathrm{E}_{d_k}^{"}}{dt} - jk\mathrm{E}_{d_k}^{"} - \sum_l \frac{\Omega_{r_{k-l}}}{\omega_s}\left(X_d^{"}\mathrm{I}_{d_l} - \mathrm{E}_{q_l}^{"}\right) - R_a\mathrm{I}_{q_k} \quad (2.195)$$

where *k*, the Fourier coefficients for *q*-axis stator voltage, can be zero or two.

The DP relation of the 0-axis stator voltage is calculated by applying the DP properties to equation (2.90) and computing the model's Fourier coefficient.

$$\mathrm{V}_{0_k} = -\frac{\left(X_l + 3X_n\right)}{\omega_s}\frac{d\mathrm{I}_{0_k}}{dt} - jk\left(X_l + 3X_n\right)\mathrm{I}_{0_k} - \left(R_a + 3R_n\right)\mathrm{I}_{0_k} \tag{2.196}$$

where *k*, the Fourier coefficients for 0-axis stator voltage, is one.

The DP relation of the *q*-axis transient emf is obtained by calculating the Fourier coefficients from equation (2.91).

$$\frac{d\mathrm{E}'_{q_k}}{dt} + jk\omega_s\mathrm{E}'_{q_k} = \frac{1}{T'_{d0}}\left[\mathrm{E}_{fd_k} - \frac{X_d - X_l}{X'_d - X_l}\mathrm{E}'_{q_k} + \frac{X_d - X'_d}{X'_d - X_l}\mathrm{E}''_{q_k} - \frac{\left(X_d - X'_d\right)\left(X''_d - X_l\right)}{X'_d - X_l}\mathrm{I}_{d_k}\right] \tag{2.197}$$

where *k*, the Fourier coefficients for *q*-axis transient emf, is zero or two.

The DP relation of the *d*-axis transient emf is obtained by calculating the Fourier coefficients from equation (2.92).

$$\frac{d\mathrm{E}'_{d_k}}{dt} + jk\omega_s\mathrm{E}'_{d_k} = \frac{1}{T'_{q0}}\left[\frac{\left(X_q - X'_q\right)\left(X''_q - X_l\right)}{X'_q - X_l}\mathrm{I}_{q_k} - \frac{X_q - X_l}{X'_q - X_l}\mathrm{E}'_{d_k} + \frac{X_q - X'_q}{X'_q - X_l}\mathrm{E}''_{d_k}\right] \tag{2.198}$$

where *k*, the Fourier coefficients for *d*-axis transient emf, is zero or two.

The DP relation of the *q*-axis sub-transient emf is obtained by calculating the Fourier coefficients from equation (2.93).

$$\frac{d\mathrm{E}''_{q_k}}{dt} + jk\omega_s\mathrm{E}''_{q_k} = \frac{1}{T''_{d0}}\left[\mathrm{E}'_{q_k} - \mathrm{E}''_{q_k} - \left(X'_d - X''_d\right)I_{d_k}\right] + \frac{X''_d - X_l}{X'_d - X_l}\left(\frac{d\mathrm{E}'_{q_k}}{dt} + jk\omega_s\mathrm{E}'_{q_k}\right) \tag{2.199}$$

where *k*, the Fourier coefficients for *q*-axis sub-transient emf, is zero or two.

The DP relation of the *d*-axis sub-transient emf is obtained by calculating the Fourier coefficients from equation (2.94).

$$\frac{d\mathrm{E}''_{d_k}}{dt} + jk\omega_s\mathrm{E}''_{d_k} = \frac{1}{T''_{q0}}\left[\mathrm{E}'_{dk} - \mathrm{E}''_{d_k} + \left(X'_q - X''_q\right)\mathrm{I}_{q_k}\right] + \frac{X''_q - X_l}{X'_q - X_l}\left(\frac{d\mathrm{E}'_{d_k}}{dt} + jk\omega_s\mathrm{E}'_d\right) \tag{2.200}$$

The DP relation of mechanical angular speed is obtained by calculating the Fourier coefficients from equation (2.107).

$$\frac{2H}{\omega_s}\left(\frac{d\Omega_{m_k}}{dt}+jk\omega_s\Omega_{m_k}\right)=T_{m_k}-\sum_l\left(\Psi_{d_{k-l}}\mathrm{I}_{q_l}-\Psi_{q_{k-l}}\mathrm{I}_{d_l}\right)-K_D\left(\Omega_{m_k}-\omega_{s_k}\right) \tag{2.201}$$

where *k*, the Fourier coefficients for mechanical angular speed, is zero or two. It should be noticed that for the zero Fourier coefficient, ω_{s_k} equals 1 pu, while for the other Fourier coefficients, ω_{s_k} equals zero.

The DP relation of the rotor angle is obtained by calculating the Fourier coefficients from equation (2.114). The rotor angle used in equation (2.168) is a time domain variable, therefore it is calculated for the zero Fourier coefficient.

$$\frac{d\delta}{dt}=\frac{P}{2}\left(\Omega_{m_0}-\omega_s\right) \tag{2.202}$$

The DP relation of the *d*- and *q*- axes flux are obtained by calculating the Fourier coefficients from equations (2.105) and (2.106), respectively.

$$\Psi_{d_k}=-X_d^{''}\mathrm{I}_{d_k}+\mathrm{E}_{q_k}^{''} \tag{2.203}$$

$$\Psi_{q_k}=-X_q^{''}\mathrm{I}_{q_k}-\mathrm{E}_{d_k}^{''} \tag{2.204}$$

where *k*, the Fourier coefficients for the flux, is zero or two.

2.2.1 Discretized equations

The discretized equations of the DP model of synchronous machine employing the Trapezoidal rule are provided in this section.

Equations (2.197)-(2.200) are rewritten using stated parameters in equations (2.115)-(2.122), yielding:

$$\frac{d\mathrm{E}_{q_k}^{'}}{dt}+jk\omega_s\mathrm{E}_{q_k}^{'}=-a_1\mathrm{E}_{q_k}^{'}+a_2\mathrm{E}_{q_k}^{''}-a_3\mathrm{I}_{d_k}+\frac{E_{fd}}{T_{d0}^{'}} \tag{2.205}$$

$$\frac{d\mathrm{E}''_{q_k}}{dt} + jk\omega_s \mathrm{E}''_{q_k} = a_4 \frac{d\mathrm{E}'_{q_k}}{dt} + jk\omega_s a_4 \mathrm{E}'_{q_k} + \frac{1}{T''_{d0}}\left[\mathrm{E}'_{q_k} - \mathrm{E}''_{q_k} - \left(X'_d - X''_d\right) I_{d_k}\right] \tag{2.206}$$

$$\frac{d\mathrm{E}'_{d_k}}{dt} + jk\omega_s \mathrm{E}'_{d_k} = -b_1 \mathrm{E}'_{d_k} + b_2 \mathrm{E}''_{d_k} + b_3 \mathrm{I}_{q_k} \tag{2.207}$$

$$\frac{d\mathrm{E}''_{d_k}}{dt} + jk\omega_s \mathrm{E}''_{d_k} = \frac{1}{T''_{q0}}\left[\mathrm{E}'_{d_k} - \mathrm{E}''_{d_k} + \left(X'_q - X''_q\right)\mathrm{I}_{q_k}\right] + b_4 \frac{d\mathrm{E}'_{d_k}}{dt} + jk\omega_s b_4 \mathrm{E}'_{d_k} \tag{2.208}$$

The transient emf on *q*-axis, given in (2.205), is discretized as follows:

$$\mathrm{E}'_{q_{k,n}} = \frac{a_2 \mathrm{E}''_{q_{k,n}} - a_3 \mathrm{I}_{d_{k,n}} + \mathrm{E}'_{hq_{k,n}}}{\frac{2}{\Delta t} + jk\omega_s + a_1} \tag{2.209}$$

where the history term is:

$$\mathrm{E}'_{hq_{k,n}} = \frac{\mathrm{E}_{fD_{k,n}}}{T'_{d0}} + \frac{\mathrm{E}_{fD_{k,n-1}}}{T'_{d0}} + \left(\frac{2}{\Delta t} - jk\omega_s - a_1\right)\mathrm{E}'_{q_{k,n-1}} + a_2 \mathrm{E}''_{q_{k,n-1}} - a_3 \mathrm{I}_{d_{k,n-1}} \tag{2.210}$$

The number of Fourier coefficients is denoted by the subscript *k*, while the value of the variable at the *n*-th time step ($x\left(t_n\right) = x_n$) is denoted by the subscript *n*.

The sub-transient emf on *d*-axis, given in (2.206), is discretized as follows:

$$\mathrm{E}''_{q_{k,n}} = \frac{\left(\frac{2a_4}{\Delta t} + jka_4\omega_s + \frac{1}{T''_{d0}}\right)\mathrm{E}'_{q_{k,n}} - \frac{1}{T''_{d0}}\left(x'_d - x''_d\right)\mathrm{I}_{d_{k,n}} + \mathrm{E}''_{hq_{k,n}}}{\frac{2}{\Delta t} + jk\omega_s + \frac{1}{T''_{d0}}} \tag{2.211}$$

where the history term is:

$$\begin{aligned}\mathrm{E}''_{hq_{k,n}} = &-\left(\frac{2a_4}{\Delta t} - jka_4\omega_s - \frac{1}{T''_{d0}}\right)\mathrm{E}'_{q_{k,n-1}} + \left(\frac{2}{\Delta t} - jk\omega_s - \frac{1}{T''_{d0}}\right)\mathrm{E}''_{q_{k,n-1}} \\ &- \frac{1}{T''_{d0}}\left(x'_d - x''_d\right)\mathrm{I}_{d_{k,n-1}}\end{aligned} \tag{2.212}$$

To derive the transient and the sub-transient emf on the *d*-axis depending on the input current, the set of equations (2.209) and (2.211) are rearranged, yielding the following result:

$$\begin{aligned}\mathrm{E}'_{q_{k,n}} = &-\frac{\frac{1}{T''_{d0}}\left(x'_d - x''_d\right)a_2 + \left(\frac{2}{\Delta t} + jk\omega_s + \frac{1}{T''_{d0}}\right)a_3}{\left(\frac{2}{\Delta t} + jk\omega_s + \frac{1}{T''_{d0}}\right)\left(\frac{2}{\Delta t} + jk\omega_s + a_1\right) - \left(\frac{2a_4}{\Delta t} + jka_4\omega_s + \frac{1}{T''_{d0}}\right)a_2}\mathrm{I}_{d_{k,n}} \\ &+\frac{\left(\frac{2}{\Delta t} + jk\omega_s + \frac{1}{T''_{d0}}\right)\mathrm{E}'_{hq,k,n} + a_2\,\mathrm{E}''_{hq,k,n}}{\left(\frac{2}{\Delta t} + jk\omega_s + \frac{1}{T''_{d0}}\right)\left(\frac{2}{\Delta t} + jk\omega_s + a_1\right) - \left(\frac{2a_4}{\Delta t} + jka_4\omega_s + \frac{1}{T''_{d0}}\right)a_2}\end{aligned} \tag{2.213}$$

$$\begin{aligned}\mathrm{E}''_{q_{k,n}} = &-\frac{\frac{1}{T''_{d0}}\left(x'_d - x''_d\right)\left(\frac{2}{\Delta t} + jk\omega_s + a_1\right) + \left(\frac{2a_4}{\Delta t} + jka_4\omega_s + \frac{1}{T''_{d0}}\right)a_3}{\left(\frac{2}{\Delta t} + jk\omega_s + \frac{1}{T''_{d0}}\right)\left(\frac{2}{\Delta t} + jk\omega_s + a_1\right) - \left(\frac{2a_4}{\Delta t} + jka_4\omega_s + \frac{1}{T''_{d0}}\right)a_2}\mathrm{I}_{d_{k,n}} \\ &+\frac{\left(\frac{2a_4}{\Delta t} + jka_4\omega_s + \frac{1}{T''_{d0}}\right)\mathrm{E}'_{hq_{k,n}} + \left(\frac{2}{\Delta t} + jk\omega_s + a_1\right)\mathrm{E}''_{hq_{k,n}}}{\left(\frac{2}{\Delta t} + jk\omega_s + \frac{1}{T''_{d0}}\right)\left(\frac{2}{\Delta t} + jk\omega_s + a_1\right) - \left(\frac{2a_4}{\Delta t} + jka_4\omega_s + \frac{1}{T''_{d0}}\right)a_2}\end{aligned} \tag{2.214}$$

The transient emf on *q*-axis, given in (2.207), is discretized as follows:

$$\mathrm{E}'_{d_{k,n}} = \frac{b_2\,\mathrm{E}''_{d_{k,n}} + b_3\,\mathrm{I}_{q_{k,n}} + \mathrm{E}'_{hd_{k,n}}}{\frac{2}{\Delta t} + jk\omega_s + b_1} \tag{2.215}$$

where the history term is:

$$\mathrm{E}'_{hd_{k,n}} = \left(\frac{2}{\Delta t} - jk\omega_s - b_1\right)\mathrm{E}'_{d_{k,n-1}} + b_2\,\mathrm{E}''_{d_{k,n-1}} + b_3\,\mathrm{I}_{q_{k,n-1}} \tag{2.216}$$

The sub-transient emf on *q*-axis, given in (2.208), is discretized as follows:

$$\mathrm{E}''_{d_{k,n}} = \frac{\left(\frac{2b_4}{\Delta t} + jkb_4\omega_s + \frac{1}{T''_{q0}}\right)\mathrm{E}'_{d_{k,n}} + \frac{1}{T''_{q0}}\left(x'_q - x''_q\right)\mathrm{I}_{q_{k,n}} + \mathrm{E}''_{hd_{k,n}}}{\frac{2}{\Delta t} + jk\omega_s + \frac{1}{T''_{q0}}} \tag{2.217}$$

where the history term is:

$$\mathrm{E}''_{hd_{k,n}} = \left(\frac{2}{\Delta t} - jk\omega_s - \frac{1}{T''_{q0}}\right)\mathrm{E}''_{d_{k,n-1}} - \left(\frac{2b_4}{\Delta t} - jkb_4\omega_s - \frac{1}{T''_{q0}}\right)\mathrm{E}'_{d_{k,n-1}} + \frac{1}{T''_{q0}}\left(x'_q - x''_q\right)\mathrm{I}_{q_{k,n-1}} \tag{2.218}$$

To derive the transient and the sub-transient emf on the *q*-axis depending on the input current, the set of equations (2.215) and (2.217) are rearranged, yielding the following result:

$$\begin{aligned}\mathrm{E}'_{d_{k,n}} &= \frac{\left(\frac{2}{\Delta t} + jk\omega_s + \frac{1}{T''_{q0}}\right)b_3 + \frac{1}{T''_{q0}}\left(x'_q - x''_q\right)b_2}{\left(\frac{2}{\Delta t} + jk\omega_s + \frac{1}{T''_{q0}}\right)\left(\frac{2}{\Delta t} + jk\omega_s + b_1\right) - \left(\frac{2b_4}{\Delta t} + jkb_4\omega_s + \frac{1}{T''_{q0}}\right)b_2}\mathrm{I}_{q_{k,n}} \\ &+ \frac{\left(\frac{2}{\Delta t} + jk\omega_s + \frac{1}{T''_{q0}}\right)\mathrm{E}'_{d_{k,n}} + b_2\,\mathrm{E}''_{hd_{k,n}}}{\left(\frac{2}{\Delta t} + jk\omega_s + \frac{1}{T''_{q0}}\right)\left(\frac{2}{\Delta t} + jk\omega_s + b_1\right) - \left(\frac{2b_4}{\Delta t} + jkb_4\omega_s + \frac{1}{T''_{q0}}\right)b_2}\end{aligned} \tag{2.219}$$

$$\begin{aligned}\mathrm{E}''_{d_{k,n}} &= \frac{\left(\frac{2b_4}{\Delta t} + jkb_4\omega_s + \frac{1}{T''_{q0}}\right)b_3 + \frac{1}{T''_{q0}}\left(x'_q - x''_q\right)\left(\frac{2}{\Delta t} + jk\omega_s + b_1\right)}{\left(\frac{2}{\Delta t} + jk\omega_s + \frac{1}{T''_{q0}}\right)\left(\frac{2}{\Delta t} + jk\omega_s + b_1\right) - \left(\frac{2b_4}{\Delta t} + jkb_4\omega_s + \frac{1}{T''_{q0}}\right)b_2}\mathrm{I}_{q_{k,n}} \\ &+ \frac{\left(\frac{2b_4}{\Delta t} + jkb_4\omega_s + \frac{1}{T''_{q0}}\right)\mathrm{E}'_{hd_{k,n}} + \left(\frac{2}{\Delta t} + jk\omega_s + b_1\right)\mathrm{E}''_{hd_{k,n}}}{\left(\frac{2}{\Delta t} + jk\omega_s + \frac{1}{T''_{q0}}\right)\left(\frac{2}{\Delta t} + jk\omega_s + b_1\right) - \left(\frac{2b_4}{\Delta t} + jkb_4\omega_s + \frac{1}{T''_{q0}}\right)b_2}\end{aligned} \tag{2.220}$$

The voltage on *d*-axis, given in (2.194), is discretized as follows:

$$\begin{aligned}\mathrm{V}_{d_{k,n}} = &-\left(R_s + \frac{2X_d^{"}}{\omega_s \Delta t} + jkX_d^{"}\right)\mathrm{I}_{d_{k,n}} + \left(\frac{2}{\omega_s \Delta t} + jk\right)\mathrm{E}_{q_{k,n}}^{"} \\ &+ \frac{\Omega_{r_{0,n}}}{\omega_s}\left(X_q^{"}\,\mathrm{I}_{q_{k,n}} + \mathrm{E}_{d_{k,n}}^{"}\right) + \mathrm{V}_{hd_{k,n}}\end{aligned} \tag{2.221}$$

where the history term is:

$$\begin{aligned}\mathrm{V}_{hd_{k,n-1}} = &-\mathrm{V}_{d_{k,n-1}} - \left(R_s - \frac{2X_d^{"}}{\omega_s \Delta t} + jkX_d^{"}\right)\mathrm{I}_{d_{2,n-1}} - \left(\frac{2}{\omega_s \Delta t} - jk\right)\mathrm{E}_{q_{2,n-1}}^{"} \\ &+ \sum_{l} \frac{\Omega_{r_{k-l,n-1}}}{\omega_s}\left(X_q^{"}\,\mathrm{I}_{q_{l,n-1}} + \mathrm{E}_{d_{l,n-1}}^{"}\right) + \sum_{l \neq k} \frac{\Omega_{r_{k-l,n}}}{\omega_s}\left(X_q^{"}\,\mathrm{I}_{q_{l,n}} + \mathrm{E}_{d_{l,n}}^{"}\right)\end{aligned} \tag{2.222}$$

To define the voltage on *q*-axis voltage as a function of input currents, equations (2.214) and (2.220) are replaced in (2.220). Then, the obtained function is rearranged as follow:

$$\mathrm{V}_{d_{k,n}} = -\mathrm{Z}_{dd_k}\,\mathrm{I}_{d_{k,n}} + \mathrm{Z}_{dq_{k,n}}\,\mathrm{I}_{q_{k,n}} + \mathrm{E}_{hd_{k,n}} \tag{2.223}$$

where Z_{dd_k} is given by:

$$\begin{aligned}\mathrm{Z}_{dd_k} = &R_s + \frac{X_d^{"}}{\omega_s}\left(\frac{2}{\Delta t} + jk\omega_s\right) \\ &+ \frac{1}{\omega_s}\left(\frac{2}{\Delta t} + jk\omega_s\right)\frac{\left(\frac{2a_4}{\Delta t} + ja_4 k\omega_s + \frac{1}{T_{d0}^{"}}\right)a_3 + \frac{1}{T_{d0}^{"}}\left(x_d^{'} - x_d^{"}\right)\left(\frac{2}{\Delta t} + jk\omega_s + a_1\right)}{\left(\frac{2}{\Delta t} + jk\omega_s + \frac{1}{T_{d0}^{"}}\right)\left(\frac{2}{\Delta t} + jk\omega_s + a_1\right) - \left(\frac{2a_4}{\Delta t} + ja_4 k\omega_s + \frac{1}{T_{d0}^{"}}\right)a_2}\end{aligned} \tag{2.224}$$

and $\mathrm{Z}_{dq_{k,n}}$ is given by:

$$\mathrm{Z}_{dq_{k,n}} = \frac{\Omega_{r_{0,n}}}{\omega_s}\left(X_q^{"} + \frac{\left(\frac{2b_4}{\Delta t} + jb_4 k\omega_s + \frac{1}{T_{q0}^{"}}\right)b_3 + \frac{1}{T_{q0}^{"}}\left(x_q^{'} - x_q^{"}\right)\left(\frac{2}{\Delta t} + jk\omega_s + b_1\right)}{\left(\frac{2}{\Delta t} + jk\omega_s + \frac{1}{T_{q0}^{"}}\right)\left(\frac{2}{\Delta t} + jk\omega_s + b_1\right) - \left(\frac{2b_4}{\Delta t} + jb_4 k\omega_s + \frac{1}{T_{q0}^{"}}\right)b_2}\right) \tag{2.225}$$

Unlike Z_{dd_k}, which is constant, $\mathrm{Z}_{dq_{k,n}}$ is variable and depends on rotor speed.

The total history term of *d*-axis voltage in equation (2.223) is:

$$\begin{aligned}\mathrm{E}_{hd_{k,n-1}} &= \mathrm{V}_{hd_{k,n-1}} + \\ &+\frac{1}{\omega_s}\left(\frac{2}{\Delta t}+jk\omega_s\right)\frac{\left(\frac{2a_4}{\Delta t}+ja_4k\omega_s+\frac{1}{T_{d0}^{"}}\right)\mathrm{E}_{hq_{k,n-1}}^{'}+\left(\frac{2}{\Delta t}+jk\omega_s+a_1\right)\mathrm{E}_{hq_{k,n-1}}^{"}}{\left(\frac{2}{\Delta t}+jk\omega_s+\frac{1}{T_{d0}^{"}}\right)\left(\frac{2}{\Delta t}+jk\omega_s+a_1\right)-\left(\frac{2a_4}{\Delta t}+ja_4k\omega_s+\frac{1}{T_{d0}^{"}}\right)a_2} \\ &+\frac{\Omega_{r_{0,n-1}}}{\omega_s}\frac{\left(\frac{2b_4}{\Delta t}+jb_4k\omega_s+\frac{1}{T_{q0}^{"}}\right)\mathrm{E}_{hd_{k,n-1}}^{'}+\left(\frac{2}{\Delta t}+jk\omega_s+b_1\right)\mathrm{E}_{hd_{k,n-1}}^{"}}{\left(\frac{2}{\Delta t}+jk\omega_s+\frac{1}{T_{q0}^{"}}\right)\left(\frac{2}{\Delta t}+jk\omega_s+b_1\right)-\left(\frac{2b_4}{\Delta t}+jb_4k\omega_s+\frac{1}{T_{q0}^{"}}\right)b_2}\end{aligned} \tag{2.226}$$

The voltage on *q*-axis, given in (2.195), is discretized as follows:

$$\begin{aligned}\mathrm{V}_{q_{k,n}} = &-\left(R_s+\frac{2X_q^{"}}{\omega_s\Delta t}+jkX_q^{"}\right)\mathrm{I}_{q_{k,n}}-\left(\frac{2}{\omega_s\Delta t}+jk\right)\mathrm{E}_{d_{k,n}}^{"} \\ &-\frac{\Omega_{r_{0,n}}}{\omega_s}\left(X_d^{"}\,\mathrm{I}_{d_{k,n}}+\mathrm{E}_{q_n}^{"}\right)+\mathrm{V}_{hq_{k,n-1}}\end{aligned} \tag{2.227}$$

where the history term is:

$$\begin{aligned}\mathrm{V}_{hq_{k,n-1}} = &-\mathrm{V}_{q_{k,n-1}}-\left(R_s-\frac{2X_q^{"}}{\omega_s\Delta t}+jkX_q^{"}\right)\mathrm{I}_{q_{k,n-1}}+\left(\frac{2}{\omega_s\Delta t}-jk\right)\mathrm{E}_{d_{k,n-1}}^{"} \\ &-\sum_{l}\frac{\Omega_{r_{k-l,n-1}}}{\omega_s}\left(X_d^{"}\,\mathrm{I}_{d_{l,n-1}}-\mathrm{E}_{q_{l,n-1}}^{"}\right)-\sum_{l\neq k}\frac{\Omega_{r_{k-l,n}}}{\omega_s}\left(X_d^{"}\,\mathrm{I}_{d_{l,n}}-\mathrm{E}_{q_{l,n}}^{"}\right)\end{aligned} \tag{2.228}$$

To define the voltage on *q*-axis voltage as a function of input currents, (2.214) and (2.220) are replaced in (2.227). Then, the obtained function is rearranged as follow:

$$\mathrm{V}_{q_{k,n}} = -\mathrm{Z}_{qd_{k,n}}\,\mathrm{I}_{d_{k,n}}-\mathrm{Z}_{qq_k}\,\mathrm{I}_{q_{k,n}}+\mathrm{E}_{hq_{k,n}} \tag{2.229}$$

where Z_{qq_k} is given by:

$$\mathrm{Z}_{qq_k} = R_s + \frac{X_q^{"}}{\omega_s}\left(\frac{2}{\Delta t} + jk\omega_s\right) + \frac{1}{\omega_s}\left(\frac{2}{\Delta t} + jk\omega_s\right)\frac{\left(\frac{2b_4}{\Delta t} + jb_4k\omega_s + \frac{1}{T_{q0}^{"}}\right)b_3 + \frac{\left(x_q^{'} - x_q^{"}\right)}{T_{q0}^{"}}\left(\frac{2}{\Delta t} + jk\omega_s + b_1\right)}{\left(\frac{2}{\Delta t} + jk\omega_s + \frac{1}{T_{q0}^{"}}\right)\left(\frac{2}{\Delta t} + jk\omega_s + b_1\right) - \left(\frac{2b_4}{\Delta t} + jb_4k\omega_s + \frac{1}{T_{q0}^{"}}\right)b_2} \quad (2.230)$$

and $\mathrm{Z}_{qd_{k,n}}$ is given by:

$$\mathrm{Z}_{qd_{k,n}} = \frac{\Omega_{r_{0,n}}}{\omega_s}\left(X_d^{"} + \frac{\left(\frac{2a_4}{\Delta t} + ja_4k\omega_s + \frac{1}{T_{d0}^{"}}\right)a_3 + \frac{\left(x_d^{'} - x_d^{"}\right)}{T_{d0}^{"}}\left(\frac{2}{\Delta t} + jk\omega_s + a_1\right)}{\left(\frac{2}{\Delta t} + jk\omega_s + \frac{1}{T_{d0}^{"}}\right)\left(\frac{2}{\Delta t} + jk\omega_s + a_1\right) - \left(\frac{2a_4}{\Delta t} + ja_4k\omega_s + \frac{1}{T_{d0}^{"}}\right)a_2}\right) \quad (2.231)$$

Unlike Z_{qq_k}, which is constant, $\mathrm{Z}_{qd_{k,n}}$ is variable and depends on rotor speed.

The total history term of *q*-axis voltage in equation (2.223) is:

$$\mathrm{E}_{hq_{k,n-1}} = \mathrm{V}_{hq_{k,n-1}} + -\frac{1}{\omega_s}\left(\frac{2}{\Delta t} + jk\omega_s\right)\frac{\left(\frac{2b_4}{\Delta t} + jb_4k\omega_s + \frac{1}{T_{q0}^{"}}\right)\mathrm{E}_{hd_{k,n-1}}^{'} + \left(\frac{2}{\Delta t} + jk\omega_s + b_1\right)\mathrm{E}_{hd_{k,n-1}}^{"}}{\left(\frac{2}{\Delta t} + jk\omega_s + \frac{1}{T_{q0}^{"}}\right)\left(\frac{2}{\Delta t} + jk\omega_s + b_1\right) - \left(\frac{2b_4}{\Delta t} + jb_4k\omega_s + \frac{1}{T_{q0}^{"}}\right)b_2} + \frac{\Omega_{r_{0,n-1}}}{\omega_s}\frac{\left(\frac{2a_4}{\Delta t} + ja_4k\omega_s + \frac{1}{T_{d0}^{"}}\right)\mathrm{E}_{hq_{k,n-1}}^{'} + \left(\frac{2}{\Delta t} + jk\omega_s + a_1\right)\mathrm{E}_{hq_{k,n-1}}^{"}}{\left(\frac{2}{\Delta t} + jk\omega_s + \frac{1}{T_{d0}^{"}}\right)\left(\frac{2}{\Delta t} + jk\omega_s + a_1\right) - \left(\frac{2a_4}{\Delta t} + ja_4k\omega_s + \frac{1}{T_{d0}^{"}}\right)a_2} \quad (2.232)$$

The first Fourier coefficient of positive sequence voltage according to equation (2.185) is:

$$\begin{aligned} \mathrm{V}_{p_{1,n}} = & \frac{1}{2}\left(-\mathrm{Z}_{dd_0}\,\mathrm{I}_{d_{0,n}} + \mathrm{Z}_{dq_{0,n}}\,\mathrm{I}_{q_{0,n}} - j\left(\mathrm{Z}_{qd_{0,n}}\,\mathrm{I}_{d_{0,n}} + \mathrm{Z}_{qq_0}\,\mathrm{I}_{q_{0,n}}\right)\right)e^{j\left(\delta_n-\frac{\pi}{2}\right)} \\ & + \frac{1}{2}\left(\mathrm{E}_{hd_{0,n-1}} + j\,\mathrm{E}_{hq_{0,n-1}}\right)e^{j\left(\delta_n-\frac{\pi}{2}\right)} \end{aligned} \tag{2.233}$$

The first Fourier coefficient of negative sequence voltage according to equation (2.186) is:

$$\begin{aligned} \mathrm{V}_{n_{1,n}} = & \frac{1}{2}\left(-\mathrm{Z}_{dd_2}\,\mathrm{I}_{d_{2,n}} + \mathrm{Z}_{dq_{2,n}}\,\mathrm{I}_{q_{2,n}} + j\left(\mathrm{Z}_{qd_{2,n}}\,\mathrm{I}_{d_{2,n}} + \mathrm{Z}_{qq_2}\,\mathrm{I}_{q_{2,n}}\right)\right)e^{-j\left(\delta_n-\frac{\pi}{2}\right)} \\ & + \frac{1}{2}\left(\mathrm{E}_{hd_{2,n-1}} - j\,\mathrm{E}_{hq_{2,n-1}}\right)e^{-j\left(\delta_n-\frac{\pi}{2}\right)} \end{aligned} \tag{2.234}$$

To have DP model of SM in symmetrical components, equation (2.233) needs to be rewritten as:

$$\mathrm{V}_{p_{1,n}} = -\mathrm{Z}_{p_{1,n}}\,\mathrm{I}_{p_{1,n}} + \mathrm{V}_{hp_{1,n-1}} \tag{2.235}$$

and equation (2.234) needs to be rewritten as:

$$\mathrm{V}_{n_{1,n}} = -\mathrm{Z}_{n_{1,n}}\,\mathrm{I}_{n_{1,n}} + \mathrm{V}_{hn_{1,n-1}} \tag{2.236}$$

The equivalent impedance and history term in (2.235) and (2.236) are defined as below. The equivalent impedance is:

$$\mathrm{Z}_{p_{1,n}} = \frac{\mathrm{Z}_{dd_0} + \mathrm{Z}_{qq_0} + j\left(\mathrm{Z}_{dq_{0,n}} + \mathrm{Z}_{qd_{0,n}}\right)}{2} \tag{2.237}$$

$$\mathrm{Z}_{n_{1,n}} = \frac{\mathrm{Z}_{dd_2} + \mathrm{Z}_{qq_2} - j\left(\mathrm{Z}_{dq_{2,n}} + \mathrm{Z}_{qd_{2,n}}\right)}{2} \tag{2.238}$$

and history term is:

$$\begin{aligned} \mathrm{V}_{hp_{1,n-1}} = & -\frac{\mathrm{Z}_{dd_0} - \mathrm{Z}_{qq_0} - j\left(\mathrm{Z}_{dq_{0,n}} - \mathrm{Z}_{qd_{0,n}}\right)}{2}\left(\mathrm{I}_{d_{0,n}} - j\,\mathrm{I}_{q_{0,n}}\right)e^{j\left(\delta_n-\frac{\pi}{2}\right)} \\ & + \left(\mathrm{E}_{hd_{0,n-1}} + j\,\mathrm{E}_{h\mathrm{q}_{0,n-1}}\right)e^{j\left(\delta_n-\frac{\pi}{2}\right)} \end{aligned} \tag{2.239}$$

$$\begin{aligned}\mathrm{V}_{hn_{1,n-1}} = &-\frac{\mathrm{Z}_{dd_2}-\mathrm{Z}_{qq_2}+j\left(\mathrm{Z}_{dq_{2,n}}-\mathrm{Z}_{qd_{2,n}}\right)}{2}\left(\mathrm{I}_{d_{2,n}}+j\,\mathrm{I}_{q_{2,n}}\right)e^{-j\left(\delta_n-\frac{\pi}{2}\right)} \\ &+\left(\mathrm{E}_{d_{2,n-1}}-j\,\mathrm{E}_{hq_{2,n-1}}\right)e^{-j\left(\delta_n-\frac{\pi}{2}\right)}\end{aligned} \tag{2.240}$$

The history term depends on both present and prior states. To obtain the proper SM equivalent, an iterative solver is required.

The voltage on 0-axis, given in (2.196), is discretized as follows:

$$\mathrm{V}_{0_{1,n}} = -\mathrm{Z}_{00_1}\,\mathrm{I}_{0_{1,n}} + \mathrm{E}_{h0_{1,n-1}} \tag{2.241}$$

where Z_{00_1} is given by:

$$\mathrm{Z}_{00_1} = \frac{X_l + 3X_n}{\omega_s}\left(\frac{2}{\Delta t} + j\omega_s\right) + R_a + 3R_n \tag{2.242}$$

and the history term of 0-axis voltage in equation (2.241) is:

$$\mathrm{E}_{h0_{1,n-1}} = -\mathrm{V}_{0_{1,n-1}} + \left(\frac{X_l + 3X_n}{\omega_s}\left(\frac{2}{\Delta t} - j\omega_s\right) - \left(R_a + 3R_n\right)\right)\mathrm{I}_{0_{1,n-1}} \tag{2.243}$$

The mechanical angular speed, given in (2.201), is discretized as follows:

$$\Omega_{m_{k,n}} = \frac{\mathrm{T}_{m_{k,n}} - \sum_l \left(\psi_{d_{k-l,n}}\mathrm{I}_{q_{l,n}} - \psi_{q_{k-l,n}}\mathrm{I}_{d_{l,n}}\right)}{\frac{2H}{\omega_s}\left(\frac{2}{\Delta t} + jk\omega_s\right) + K_D} + \Omega_{hm_{k,n-1}} \tag{2.244}$$

where the history term is:

$$\begin{aligned}\Omega_{hm_{k,n-1}} = &-\frac{\left(\frac{2}{\Delta t} - jk\omega_s\right) - K_D}{\left(\frac{2}{\Delta t} + jk\omega_s\right) + K_D}\Omega_{m_{k,n-1}} \\ &+\frac{\mathrm{T}_{m_{k,n-1}} - \sum_l \left(\psi_{d_{k-l,n-1}}\mathrm{I}_{q_{l,n-1}} - \psi_{q_{k-l,n-1}}\mathrm{I}_{d_{l,n-1}}\right) + 2\omega_{s_k}}{\frac{2H}{\omega_s}\left(\frac{2}{\Delta t} + jk\omega_s\right) + K_D}\end{aligned} \tag{2.245}$$

The rotor angle used in equation (2.168) is a time domain variable, therefore it is calculated for the zero Fourier coefficient. The rotor angle, given in (2.204), is discretized as follows:

$$\delta_{0,n} = \frac{P\Delta t}{4}\Omega_{m_{0,n}} + \delta_{h_{0,n-1}} \tag{2.246}$$

where the history term is:

$$\delta_{h_{0,n-1}} = \delta_{0,n-1} + \frac{P\Delta t}{4}\left(\Omega_{m_{0,n-1}} - 2\omega_s\right) \tag{2.247}$$

2.2.2 Norton equivalent circuit of SM

The DP model of SM by symmetrical components is expressed as follows using equations (2.235), (2.236), and (2.241):

$$\mathrm{V}_{pnz_{1,n}} = -\mathrm{Z}_{pnz_{1,n}}\mathrm{I}_{pnz_{1,n}} + \mathrm{E}_{hpnz_{1,n-1}} \tag{2.248}$$

where the $\mathrm{Z}_{pnz_{1,n}}$ matrix is the SM equivalent impedance by symmetrical components. It should be noted that the *dq0* impedance is not constant and is a function of rotor speed.

$$\mathrm{Z}_{pnz_{1,n}} = \begin{bmatrix} \mathrm{Z}_{p_{1,n}} & 0 & 0 \\ 0 & \mathrm{Z}_{n_{1,n}} & 0 \\ 0 & 0 & \mathrm{Z}_{z_{1,n}} \end{bmatrix} \tag{2.249}$$

and $\mathrm{E}_{hpnz_{1,n-1}}$, vector of history term, is:

$$\mathrm{E}_{hdq0_{1,n-1}} = \begin{bmatrix} \mathrm{E}_{hp_{1,n-1}} & \mathrm{E}_{hn_{1,n-1}} & \mathrm{E}_{hz_{1,n-1}} \end{bmatrix}^T \tag{2.250}$$

To add the equivalent SM model to the MANA matrix, the symmetrical components model explained in (2.248) needs to transform to the *abc* frame.

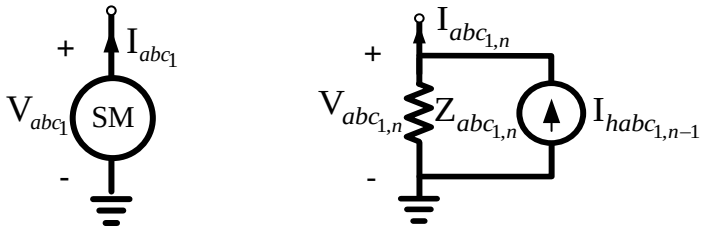

a) b)

Figure 2.9 a) Synchronous machine, b) Equivalent SM circuit, DP models

Figure 2.9 shows the DP Norton equivalent circuit by Trapezoidal rule. The equivalent impedance and history terms in the *abc* frame shown in Figure 2.9 are computed as follows:

$$\mathrm{Z}_{abc_{1,n}} = \mathbf{A}^{-1}\mathrm{Z}_{pnz_{1,n}}\mathbf{A} \tag{2.251}$$

$$\mathrm{I}_{habc_{1,n}} = \mathbf{A}^{-1}\mathrm{Z}^{-1}_{pnz_{1,n}}\mathrm{E}_{hpnz_{1,n}} \tag{2.252}$$

The equivalent impedance of a linear component, such as an inductor or a capacitor, is constant, and the history term calculated using the Trapezoidal method is dependent on the component's voltage and current in the last time step. The equivalent impedance of SM, on the other hand, is not constant, and the history term is affected by present and prior states.

2.2.3 Simulation steps

The following are the steps in a DP simulation approach:

1. Calculate the three phase load-flow: to simulate unbalanced network from initial state, a three-phase load flow is used
2. Initialization
    a. Convert the loads to constant impedances
    b. Calculate the equivalent circuit of elements by discretized method
    c. Build the MANA matrix (equation (1.8)) of the network (exclude the SMs)
    d. Calculate the history terms for the first time-step based on the load flow results

3. Dynamic simulation

    a. Calculate the equivalent impedance and the injection current using (2.251) and (2.252) for all SMs

    b. Add the equivalent impedance of SMs to admittance submatrix of MANA, add the injection current of SMs to the $\mathrm{B}_{1,n}$ vector, and solve $\mathrm{A}_{1,n}\mathrm{X}_{1,n} = \mathrm{B}_{1,n}$

    c. Update the *dq*0-axes currents (equations (2.235), (2.236), and (2.241)), rotor speed (equation (2.244)), and rotor angle (equation (2.246)) for all SMs

    d. If the angular speed relative error of all SMs is less than the allowed error for two consecutive iterations, the solution is converged, and can proceed to step 3.e. If not, the solution has not converged, and the next iteration should begin at step 3.a.

    e. Calculate the controllers' model of zero Fourier coefficient for the next time step

    f. Predict the SM quantities of rotor speed, rotor angle, *d*- and *q*- axes currents of zero and second Fourier coefficients

    g. Calculate the history terms of all elements except SMs (the history term of an inductor, for example, as indicated in equation (1.19)), then update the $\mathrm{B}_{1,n}$ vector and proceed to step 3.a for the next time step

The prediction of variables in step 3.f reduces the number of iterations. Equation (2.163) represents the prediction relationship. In step 3.d, the relationship of relative error is given as (2.164).

2.3 Three phase phasor domain of synchronous machine

In 3pPD method of SM, the electromechanical transients are represented by the zero Fourier coefficient, and non-zero Fourier coefficient transients are ignored. Therefore, the zero Fourier coefficient of the *d*-axis stator voltage, according to (2.88), is:

$$\begin{aligned}\mathbf{V}_{d_0} = &-\frac{X_d^{''}}{\omega_s}\frac{d\mathbf{I}_{d_0}}{dt} + \frac{1}{\omega_s}\frac{d\mathbf{E}_{q_0}^{''}}{dt} + \frac{\boldsymbol{\Omega}_{r_0}}{\omega_s}\left(X_q^{''}\mathbf{I}_{q_0} + \mathbf{E}_{d_0}^{''}\right) + \frac{\boldsymbol{\Omega}_{r_2}}{\omega_s}\left(X_q^{''}\mathbf{I}_{q_2}^{\ *} + \mathbf{E}_{d_2}^{''\ *}\right) \\ &+ \frac{\boldsymbol{\Omega}_{r_2}^{\ *}}{\omega_s}\left(X_q^{''}\mathbf{I}_{q_2} + \mathbf{E}_{d_2}^{''}\right) - R_a\mathbf{I}_{d_0}\end{aligned} \tag{2.253}$$

and the second Fourier coefficient of the *d*-axis stator voltage is:

$$\mathbf{V}_{d_2} = -j2X_d^{''}\mathbf{I}_{d_2} + j2\mathbf{E}_{q_2}^{''} + \frac{\boldsymbol{\Omega}_{r_2}}{\omega_s}\left(X_q^{''}\mathbf{I}_{q_0} + \mathbf{E}_{d_0}^{''}\right) + \frac{\boldsymbol{\Omega}_{r_0}}{\omega_s}\left(X_q^{''}\mathbf{I}_{q_2} + \mathbf{E}_{d_2}^{''}\right) - R_a\mathbf{I}_{d_2} \tag{2.254}$$

The zero Fourier coefficient of the *q*-axis stator voltage, according to (2.89), is:

$$\begin{aligned}\mathbf{V}_{q_0} = &-\frac{X_q^{''}}{\omega_s}\frac{d\mathbf{I}_{q_0}}{dt} - \frac{1}{\omega_s}\frac{d\mathbf{E}_{d_0}^{''}}{dt} - \frac{\boldsymbol{\Omega}_{r_0}}{\omega_s}\left(X_d^{''}\mathbf{I}_{d_0} - \mathbf{E}_{q_0}^{''}\right) \\ &-\frac{\boldsymbol{\Omega}_{r_2}}{\omega_s}\left(X_d^{''}\mathbf{I}_{d_2}^{\ *} - \mathbf{E}_{q_2}^{''\ *}\right) - \frac{\boldsymbol{\Omega}_{r_2}^{\ *}}{\omega_s}\left(X_d^{''}\mathbf{I}_{d_2} - \mathbf{E}_{q_2}^{''}\right) - R_a\mathbf{I}_{q_0}\end{aligned} \tag{2.255}$$

and the second Fourier coefficient of the *q*-axis stator voltage is:

$$\mathbf{V}_{q_2} = -j2X_q^{''}\mathbf{I}_{q_2} - j2\mathbf{E}_{d_2}^{''} - \frac{\boldsymbol{\Omega}_{r_2}}{\omega_s}\left(X_d^{''}\mathbf{I}_{d_0} - \mathbf{E}_{q_0}^{''}\right) - \frac{\boldsymbol{\Omega}_{r_0}}{\omega_s}\left(X_d^{''}\mathbf{I}_{d_2} - \mathbf{E}_{q_2}^{''}\right) - R_a\mathbf{I}_{q_2} \tag{2.256}$$

The zero Fourier coefficient of the 0-axis stator voltage, according to (2.90), is:

$$\mathbf{V}_{0_1} = -\left(R_a + 3R_n + j\left(X_l + 3X_n\right)\right)\mathbf{I}_{0_1} \tag{2.257}$$

The zero Fourier coefficient of the *q*-axis transient emf, according to (2.91), is:

$$\frac{d\mathbf{E}_{q_0}^{'}}{dt} = \frac{1}{T_{d0}^{'}}\left[E_{fd} - \frac{\left(X_d - X_d^{'}\right)\left(X_d^{''} - X_l\right)}{X_d^{'} - X_l}\mathbf{I}_{d_0} - \frac{X_d - X_l}{X_d^{'} - X_l}\mathbf{E}_{q_0}^{'} + \frac{X_d - X_d^{'}}{X_d^{'} - X_l}\mathbf{E}_{q_0}^{''}\right] \tag{2.258}$$

and the second Fourier coefficient of the *q*-axis transient emf is:

$$j2\omega_s\mathbf{E}_{q_2}^{'} = \frac{1}{T_{d0}^{'}}\left[-\frac{\left(X_d - X_d^{'}\right)\left(X_d^{''} - X_l\right)}{X_d^{'} - X_l}\mathbf{I}_{d_2} - \frac{X_d - X_l}{X_d^{'} - X_l}\mathbf{E}_{q_2}^{'} + \frac{X_d - X_d^{'}}{X_d^{'} - X_l}\mathbf{E}_{q_2}^{''}\right] \tag{2.259}$$

The zero Fourier coefficient of the *d*-axis transient emf, according to (2.92), is:

$$\frac{d\mathbf{E}_{d_0}^{'}}{dt} = \frac{1}{T_{q0}^{'}}\left[\frac{\left(X_q - X_q^{'}\right)\left(X_q^{''} - X_l\right)}{X_q^{'} - X_l}\mathbf{I}_{q_0} - \frac{X_q - X_l}{X_q^{'} - X_l}\mathbf{E}_{d_0}^{'} + \frac{X_q - X_q^{'}}{X_q^{'} - X_l}\mathbf{E}_{d_0}^{''}\right] \tag{2.260}$$

and the second Fourier coefficient of the *d*-axis transient emf is:

$$j2\omega_s \mathbf{E}'_{d_2} = \frac{1}{T'_{q0}}\left[\frac{\left(X_q - X'_q\right)\left(X''_q - X_l\right)}{X'_q - X_l}\mathbf{I}_{q_2} - \frac{X_q - X_l}{X'_q - X_l}\mathbf{E}'_{d_2} + \frac{X_q - X'_q}{X'_q - X_l}\mathbf{E}''_{d_2}\right] \tag{2.261}$$

The zero Fourier coefficient of the *q*-axis sub-transient emf, according to (2.93), is:

$$\frac{d\mathbf{E}''_{q_0}}{dt} = \frac{1}{T''_{do}}\left[\mathbf{E}'_{q_0} - \mathbf{E}''_{q_0} - \left(X'_d - X''_d\right)\mathbf{I}_{d_0}\right] + \frac{X''_d - X_l}{X'_d - X_l}\frac{d\mathbf{E}'_{q_0}}{dt} \tag{2.262}$$

and the second Fourier coefficient of the *q*-axis sub-transient emf is:

$$j2\omega_s \mathbf{E}''_{q_2} = \frac{1}{T''_{d0}}\left[\mathbf{E}'_{q_2} - \mathbf{E}''_{q_2} - \left(X'_d - X''_d\right)\mathbf{I}_{d_2}\right] + j2\omega_s \frac{X''_d - X_l}{X'_d - X_l}\mathbf{E}'_{q_2} \tag{2.263}$$

The zero Fourier coefficient of the *d*-axis sub-transient emf, according to (2.93), is:

$$\frac{d\mathbf{E}''_{d_0}}{dt} = \frac{1}{T''_{q0}}\left[\mathbf{E}'_{d_0} - \mathbf{E}''_{d_0} + \left(X'_q - X''_q\right)\mathbf{I}_{q_0}\right] + \frac{X''_q - X_l}{X'_q - X_l}\frac{d\mathbf{E}'_{d_0}}{dt} \tag{2.264}$$

and the second Fourier coefficient of the *d*-axis sub-transient emf is:

$$j2\omega_s \mathbf{E}''_{d_2} = \frac{1}{T''_{q0}}\left[\mathbf{E}'_{d_2} - \mathbf{E}''_{d_2} + \left(X'_q - X''_q\right)\mathbf{I}_{q_2}\right] + j2\omega_s \frac{X''_q - X_l}{X'_q - X_l}\mathbf{E}'_{d_2} \tag{2.265}$$

The zero Fourier coefficient of the mechanical angular speed is obtained by calculating the zero Fourier coefficients from equation (2.107).

$$\begin{aligned}\frac{2H}{\omega_s}\frac{d\boldsymbol{\Omega}_{m_0}}{dt} = T_m &- \left(\boldsymbol{\Psi}_{d_0}\mathbf{I}_{q_0} - \boldsymbol{\Psi}_{q_0}\mathbf{I}_{d_0}\right) - \left(\boldsymbol{\Psi}_{d_2}\mathbf{I}_{q_2}{}^{*} - \boldsymbol{\Psi}_{q_2}\mathbf{I}_{d_2}{}^{*}\right) \\ &- \left(\boldsymbol{\Psi}_{d_2}{}^{*}\mathbf{I}_{q_2} - \boldsymbol{\Psi}_{q_2}{}^{*}\mathbf{I}_{d_2}\right) - K_D\left(\boldsymbol{\Omega}_{m_0} - \omega_s\right)\end{aligned} \tag{2.266}$$

and the second Fourier coefficient of the mechanical angular speed is:

$$j4H\boldsymbol{\Omega}_{m_2} = -\left(\boldsymbol{\Psi}_{d_2}\mathbf{I}_{q_0} - \boldsymbol{\Psi}_{q_2}\mathbf{I}_{d_0}\right) - \left(\boldsymbol{\Psi}_{d_0}\mathbf{I}_{q_2} - \boldsymbol{\Psi}_{q_0}\mathbf{I}_{d_2}\right) - K_D\boldsymbol{\Omega}_{m_2} \tag{2.267}$$

The relation of the rotor angle is obtained by calculating the Fourier coefficients from equation (2.114). The rotor angle used in equation (2.168) is a time domain variable, therefore it is calculated for the zero Fourier coefficient.

$$\frac{d\delta}{dt} = \frac{P}{2}\left(\mathbf{\Omega}_{m_0} - \omega_s\right) \tag{2.268}$$

The relation of the *d*- and *q*- axes flux are obtained by calculating the Fourier coefficients from equations (2.105) and (2.106), respectively.

$$\mathbf{\Psi}_{d_k} = -X_d^{''}\mathbf{I}_{d_k} + \mathbf{E}_{q_k}^{''} \tag{2.269}$$

$$\mathbf{\Psi}_{q_k} = -X_q^{''}\mathbf{I}_{q_k} - \mathbf{E}_{d_k}^{''} \tag{2.270}$$

where *k*, the Fourier coefficients for the flux, is zero or two.

2.3.1 Discretized equations

The discretized equations of the 3pPD model of synchronous machine employing the Trapezoidal rule are provided in this section.

Equations (2.258), (2.260), (2.262), and (2.264), the zero Fourier coefficient of the transient and the sub-transient emfs are rewritten using stated parameters in equations (2.115)-(2.122), yielding:

$$\frac{d\mathbf{E}_{q_0}^{'}}{dt} = \frac{E_{fd}}{T_{do}^{'}} - a_1\mathbf{E}_{q_0}^{'} + a_2\mathbf{E}_{q_0}^{''} - a_3\mathbf{I}_{d_0} \tag{2.271}$$

$$\frac{d\mathbf{E}_{q_0}^{''}}{dt} = \frac{1}{T_{d0}^{''}}\left[\mathbf{E}_{q_0}^{'} - \mathbf{E}_{q_0}^{''} - \left(X_d^{'} - X_d^{''}\right)\mathbf{I}_{d_0}\right] + a_4\frac{d\mathbf{E}_{q_0}^{'}}{dt} \tag{2.272}$$

$$\frac{d\mathbf{E}_{d_0}^{'}}{dt} = -b_1\mathbf{E}_{d_0}^{'} + b_2\mathbf{E}_{d_0}^{''} + b_3\mathbf{I}_{q_0} \tag{2.273}$$

$$\frac{d\mathbf{E}_{d_0}^{''}}{dt} = \frac{1}{T_{q0}^{''}}\left[\mathbf{E}_{d_0}^{'} - \mathbf{E}_{d_0}^{''} + \left(X_q^{'} - X_q^{''}\right)\mathbf{I}_{q_0}\right] + b_4\frac{d\mathbf{E}_{d_0}^{'}}{dt} \tag{2.274}$$

The zero Fourier coefficient of transient emf on *q*-axis, given in (2.271), is discretized as follows:

$$\mathbf{E}'_{q_{0,n}} = \frac{a_2\mathbf{E}''_{q_{0,n}} - a_3\mathbf{I}_{d_{0,n}} + \mathbf{E}'_{hq_{0,n-1}}}{\frac{2}{\Delta t} + a_1} \tag{2.275}$$

where the history term is:

$$\mathbf{E}'_{hq_{0,n-1}} = \frac{\mathbf{E}_{fD_{0,n}}}{T'_{d0}} + \frac{\mathbf{E}_{fD_{0,n-1}}}{T'_{d0}} + \left(\frac{2}{\Delta t} - a_1\right)\mathbf{E}'_{q_{0,n-1}} + a_2\mathbf{E}''_{q_{0,n-1}} - a_3\mathbf{I}_{d_{0,n-1}} \tag{2.276}$$

Equation (2.272), the zero Fourier coefficient of sub-transient emf on *d*-axis, is discretized as follows:

$$\mathbf{E}''_{q_{0,n}} = \frac{\left(\frac{2a_4}{\Delta t}_s + \frac{1}{T''_{d0}}\right)\mathbf{E}'_{q_{0,n}} - \frac{1}{T''_{d0}}\left(x'_d - x''_d\right)\mathbf{I}_{d_{0,n}} + \mathbf{E}''_{hq_{0,n-1}}}{\frac{2}{\Delta t} + \frac{1}{T''_{d0}}} \tag{2.277}$$

where the history term is:

$$\mathbf{E}''_{hq_{0,n-1}} = -\left(\frac{2a_4}{\Delta t} - \frac{1}{T''_{d0}}\right)\mathbf{E}'_{q_{0,n-1}} + \left(\frac{2}{\Delta t} - \frac{1}{T''_{d0}}\right)\mathbf{E}''_{q_{0,n-1}} - \frac{1}{T''_{d0}}\left(x'_d - x''_d\right)\mathbf{I}_{d_{0,n-1}} \tag{2.278}$$

To derive the zero Fourier coefficient of the transient and the sub-transient emfs on the *d*-axis depending on the input current, (2.275) and (2.278) are rearranged, yielding the following result:

$$\begin{aligned}\mathbf{E}'_{q_{0,n}} = &-\frac{\frac{1}{T''_{d0}}\left(x'_d - x''_d\right)a_2 + \left(\frac{2}{\Delta t} + \frac{1}{T''_{d0}}\right)a_3}{\left(\frac{2}{\Delta t} + \frac{1}{T''_{d0}}\right)\left(\frac{2}{\Delta t} + a_1\right) - \left(\frac{2a_4}{\Delta t} + \frac{1}{T''_{d0}}\right)a_2}\mathbf{I}_{d_{0,n}} \\ &+ \frac{\left(\frac{2}{\Delta t} + \frac{1}{T''_{d0}}\right)\mathbf{E}'_{hq_{0,n-1}} + a_2\mathbf{E}''_{hq_{0,n-1}}}{\left(\frac{2}{\Delta t} + \frac{1}{T''_{d0}}\right)\left(\frac{2}{\Delta t} + a_1\right) - \left(\frac{2a_4}{\Delta t} + \frac{1}{T''_{d0}}\right)a_2}\end{aligned} \tag{2.279}$$

$$\mathbf{E}''_{q_{0,n}} = -\frac{\frac{1}{T''_{d0}}\left(x'_d - x''_d\right)\left(\frac{2}{\Delta t}+a_1\right)+\left(\frac{2a_4}{\Delta t}+\frac{1}{T''_{d0}}\right)a_3}{\left(\frac{2}{\Delta t}+\frac{1}{T''_{d0}}\right)\left(\frac{2}{\Delta t}+a_1\right)-\left(\frac{2a_4}{\Delta t}+\frac{1}{T''_{d0}}\right)a_2}\mathbf{I}_{d_{0,n}} + \frac{\left(\frac{2a_4}{\Delta t}+\frac{1}{T''_{d0}}\right)\mathbf{E}'_{q_{0,n}}+\left(\frac{2}{\Delta t}+a_1\right)\mathbf{E}''_{q_{0,n}}}{\left(\frac{2}{\Delta t}+\frac{1}{T''_{d0}}\right)\left(\frac{2}{\Delta t}+a_1\right)-\left(\frac{2a_4}{\Delta t}+\frac{1}{T''_{d0}}\right)a_2} \tag{2.280}$$

The zero Fourier coefficient of transient emf on *d*-axis, given in (2.273), is discretized as follows:

$$\mathbf{E}'_{d_{0,n}} = \frac{b_2\mathbf{E}''_{d_{0,n}} + b_3\mathbf{I}_{q_{0,n}} + \mathbf{E}'_{hd_{0,n-1}}}{\frac{2}{\Delta t}+b_1} \tag{2.281}$$

where the history term is:

$$\mathbf{E}'_{hd_{0,n-1}} = \left(\frac{2}{\Delta t}-b_1\right)\mathbf{E}'_{d_{0,n-1}} + b_2\mathbf{E}''_{d_{0,n-1}} + b_3\mathbf{I}_{q_{0,n-1}} \tag{2.282}$$

The zero Fourier coefficient of sub-transient emf on *d*-axis, given in (2.274), is discretized as follows:

$$\mathbf{E}''_{d_{0,n}} = \frac{\left(\frac{2b_4}{\Delta t}+\frac{1}{T''_{q0}}\right)\mathbf{E}'_{d_{0,n}} + \frac{1}{T''_{q0}}\left(x'_q - x''_q\right)\mathbf{I}_{q_{0,n}} + \mathbf{E}''_{hd_{0,n-1}}}{\frac{2}{\Delta t}+\frac{1}{T''_{q0}}} \tag{2.283}$$

where the history term is:

$$\mathbf{E}''_{hd_{0,n-1}} = \left(\frac{2}{\Delta t}-\frac{1}{T''_{q0}}\right)\mathbf{E}''_{d_{0,n-1}} - \left(\frac{2b_4}{\Delta t}-\frac{1}{T''_{q0}}\right)\mathbf{E}'_{d_{0,n-1}} + \frac{1}{T''_{q0}}\left(x'_q - x''_q\right)\mathbf{I}_{q_{0,n-1}} \tag{2.284}$$

To derive the zero Fourier coefficient of the transient and the sub-transient emfs on the *q*-axis depending on the input current, (2.281) and (2.283) are rearranged, yielding the following result:

$$\begin{aligned}\mathbf{E}'_{d_{0,n}} &= \frac{\left(\frac{2}{\Delta t}+\frac{1}{T''_{q0}}\right)b_3+\frac{1}{T''_{q0}}\left(x'_q-x''_q\right)b_2}{\left(\frac{2}{\Delta t}+\frac{1}{T''_{q0}}\right)\left(\frac{2}{\Delta t}+b_1\right)-\left(\frac{2b_4}{\Delta t}+\frac{1}{T''_{q0}}\right)b_2}\mathbf{I}_{q_{0,n}} \\ &+\frac{\left(\frac{2}{\Delta t}+\frac{1}{T''_{q0}}\right)\mathbf{E}'_{hd_{0,n-1}}+b_2\mathbf{E}''_{hd_{0,n-1}}}{\left(\frac{2}{\Delta t}+\frac{1}{T''_{q0}}\right)\left(\frac{2}{\Delta t}+b_1\right)-\left(\frac{2b_4}{\Delta t}+\frac{1}{T''_{q0}}\right)b_2}\end{aligned} \tag{2.285}$$

$$\begin{aligned}\mathbf{E}''_{d_{0,n}} &= \frac{\left(\frac{2b_4}{\Delta t}+\frac{1}{T''_{q0}}\right)b_3+\frac{1}{T''_{q0}}\left(x'_q-x''_q\right)\left(\frac{2}{\Delta t}+b_1\right)}{\left(\frac{2}{\Delta t}+\frac{1}{T''_{q0}}\right)\left(\frac{2}{\Delta t}+b_1\right)-\left(\frac{2b_4}{\Delta t}+\frac{1}{T''_{q0}}\right)b_2}\mathbf{I}_{q_{0,n}} \\ &+\frac{\left(\frac{2b_4}{\Delta t}+\frac{1}{T''_{q0}}\right)\mathbf{E}'_{hd_{0,n-1}}+\left(\frac{2}{\Delta t}+b_1\right)\mathbf{E}''_{hd_{0,n-1}}}{\left(\frac{2}{\Delta t}+\frac{1}{T''_{q0}}\right)\left(\frac{2}{\Delta t}+b_1\right)-\left(\frac{2b_4}{\Delta t}+\frac{1}{T''_{q0}}\right)b_2}\end{aligned} \tag{2.286}$$

The zero Fourier coefficient of *d*-axis voltage, given in (2.253), is discretized as follows:

$$\mathbf{V}_{d_{0,n}} = -\left(R_s+\frac{2X''_d}{\omega_s\Delta t}\right)\mathbf{I}_{d_{0,n}}+\frac{2}{\omega_s\Delta t}\mathbf{E}''_{q_{0,n}}+\frac{\mathbf{\Omega}_{r_{0,n}}}{\omega_s}\left(X''_q\mathbf{I}_{q_{0,n}}+\mathbf{E}''_{d_{0,n}}\right)+\mathbf{V}_{hd_{0,n-1}} \tag{2.287}$$

where the history term is:

$$\begin{aligned}\mathbf{V}_{hd_{0,n-1}} &= -\left(R_s-\frac{2X''_d}{\omega_s\Delta t}\right)\mathbf{I}_{d_{0,n-1}}-\frac{2}{\omega_s\Delta t}\mathbf{E}''_{q_{0,n-1}}+\frac{\mathbf{\Omega}_{r_{0,n-1}}}{\omega_s}\left(X''_q\mathbf{I}_{q_{0,n-1}}+\mathbf{E}''_{d_{0,n-1}}\right) \\ &+\frac{\mathbf{\Omega}_{r_{2,n-1}}^{\ *}}{\omega_s}\left(X''_q\mathbf{I}_{q_{2,n-1}}+\mathbf{E}''_{d_{2,n-1}}\right)+\frac{\mathbf{\Omega}_{r_{2,n-1}}}{\omega_s}\left(X''_q\mathbf{I}_{q_{2,n-1}}^{\ *}+\mathbf{E}''_{d_{2,n-1}}^{\ *}\right) \\ &+\frac{\mathbf{\Omega}_{r_{2,n}}^{\ *}}{\omega_s}\left(X''_q\mathbf{I}_{q_{2,n}}+\mathbf{E}''_{d_{2,n}}\right)+\frac{\mathbf{\Omega}_{r_{2,n}}}{\omega_s}\left(X''_q\mathbf{I}_{q_{2,n}}^{\ *}+\mathbf{E}''_{d_{2,n}}^{\ *}\right)-\mathbf{V}_{d_{0,n-1}}\end{aligned} \tag{2.288}$$

To derive the zero Fourier coefficient of voltage on the *d*-axis depending on the input current, the set of equations (2.280) and (2.286) are replaced in equation (2.287), yielding the following result:

$$\mathbf{V}_{d_{0,n}} = -\mathbf{Z}_{dd_0}\mathbf{I}_{d_{0,n}} + \mathbf{Z}_{dq_{0,n}}\mathbf{I}_{q_{0,n}} + \mathbf{E}_{hd_{0,n-1}} \tag{2.289}$$

where $\mathbf{Z}_{dd_0}$ is given by:

$$\mathbf{Z}_{dd_0} = R_s + \frac{2X_d^{''}}{\Delta t\omega_s} + \frac{2}{\Delta t\omega_s}\frac{\left(\frac{2a_4}{\Delta t}+\frac{1}{T_{d0}^{''}}\right)a_3 + \frac{1}{T_{d0}^{''}}\left(x_d^{'}-x_d^{''}\right)\left(\frac{2}{\Delta t}+a_1\right)}{\left(\frac{2}{\Delta t}+\frac{1}{T_{d0}^{''}}\right)\left(\frac{2}{\Delta t}+a_1\right)-\left(\frac{2a_4}{\Delta t}+\frac{1}{T_{d0}^{''}}\right)a_2} \tag{2.290}$$

and $\mathbf{Z}_{dq_{0,n}}$ is given by:

$$\mathbf{Z}_{dq_{0,n}} = \frac{\mathbf{\Omega}_{r_{0,n}}}{\omega_s}\left(X_q^{''} + \frac{\left(\frac{2b_4}{\Delta t}+\frac{1}{T_{q0}^{''}}\right)b_3 + \frac{1}{T_{q0}^{''}}\left(x_q^{'}-x_q^{''}\right)\left(\frac{2}{\Delta t}+b_1\right)}{\left(\frac{2}{\Delta t}+\frac{1}{T_{q0}^{''}}\right)\left(\frac{2}{\Delta t}+b_1\right)-\left(\frac{2b_4}{\Delta t}+\frac{1}{T_{q0}^{''}}\right)b_2}\right) \tag{2.291}$$

The $\mathbf{Z}_{dd_0}$ is constant and $\mathbf{Z}_{dq_{0,n}}$ is a function of rotor speed.

The total history term in equation (2.289) is:

$$\begin{aligned}\mathbf{E}_{hd_{0,n-1}} = {} & \mathbf{V}_{hd_{0,n-1}} \\ & + \frac{2}{\omega_s\Delta t}\frac{\left(\frac{2a_4}{\Delta t}+\frac{1}{T_{d0}^{''}}\right)\mathbf{E}_{hq_{0,n-1}}^{'} + \left(\frac{2}{\Delta t}+a_1\right)\mathbf{E}_{hq_{0,n-1}}^{''}}{\left(\frac{2}{\Delta t}+\frac{1}{T_{d0}^{''}}\right)\left(\frac{2}{\Delta t}+a_1\right)-\left(\frac{2a_4}{\Delta t}+\frac{1}{T_{d0}^{''}}\right)a_2} \\ & + \frac{\mathbf{\Omega}_{r_{0,n-1}}}{\omega_s}\frac{\left(\frac{2b_4}{\Delta t}+\frac{1}{T_{q0}^{''}}\right)\mathbf{E}_{hd_{0,n-1}}^{'} + \left(\frac{2}{\Delta t}+b_1\right)\mathbf{E}_{hd_{0,n-1}}^{''}}{\left(\frac{2}{\Delta t}+\frac{1}{T_{q0}^{''}}\right)\left(\frac{2}{\Delta t}+b_1\right)-\left(\frac{2b_4}{\Delta t}+\frac{1}{T_{q0}^{''}}\right)b_2}\end{aligned} \tag{2.292}$$

The zero Fourier coefficient of *q*-axis voltage, given in (2.255), is discretized as follows:

$$\mathbf{V}_{q_{0,n}} = -\left(R_s + \frac{2X_q^{"}}{\omega_s \Delta t} \right) \mathbf{I}_{q_{0,n}} - \frac{2}{\omega_s \Delta t} \mathbf{E}_{d_{0,n}}^{"} - \frac{\mathbf{\Omega}_{r_{0,n}}}{\omega_s} \left(X_d^{"} \mathbf{I}_{d_{0,n}} + \mathbf{E}_{q_{0,n}}^{"} \right) + \mathbf{V}_{hq_{0,n-1}} \tag{2.293}$$

where the history term is:

$$\begin{aligned} \mathbf{V}_{hq_{0,n-1}} = & -\mathbf{V}_{q_{0,n-1}} - \left(R_s - \frac{2X_q^{"}}{\omega_s \Delta t} \right) \mathbf{I}_{q_{0,n-1}} + \frac{2}{\omega_s \Delta t} \mathbf{E}_{d_{0,n-1}}^{"} - \frac{\mathbf{\Omega}_{r_{0,n-1}}}{\omega_s} \left(X_d^{"} \mathbf{I}_{d_{0,n-1}} - \mathbf{E}_{q_{0,n-1}}^{"} \right) \\ & - \frac{\mathbf{\Omega}_{r_{2,n-1}}^{\ *}}{\omega_s} \left(X_d^{"} \mathbf{I}_{d_{2,n-1}} - \mathbf{E}_{q_{2,n-1}}^{"} \right) - \frac{\mathbf{\Omega}_{r_{2,n-1}}}{\omega_s} \left(X_d^{"} \mathbf{I}_{d_{2,n-1}}^{\ *} - \mathbf{E}_{q_{2,n-1}}^{"\ *} \right) \\ & - \frac{\mathbf{\Omega}_{r_{2,n}}^{\ *}}{\omega_s} \left(X_d^{"} \mathbf{I}_{d_{2,n}} - \mathbf{E}_{q_{2,n}}^{"} \right) - \frac{\mathbf{\Omega}_{r_{2,n}}}{\omega_s} \left(X_d^{"} \mathbf{I}_{d_{2,n}}^{\ *} - \mathbf{E}_{q_{2,n}}^{"\ *} \right) \end{aligned} \tag{2.294}$$

To derive the zero Fourier coefficient of voltage on the *q*-axis depending on the input current, the set of equations (2.280) and (2.286) are replaced in equation (2.293), yielding the following result:

$$\mathbf{V}_{q_{0,n}} = -\mathbf{Z}_{qd_{0,n}} \mathbf{I}_{d_{0,n}} - \mathbf{Z}_{qq_0} \mathbf{I}_{q_{0,n}} + \mathbf{E}_{q_{0,n-1}} \tag{2.295}$$

where $\mathbf{Z}_{qq_0}$ is given by:

$$\mathbf{Z}_{qq_0} = R_s + \frac{2X_q^{"}}{\Delta t \omega_s} + \frac{2}{\Delta t \omega_s} \frac{\left(\frac{2b_4}{\Delta t} + \frac{1}{T_{q0}^{"}} \right) b_3 + \frac{\left(x_q^{'} - x_q^{"} \right)}{T_{q0}^{"}} \left(\frac{2}{\Delta t} + b_1 \right)}{\left(\frac{2}{\Delta t} + \frac{1}{T_{q0}^{"}} \right) \left(\frac{2}{\Delta t} + b_1 \right) - \left(\frac{2b_4}{\Delta t} + \frac{1}{T_{q0}^{"}} \right) b_2} \tag{2.296}$$

and $\mathbf{Z}_{qd_{0,n}}$ is given by:

$$\mathbf{Z}_{qd_{0,n}} = \frac{\mathbf{\Omega}_{r_{0,n}}}{\omega_s} \left(X_d^{"} + \frac{\left(\frac{2a_4}{\Delta t} + \frac{1}{T_{d0}^{"}} \right) a_3 + \frac{\left(x_d^{'} - x_d^{"} \right)}{T_{d0}^{"}} \left(\frac{2}{\Delta t} + a_1 \right)}{\left(\frac{2}{\Delta t} + \frac{1}{T_{d0}^{"}} \right) \left(\frac{2}{\Delta t} + a_1 \right) - \left(\frac{2a_4}{\Delta t} + \frac{1}{T_{d0}^{"}} \right) a_2} \right) \tag{2.297}$$

The $\mathbf{Z}_{qq_0}$ is constant and $\mathbf{Z}_{qd_{0,n}}$ is a function of rotor speed.

The total history term of *q*-axis voltage in equation (2.295) is:

$$\begin{aligned}\mathbf{E}_{hq_{0,n-1}} &= \mathbf{V}_{hq_{0,n-1}} \\ &-\frac{2}{\Delta t}\frac{\left(\frac{2b_4}{\Delta t}+\frac{1}{T_{q0}^{''}}\right)\mathbf{E}_{hd_{0,n-1}}^{'}+\left(\frac{2}{\Delta t}+b_1\right)\mathbf{E}_{hd_{0,n-1}}^{''}}{\left(\frac{2}{\Delta t}+\frac{1}{T_{q0}^{''}}\right)\left(\frac{2}{\Delta t}+b_1\right)-\left(\frac{2b_4}{\Delta t}+\frac{1}{T_{q0}^{''}}\right)b_2} \\ &+\frac{\mathbf{\Omega}_{r_{0,n-1}}}{\omega_s}\frac{\left(\frac{2a_4}{\Delta t}+\frac{1}{T_{d0}^{''}}\right)\mathbf{E}_{hq_{0,n-1}}^{'}+\left(\frac{2}{\Delta t}+a_1\right)\mathbf{E}_{hq_{0,n-1}}^{''}}{\left(\frac{2}{\Delta t}+\frac{1}{T_{d0}^{''}}\right)\left(\frac{2}{\Delta t}+a_1\right)-\left(\frac{2a_4}{\Delta t}+\frac{1}{T_{d0}^{''}}\right)a_2}\end{aligned} \tag{2.298}$$

The first Fourier coefficient of positive sequence voltage according to equation (2.185) is obtained by combining equations (2.289) and (2.295):

$$\begin{aligned}\mathbf{V}_{p_{1,n}} &= \frac{1}{2}\left(-\mathbf{Z}_{dd_0}\mathbf{I}_{d_{0,n}}+\mathbf{Z}_{dq_{0,n}}\mathbf{I}_{q_{0,n}}-j\left(\mathbf{Z}_{qd_0}\mathbf{I}_{d_{0,n}}+\mathbf{Z}_{qq_0}\mathbf{I}_{q_{0,n}}\right)\right)e^{j\left(\boldsymbol{\delta}_n-\frac{\pi}{2}\right)} \\ &+\frac{1}{2}\left(\mathbf{E}_{hd_{0,n-1}}+j\mathbf{E}_{hq_{0,n-1}}\right)e^{j\left(\boldsymbol{\delta}_n-\frac{\pi}{2}\right)}\end{aligned} \tag{2.299}$$

In the SM model, the negative sequence component is caused by the second Fourier coefficients. Since the second Fourier coefficient in a traditional phasor derivative term does not exist, no numerical approach is required to discretize it. Equations (2.259), (2.261), (2.263), and (2.265) are rewritten using stated parameters in equations (2.115)-(2.122), yielding:

$$j2\omega_s\mathbf{E}_{q_2}^{'}=-a_1\mathbf{E}_{q_2}^{'}+a_2\mathbf{E}_{q_2}^{''}-a_3\mathbf{I}_{d_2} \tag{2.300}$$

$$j2\omega_s\mathbf{E}_{q_2}^{''}=\frac{1}{T_{d0}^{''}}\left[\mathbf{E}_{q_2}^{'}-\mathbf{E}_{q_2}^{''}-\left(X_d^{'}-X_d^{''}\right)\mathbf{I}_{d_2}\right]+j2\omega_s a_4\mathbf{E}_{q_2}^{'} \tag{2.301}$$

$$j2\omega_s\mathbf{E}_{d_2}^{'}=-b_1\mathbf{E}_{d_2}^{'}+b_2\mathbf{E}_{d_2}^{''}+b_3\mathbf{I}_{q_2} \tag{2.302}$$

$$j2\omega_s\mathbf{E}_{d_2}^{''}=\frac{1}{T_{q0}^{''}}\left[\mathbf{E}_{d_2}^{'}-\mathbf{E}_{d_2}^{''}+\left(X_q^{'}-X_q^{''}\right)\mathbf{I}_{q_2}\right]+j2\omega_s b_4\mathbf{E}_{d_2}^{'} \tag{2.303}$$

To derive the second Fourier coefficient of the transient and the sub-transient emfs on the *q*-axis depending on the input current, (2.300) and (2.301) are rearranged, yielding the following result:

$$\mathbf{E}'_{q_{2,n}} = -\frac{\frac{1}{T''_{d0}}\left(x'_d - x''_d\right)a_2 + \left(jk\omega_s + \frac{1}{T''_{d0}}\right)a_3}{\left(j2\omega_s + \frac{1}{T''_{d0}}\right)\left(j2\omega_s + a_1\right) - \left(j2a_4\omega_s + \frac{1}{T''_{d0}}\right)a_2}\mathbf{I}_{d_{2,n}} \tag{2.304}$$

$$\mathbf{E}''_{q_{2,n}} = -\frac{\frac{1}{T''_{d0}}\left(x'_d - x''_d\right)\left(j2\omega_s + a_1\right) + \left(j2a_4\omega_s + \frac{1}{T''_{d0}}\right)a_3}{\left(j2\omega_s + \frac{1}{T''_{d0}}\right)\left(j2\omega_s + a_1\right) - \left(j2a_4\omega_s + \frac{1}{T''_{d0}}\right)a_2}\mathbf{I}_{d_{2,n}} \tag{2.305}$$

To derive the second Fourier coefficient of the transient and the sub-transient emfs on the *d*-axis depending on the input current, (2.302) and (2.303) are rearranged, yielding the following result:

$$\mathbf{E}'_{d_{2,n}} = \frac{\left(j2\omega_s + \frac{1}{T''_{q0}}\right)b_3 + \frac{1}{T''_{q0}}\left(x'_q - x''_q\right)b_2}{\left(j2\omega_s + \frac{1}{T''_{q0}}\right)\left(j2\omega_s + b_1\right) - \left(j2b_4\omega_s + \frac{1}{T''_{q0}}\right)b_2}\mathbf{I}_{q_{2,n}} \tag{2.306}$$

$$\mathbf{E}''_{d_{2,n}} = \frac{\left(j2b_4\omega_s + \frac{1}{T''_{q0}}\right)b_3 + \frac{1}{T''_{q0}}\left(x'_q - x''_q\right)\left(j2\omega_s + b_1\right)}{\left(j2\omega_s + \frac{1}{T''_{q0}}\right)\left(j2\omega_s + b_1\right) - \left(j2b_4\omega_s + \frac{1}{T''_{q0}}\right)b_2}\mathbf{I}_{q_{2,n}} \tag{2.307}$$

The second Fourier coefficient of *d*-axis voltage, given in (2.254), is discretized as follows:

$$\begin{aligned}\mathbf{V}_{d_{2,n}} = &-\left(R_s + j2X''_d\right)\mathbf{I}_{d_{2,n}} + j2\mathbf{E}''_{q_{2,n}} + \frac{\boldsymbol{\Omega}_{r_{0,n}}}{\omega_s}\left(X''_q\mathbf{I}_{q_{2,n}} + \mathbf{E}''_{d_{2,n}}\right) \\ &+ \frac{\boldsymbol{\Omega}_{r_{2,n}}}{\omega_s}\left(X''_q\mathbf{I}_{q_{0,n}} + \mathbf{E}''_{d_{0,n}}\right)\end{aligned} \tag{2.308}$$

To derive the second Fourier coefficient of voltage on the *d*-axis depending on the input current, the set of equations (2.305) and (2.307) are replaced in equation (2.308), yielding the following result:

$$\mathbf{V}_{d_{2,n}} = -\mathbf{Z}_{dd_{2,n}}\mathbf{I}_{d_{2,n}} + \mathbf{Z}_{dq_2}\mathbf{I}_{q_{2,n}} + \mathbf{E}_{hd_{2,n-1}} \tag{2.309}$$

where $\mathbf{Z}_{dd_2}$ is given by:

$$\mathbf{Z}_{dd_2} = R_s + j2X_d^{"} + j2\frac{\left(ja_4 2\omega_s + \frac{1}{T_{d0}^{"}}\right)a_3 + \frac{1}{T_{d0}^{"}}\left(x_d^{'} - x_d^{"}\right)\left(j2\omega_s + a_1\right)}{\left(j2\omega_s + \frac{1}{T_{d0}^{"}}\right)\left(j2\omega_s + a_1\right) - \left(ja_4 2\omega_s + \frac{1}{T_{d0}^{"}}\right)a_2} \tag{2.310}$$

and $\mathbf{Z}_{dq_{2,n}}$ is given by:

$$\mathbf{Z}_{dq_{2,n}} = \frac{\mathbf{\Omega}_{r_{0,n}}}{\omega_s}\left(X_q^{"} + \frac{\left(jb_4 2\omega_s + \frac{1}{T_{q0}^{"}}\right)b_3 + \frac{1}{T_{q0}^{"}}\left(x_q^{'} - x_q^{"}\right)\left(j2\omega_s + b_1\right)}{\left(j2\omega_s + \frac{1}{T_{q0}^{"}}\right)\left(j2\omega_s + b_1\right) - \left(jb_4 2\omega_s + \frac{1}{T_{q0}^{"}}\right)b_2}\right) \tag{2.311}$$

Unlike $\mathbf{Z}_{dd_k}$, which is constant, $\mathbf{Z}_{dq_{k,n}}$ is variable and depends on rotor speed.

The total history in equation (2.309) is:

$$\mathbf{E}_{hd_{2,n-1}} = \frac{\mathbf{\Omega}_{r_{2,n}}}{\omega_s}\left(X_q^{"}\mathbf{I}_{q_{0,n}} + \mathbf{E}_{d_{0,n}}^{"}\right) \tag{2.312}$$

The second Fourier coefficient of *q*-axis voltage, given in (2.256), is discretized as follows:

$$\begin{aligned}\mathbf{V}_{q_{2,n}} = &-\left(R_s + j2X_q^{"}\right)\mathbf{I}_{q_{2,n}} - j2\mathbf{E}_{d_{2,n}}^{"} - \frac{\mathbf{\Omega}_{r_{0,n}}}{\omega_s}\left(X_d^{"}\mathbf{I}_{d_{2,n}} + \mathbf{E}_{q_{2,n}}^{"}\right) \\ &- \frac{\mathbf{\Omega}_{r_{2,n}}}{\omega_s}\left(X_d^{"}\mathbf{I}_{d_{0,n}} - \mathbf{E}_{q_{0,n}}^{"}\right)\end{aligned} \tag{2.313}$$

To derive the second Fourier coefficient of voltage on the *q*-axis depending on the input current, the set of equations (2.305) and (2.307) are replaced in equation (2.313), yielding the following result:

$$\mathbf{V}_{q_{2,n}} = -\mathbf{Z}_{qd_{2,n}}\mathbf{I}_{d_{2,n}} - \mathbf{Z}_{qq_2}\mathbf{I}_{q_{2,n}} + \mathbf{E}_{hq_{2,n-1}} \tag{2.314}$$

where $\mathbf{Z}_{qq_2}$ is given by:

$$\mathbf{Z}_{qq_2} = R_s + j2X_q^{"} + j2\frac{\left(jb_4 2\omega_s + \frac{1}{T_{q0}^{"}}\right)b_3 + \frac{\left(x_q^{'} - x_q^{"}\right)}{T_{q0}^{"}}\left(j2\omega_s + b_1\right)}{\left(j2\omega_s + \frac{1}{T_{q0}^{"}}\right)\left(j2\omega_s + b_1\right) - \left(jb_4 2\omega_s + \frac{1}{T_{q0}^{"}}\right)b_2} \tag{2.315}$$

and $\mathbf{Z}_{qd_{2,n}}$ is given by:

$$\mathbf{Z}_{qd_{2,n}} = \frac{\mathbf{\Omega}_{r_{0,n}}}{\omega_s}\left(X_d^{"} + \frac{\left(ja_4 2\omega_s + \frac{1}{T_{d0}^{"}}\right)a_3 + \frac{\left(x_d^{'} - x_d^{"}\right)}{T_{d0}^{"}}\left(j2\omega_s + a_1\right)}{\left(j2\omega_s + \frac{1}{T_{d0}^{"}}\right)\left(j2\omega_s + a_1\right) - \left(ja_4 2\omega_s + \frac{1}{T_{d0}^{"}}\right)a_2}\right) \tag{2.316}$$

Unlike $\mathbf{Z}_{qq_2}$, which is constant, $\mathbf{Z}_{qd_{2,n}}$ is variable and depends on rotor speed.

The total history term in equation (2.314) is:

$$\mathbf{E}_{hq_{2,n-1}} = -\frac{\mathbf{\Omega}_{r_{2,n}}}{\omega_s}\left(X_d^{"}\mathbf{I}_{d_{0,n}} - \mathbf{E}_{q_{0,n}}^{"}\right) \tag{2.317}$$

The first Fourier coefficient of positive sequence voltage according to equation (2.186) is obtained by combining equations (2.309) and (2.314):

$$\begin{aligned}\mathbf{V}_{n_{1,n}} = {} & \frac{1}{2}\left(-\mathbf{Z}_{dd_2}\mathbf{I}_{d_{2,n}} + \mathbf{Z}_{dq_{2,n}}\mathbf{I}_{q_{2,n}} + j\left(\mathbf{Z}_{qd_2}\mathbf{I}_{d_{2,n}} + \mathbf{Z}_{qq_2}\mathbf{I}_{q_{2,n}}\right)\right)e^{-j\left(\boldsymbol{\delta}_n - \frac{\pi}{2}\right)} \\ & + \frac{1}{2}\left(\mathbf{E}_{hd_{2,n-1}} - j\mathbf{E}_{hq_{2,n-1}}\right)e^{-j\left(\boldsymbol{\delta}_n - \frac{\pi}{2}\right)}\end{aligned} \tag{2.318}$$

To have 3pPD model of SM in symmetrical components, equation (2.299) needs to be rewritten as:

$$\mathbf{V}_{p_{1,n}} = -\mathbf{Z}_{p_{1,n}}\mathbf{I}_{p_{1,n}} + \mathbf{V}_{hp_{1,n-1}} \tag{2.319}$$

and equation (2.318) needs to be rewritten as:

$$\mathbf{V}_{n_{1,n}} = -\mathbf{Z}_{n_{1,n}}\mathbf{I}_{n_{1,n}} + \mathbf{V}_{hn_{1,n}} \tag{2.320}$$

The equivalent impedance and history term of (2.319) and (2.320) are defined as below. The equivalent impedance is:

$$\mathbf{Z}_{p_{1,n}} = \frac{\mathbf{Z}_{dd_0} + \mathbf{Z}_{qq_0} + j\left(\mathbf{Z}_{dq_{0,n}} + \mathbf{Z}_{qd_{0,n}}\right)}{2} \tag{2.321}$$

$$\mathbf{Z}_{n_{1,n}} = \frac{\mathbf{Z}_{dd_2} + \mathbf{Z}_{qq_2} - j\left(\mathbf{Z}_{dq_{2,n}} + \mathbf{Z}_{qd_{2,n}}\right)}{2} \tag{2.322}$$

and history term is:

$$\begin{aligned}\mathbf{V}_{hp_{1,n-1}} = &-\frac{\mathbf{Z}_{dd_0} - \mathbf{Z}_{qq_0} - j\left(\mathbf{Z}_{dq_{0,n}} - \mathbf{Z}_{qd_{0,n}}\right)}{2}\left(\mathbf{I}_{d_{0,n}} - j\mathbf{I}_{q_{0,n}}\right)e^{j\left(\boldsymbol{\delta}_n - \frac{\pi}{2}\right)} \\ &+\left(\mathbf{E}_{hd_{0,n-1}} + j\mathbf{E}_{hq_{0,n-1}}\right)e^{j\left(\boldsymbol{\delta}_n - \frac{\pi}{2}\right)}\end{aligned} \tag{2.323}$$

$$\begin{aligned}\mathbf{V}_{hn_{1,n-1}} = &-\frac{\mathbf{Z}_{dd_2} - \mathbf{Z}_{qq_2} + j\left(\mathbf{Z}_{dq_{2,n}} - \mathbf{Z}_{qd_{2,n}}\right)}{2}\left(\mathbf{I}_{d_{2,n}} + j\mathbf{I}_{q_{2,n}}\right)e^{-j\left(\boldsymbol{\delta}_n - \frac{\pi}{2}\right)} \\ &+\left(\mathbf{E}_{hd_{2,n-1}} - j\mathbf{E}_{hq_{2,n-1}}\right)e^{-j\left(\boldsymbol{\delta}_n - \frac{\pi}{2}\right)}\end{aligned} \tag{2.324}$$

The history term depends on both present and prior states. To obtain the proper SM equivalent, an iterative solver is required.

Since the first Fourier coefficient in a traditional phasor has no derivative equations, no numerical approach is required to discretize it. The voltage on 0-axis, given in (2.257), is discretized as follows:

$$\mathbf{V}_{0_{1,n}} = -\mathbf{Z}_{00_1}\mathbf{I}_{0_{1,n}} \tag{2.325}$$

where $\mathbf{Z}_{00_1}$ is given by:

$$\mathbf{Z}_{00_1} = j\left(X_l + 3X_n\right) + R_a + 3R_n \tag{2.326}$$

The mechanical angular speed, given in (2.266), is discretized as follows:

$$\boldsymbol{\Omega}_{m_{0,n}} = \frac{\mathbf{T}_{m_{0,n}} - \left(\boldsymbol{\psi}_{d_{0,n}}\mathbf{I}_{q_{0,n}} - \boldsymbol{\psi}_{q_{0,n}}\mathbf{I}_{d_{0,n}}\right)}{\frac{4H}{\omega_s \Delta t} + K_D} + \boldsymbol{\Omega}_{hm_{0,n}} \tag{2.327}$$

where the history term is:

$$\begin{aligned}\boldsymbol{\Omega}_{hm_{0,n-1}} = &\frac{\mathbf{T}_{m_{0,n-1}} - \left(\boldsymbol{\psi}_{d_{0,n-1}}\mathbf{I}_{q_{0,n-1}} - \boldsymbol{\psi}_{q_{0,n-1}}\mathbf{I}_{d_{0,n-1}}\right) + \left(\frac{4H}{\omega_s \Delta t} - K_D\right)\boldsymbol{\Omega}_{m_{0,n-1}} + 2K_D\omega_s}{\frac{4H}{\omega_s \Delta t} + K_D} \\ &- \frac{\left(\boldsymbol{\psi}_{d_{2,n-1}}\mathbf{I}_{q_{2,n-1}}{}^{*} - \boldsymbol{\psi}_{q_{2,n-1}}\mathbf{I}_{d_{2,n-1}}{}^{*}\right) + \left(\boldsymbol{\psi}_{d_{2,n-1}}{}^{*}\mathbf{I}_{q_{2,n-1}} - \boldsymbol{\psi}_{q_{2,n-1}}{}^{*}\mathbf{I}_{d_{2,n-1}}\right)}{\frac{4H}{\omega_s \Delta t} + K_D}\end{aligned} \tag{2.328}$$

The second Fourier coefficient of mechanical angular speed, given in (2.267), is discretized as follows:

$$\boldsymbol{\Omega}_{m_{2,n}} = -\frac{\boldsymbol{\psi}_{d_{2,n}}\mathbf{I}_{q_{0,n}} - \boldsymbol{\psi}_{q_{2,n}}\mathbf{I}_{d_{0,n}} + \boldsymbol{\psi}_{d_{0,n}}\mathbf{I}_{q_{2,n}} - \boldsymbol{\psi}_{q_{0,n}}\mathbf{I}_{d_{2,n}}}{j4H + K_D} \tag{2.329}$$

The rotor angle used in equation (2.168) is a time domain variable, therefore it is calculated for the zero Fourier coefficient. The rotor angle, given in (2.268), is discretized as follows:

$$\boldsymbol{\delta}_{0,n} = \frac{P\Delta t}{4}\boldsymbol{\Omega}_{m_{0,n}} + \boldsymbol{\delta}_{h_{0,n-1}} \tag{2.330}$$

where the history term is:

$$\boldsymbol{\delta}_{h_{n-1}} = \boldsymbol{\delta}_{n-1} + \frac{P\Delta t}{4}\left(\boldsymbol{\Omega}_{m_{0,n-1}} - 2\omega_s\right) \tag{2.331}$$

2.3.2 Norton equivalent circuit of SM

The 3pPD model of SM by symmetrical components is expressed as follows using equations (2.319), (2.320), and (2.325):

$$\mathbf{V}_{pnz_{1,n}} = -\mathbf{Z}_{pnz_{1,n}}\mathbf{I}_{pnz_n} + \mathbf{E}_{hpnz_{1,n}} \tag{2.332}$$

where the $\mathbf{Z}_{pnz_{1,n}}$ matrix is the SM equivalent impedance by symmetrical components. It should be noted that the *dq0* impedance is not constant and is a function of rotor speed.

$$\mathbf{Z}_{pnz_{1,n}} = \begin{bmatrix} \mathbf{Z}_{p_{1,n}} & 0 & 0 \\ 0 & \mathbf{Z}_{n_{1,n}} & 0 \\ 0 & 0 & \mathbf{Z}_{z_{1,n}} \end{bmatrix} \tag{2.333}$$

and $\mathbf{E}_{hpnz_{1,n-1}}$, vector of history term, is:

$$\mathbf{E}_{hdq0_{n-1}} = \begin{bmatrix} \mathbf{E}_{hp_{1,n-1}} & \mathbf{E}_{hn_{1,n-1}} & \mathbf{E}_{hz_{1,n-1}} \end{bmatrix}^T \tag{2.334}$$

To add the equivalent SM model to the MANA matrix, the symmetrical components model expressed in (2.332) needs to the transform to the *abc* frame.

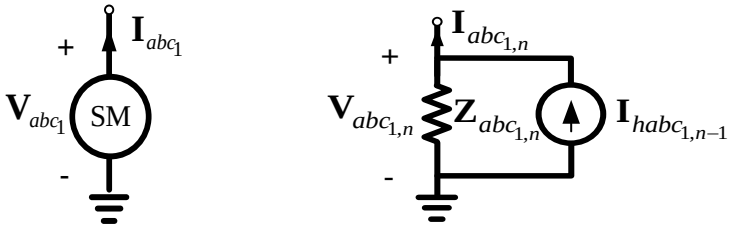

a) b)

Figure 2.10 a) Three phase phasor domain SM, b) Equivalent circuit, 3pPD model

Figure 2.10 shows the 3pPD Norton equivalent circuit by Trapezoidal rule. The equivalent impedance and history terms in the *abc* frame shown in Figure 2.10 are computed as follows:

$$\mathbf{Z}_{abc_{1,n}} = \mathbf{A}^{-1}\mathbf{Z}_{pnz_{1,n}}\mathbf{A} \tag{2.335}$$

$$\mathbf{I}_{habc_{1,n}} = \mathbf{A}^{-1}\mathbf{Z}^{-1}_{pnz_{1,n}}\mathbf{E}_{hpnz_{1,n-1}} \tag{2.336}$$

The equivalent impedance of a linear component, such as an inductor or a capacitor, is constant, and the history term calculated using the Trapezoidal method is dependent on the component's voltage and current in the last time step. The equivalent impedance of SM, on the other hand, is not constant, and the history term is affected by present and prior states.

2.3.3 Simulation steps

The following are the steps in a 3pPD simulation approach:

1. Calculate the three phase Load-flow: to simulate unbalanced network from initial state, a three-phase load flow is used
2. Initialization
    a. Convert the loads to constant impedances
    b. Calculate the equivalent circuit of elements by discretized method
    c. Build the MANA matrix (equation (1.8)) of the network (exclude the SMs)
    d. Calculate the history terms for the first time-step based on the load flow results
3. Dynamic simulation
    a. Calculate the equivalent impedance and the injection current using (2.335) and (2.336) for all SMs
    b. Add the equivalent impedance of SMs to the admittance submatrix of MANA, add the injection current of SMs to the $\mathbf{B}_{1,n}$ vector, and solve $\mathbf{A}_{1,n}\mathbf{X}_{1,n} = \mathbf{B}_{1,n}$
    c. Update the *dq*0-axes currents (equations (2.319), (2.320), and (2.325)), rotor speed (equation (2.327)), and rotor angle (equation (2.330)) for all SMs
    d. If the angular speed relative error of all SMs is less than the allowed error for two consecutive iterations, the solution is converged, and can proceed to step 3.e. If not, the solution has not converged, and the next iteration should begin at step 3.a.
    e. Calculate the controllers' model of zero Fourier coefficient for the next time step

f. Predict the SM quantities of rotor speed, rotor angle, *d*- and *q*- axes currents of zero and second Fourier coefficients, then proceed to step 3.a for the next time step

The prediction of variables in step 3.f reduces the number of iterations. Equation (2.163) represents the prediction relationship. In step 3.d, the relationship of relative error is given as (2.164).

2.4 Phasor domain model of synchronous machine (traditional)

The traditional PD method only considers the power system's positive sequence, ignoring the negative and zero symmetric components. As a result, the PD approach models electromechanical transients under balanced conditions. On the *d*- and *q*-axes, the zero Fourier coefficient is used to describe the electromechanical transient. The second Fourier coefficient does not exist in the SM model since the negative component is not modelled in the system. Also, the *0*-frame does not exist in the SM model because the zero symmetrical component is not modelled in the system.

Moreover, the traditional PD method neglects the transients of rotor on the stator ($\frac{d\mathbf{\Psi}_{d_0}}{dt} = 0$ and $\frac{d\mathbf{\Psi}_{q_0}}{dt} = 0$). The equations of the PD method are summarized as bellow.

$$\mathbf{V}_{d_0} = \frac{\mathbf{\Omega}_{r_0}}{\omega_s}\left(X_q^{"}\mathbf{I}_{q_0} + \mathbf{E}_{d_0}^{"} \right) - R_a\mathbf{I}_{d_0} \tag{2.337}$$

$$\mathbf{V}_{q_0} = -\frac{\mathbf{\Omega}_{r_0}}{\omega_s}\left(X_d^{"}\mathbf{I}_{d_0} - \mathbf{E}_{q_0}^{"} \right) - R_a\mathbf{I}_{q_0} \tag{2.338}$$

The zero Fourier coefficient of the transient and the sub-transient emf equations are the same as expressed in (2.258), (2.260), (2.262), and (2.264) at section 2.2.

The zero Fourier coefficient of the mechanical angular speed is obtained by calculating the zero Fourier coefficients from equation (2.107).

$$\frac{2H}{\omega_s}\frac{d\mathbf{\Omega}_{m_0}}{dt} = \mathbf{T}_{m_0} - \left(\mathbf{\Psi}_{d_0}\mathbf{I}_{q_0} - \mathbf{\Psi}_{q_0}\mathbf{I}_{d_0} \right) - K_D\left(\mathbf{\Omega}_{m_0} - \omega_s \right) \tag{2.339}$$

The rotor angle PD relation is the same as the equation given in (2.268). Calculating the zero Fourier coefficients from equations (2.105) and (2.106), respectively, yields the PD relation of the *d*- and *q*-axes flux.

$$\mathbf{\Psi}_{d_0} = -X_d^{''}\mathbf{I}_{d_0} + \mathbf{E}_{q_0}^{''} \tag{2.340}$$

$$\mathbf{\Psi}_{q_0} = -X_q^{''}\mathbf{I}_{q_0} - \mathbf{E}_{d_0}^{''} \tag{2.341}$$

2.4.1 Discretized equations

The discretized equations of the PD model of synchronous machine employing the Trapezoidal rule are provided in this section.

The equations (2.279), (2.280), (2.285), and (2.286) can be used for discretized PD model of zero Fourier coefficient of the transient and the sub-transient emfs.

Equation (2.337), the zero Fourier coefficient of *d*-axis voltage, is discretized as follows:

$$\begin{aligned}
\mathbf{V}_{d_{0,n}} &= -\left(R_s + \frac{2X_d^{''}}{\omega_s \Delta t}\right)\mathbf{I}_{d_{0,n}} + \frac{2}{\omega_s \Delta t}\mathbf{E}_{q_{0,n}}^{''} + \mathbf{V}_{hd_{0,n-1}} \\
\mathbf{V}_{d_0} &= \frac{\mathbf{\Omega}_{r_0}}{\omega_s}\left(X_q^{''}\mathbf{I}_{q_0} + \mathbf{E}_{d_0}^{''}\right) - R_a\mathbf{I}_{d_0}
\end{aligned} \tag{2.342}$$

where the history term is:

$$\mathbf{V}_{hd_{0,n-1}} = -\left(R_s - \frac{2X_d^{''}}{\omega_s \Delta t}\right)\mathbf{I}_{d_{0,n-1}} - \frac{2}{\omega_s \Delta t}\mathbf{E}_{q_{0,n-1}}^{''} - \mathbf{V}_{d_{0,n-1}} \tag{2.343}$$

To derive the zero Fourier coefficient of the voltage on the *d*-axis depending on the input current, the equation (2.280) is replaced in equation (2.342), yielding the following result:

$$\mathbf{V}_{d_{0,n}} = -\mathbf{Z}_{dd_0}\mathbf{I}_{d_{0,n}} + \mathbf{Z}_{dq_{0,n}}\mathbf{I}_{q_{0,n}} + \mathbf{E}_{hd_{0,n}} \tag{2.344}$$

where $\mathbf{Z}_{dd_0}$ is given by:

$$\mathbf{Z}_{dd_0} = R_s \tag{2.345}$$

and $\mathbf{Z}_{dq_0}$ is given by:

$$\mathbf{Z}_{dq_0} = \frac{\mathbf{\Omega}_{r_0}}{\omega_s} X_q^{"} \tag{2.346}$$

The total history term in equation (2.344) is:

$$\mathbf{E}_{hd_{0,n-1}} = \frac{\mathbf{\Omega}_{r_{0,n}}}{\omega_s} \mathbf{E}_{d_{0,n}}^{"} \tag{2.347}$$

The zero Fourier coefficient of *q*-axis voltage, given in (2.338), is discretized as follows:

$$\mathbf{V}_{q_{0,n}} = -\left(R_s + \frac{2X_q^{"}}{\omega_s \Delta t} \right) \mathbf{I}_{q_{0,n}} - \frac{2}{\omega_s \Delta t} \mathbf{E}_{d_{0,n}}^{"} + \mathbf{V}_{hq_{0,n-1}} \tag{2.348}$$

where the history term is:

$$\mathbf{V}_{hq_{0,n-1}} = -\left(R_s - \frac{2X_q^{"}}{\omega_s \Delta t} \right) \mathbf{I}_{q_{0,n-1}} + \frac{2}{\omega_s \Delta t} \mathbf{E}_{d_{0,n-1}}^{"} - \mathbf{V}_{q_{0,n-1}} \tag{2.349}$$

To derive the zero Fourier coefficient of the voltage on the *q*-axis depending on the input current, the (2.286) is replaced in (2.348), yielding the following result:

$$\mathbf{V}_{q_{0,n}} = -\mathbf{Z}_{qq_0} \mathbf{I}_{q_{0,n}} - \mathbf{Z}_{qd_0} \mathbf{I}_{d_{0,n}} + \mathbf{E}_{hq_{0,n}} \tag{2.350}$$

where $\mathbf{Z}_{qq_0}$ is given by:

$$\mathbf{Z}_{qq_0} = R_s \tag{2.351}$$

and $\mathbf{Z}_{qd_0}$ is given by:

$$\mathbf{Z}_{qd_{0,n}} = \frac{\mathbf{\Omega}_{r_{0,n}}}{\omega_s} X_d^{"} \tag{2.352}$$

The total history term of *q*-axis voltage in (2.350) is:

$$\mathbf{E}_{hq_{0,n-1}} = \frac{\mathbf{\Omega}_{r_{0,n}}}{\omega_s} \mathbf{E}_{q_{0,n}}^{"} \tag{2.353}$$

The first Fourier coefficient of the positive sequence voltage according to (2.185) is obtained by combining (2.344) and (2.350):

$$\begin{aligned}\mathbf{V}_{p_{1,n}} &= \frac{1}{2}\left(-R_s\left(\mathbf{I}_{d_{0,n}} + j\mathbf{I}_{q_{0,n}}\right) + j\frac{\boldsymbol{\Omega}_{r_{0,n}}}{\omega_s}\left(X_q^{"}\mathbf{I}_{d_{0,n}} + jX_q^{"}\mathbf{I}_{q_{0,n}}\right)\right)e^{j\left(\boldsymbol{\delta}_n-\frac{\pi}{2}\right)} \\ &+ \frac{1}{2}\frac{\boldsymbol{\Omega}_{r_{0,n}}}{\omega_s}\left(\mathbf{E}_{d_{0,n}}^{"} + j\mathbf{E}_{q_{0,n}}^{"}\right)e^{j\left(\boldsymbol{\delta}_n-\frac{\pi}{2}\right)}\end{aligned} \tag{2.354}$$

The solver needs to have a voltage-current function of positive sequence fundamental frequency for (2.354):

$$\mathbf{V}_{p_{1,n}} = -\mathbf{Z}_{p_{1,n}}\mathbf{I}_{p_{1,n}} + \mathbf{V}_{hp_{1,n-1}} \tag{2.355}$$

The equivalent impedance and history term of (2.355) are defined as below. The equivalent impedance is:

$$\mathbf{Z}_{p_{1,n}} = \frac{\mathbf{Z}_{dd_0} + \mathbf{Z}_{qq_0} + j\left(\mathbf{Z}_{dq_{0,n}} + \mathbf{Z}_{qd_{0,n}}\right)}{2} = R_s + j\frac{\boldsymbol{\Omega}_{r_{0,n}}}{\omega_s}\frac{X_d^{"} + X_q^{"}}{2} \tag{2.356}$$

and the history term is:

$$\begin{aligned}\mathbf{V}_{hp_{1,n-1}} &= \frac{1}{2}\left(-\frac{\mathbf{Z}_{dd_0} - \mathbf{Z}_{qq_0}}{2}\left(\mathbf{I}_{d_{0,n}} - j\mathbf{I}_{q_{0,n}}\right) + \mathbf{E}_{hd_{0,n-1}} + j\mathbf{E}_{hq_{0,n-1}}\right)e^{j\left(\boldsymbol{\delta}_n-\frac{\pi}{2}\right)} \\ &= \frac{1}{2}\frac{\boldsymbol{\Omega}_{r_{0,n}}}{\omega_s}\left(-\frac{X_d^{"} - X_q^{"}}{2}\left(\mathbf{I}_{d_{0,n}} - j\mathbf{I}_{q_{0,n}}\right) + \mathbf{E}_{d_{0,n}}^{"} + j\mathbf{E}_{d_{0,n}}^{"}\right)e^{j\left(\boldsymbol{\delta}_n-\frac{\pi}{2}\right)}\end{aligned} \tag{2.357}$$

The history term depends on not only the quantities in the previous time step, but also the quantities in the current time step. Therefore, an iterative solve is required to solve the model.

The mechanical angular speed, given in (2.339), is discretized as follows:

$$\boldsymbol{\Omega}_{m_{0,n}} = \frac{\mathbf{T}_{m_{0,n}} - \left(\boldsymbol{\psi}_{d_{0,n}}\mathbf{I}_{q_{0,n}} - \boldsymbol{\psi}_{q_{0,n}}\mathbf{I}_{d_{0,n}}\right)}{\frac{4H}{\omega_s\Delta t} + K_D} + \boldsymbol{\Omega}_{hm_{0,n}} \tag{2.358}$$

where the history term is:

$$\boldsymbol{\Omega}_{hm_{0,n-1}} = \frac{\mathbf{T}_{m_{0,n-1}} - \left(\boldsymbol{\psi}_{d_{0,n-1}}\mathbf{I}_{q_{0,n-1}} - \boldsymbol{\psi}_{q_{0,n-1}}\mathbf{I}_{d_{0,n-1}}\right) + \left(\frac{4H}{\omega_s \Delta t} - K_D\right)\boldsymbol{\Omega}_{m_{0,n-1}} + 2K_D\omega_s}{\frac{4H}{\omega_s \Delta t} + K_D} \tag{2.359}$$

The rotor angle, given in (2.268), is discretized as follows:

$$\boldsymbol{\delta}_n = \frac{P\Delta t}{4}\boldsymbol{\Omega}_{m_{0,n}} + \boldsymbol{\delta}_{h_n} \tag{2.360}$$

where the history term is:

$$\boldsymbol{\delta}_{h_n} = \boldsymbol{\delta}_{n-1} + \frac{P\Delta t}{4}\left(\boldsymbol{\Omega}_{m_{0,n-1}} - 2\omega_s\right) \tag{2.361}$$

2.4.2 Norton equivalent circuit of SM for phasor-domain solution

The traditional PD method uses the positive sequence representation of the system. To add the equivalent SM model to the Nodal matrix, the equation (2.355) is used.

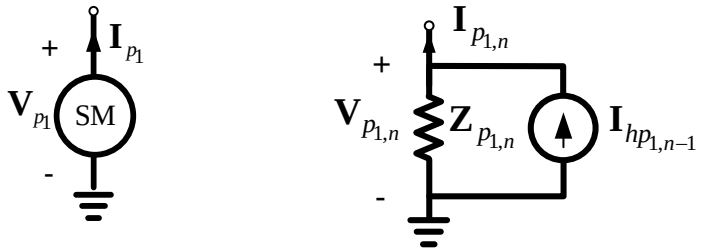

a) b)

Figure 2.11 a) Synchronous machine, b) SM Equivalent circuit in phasor-domain

In Figure 2.11 the injected current is:

$$\mathbf{I}_{hp_{1,n-1}} = \frac{\mathbf{V}_{hp_{1,n-1}}}{\mathbf{Z}_{p_{1,n}}} \tag{2.362}$$

The history term of SM model is a function of state of the network at current state of the network. Thus, an iterative method is needed to solve a system of equations that includes SM models.

2.4.3 Simulation steps

The following are the steps in a PD simulation approach:

1. Calculate the positive sequence load-flow: the PD method present the positive sequence of the system, therefore, the load-flow ignores the negative and the zero sequences
2. Initialization
    a. Convert the loads to constant impedances
    b. Build the impedance matrix of the system. The equivalent impedance of the machine is assumed to be constant in traditional PD method; therefore, unlike TD, DP, and 3pPD, the equivalent impedance of the SMs is added in this step
3. Dynamic simulation
    a. Calculate the injected current of SMs using equation (2.362)
    b. Add the injected currents to vector **i** of the nodal analysis, and solve **Yv = i** equation (1.7)
    c. Update the *dq*-axes currents (equations (2.344) and (2.350)), rotor speed (equation (2.358)), and rotor angle (equation (2.360)) for all SMs
    d. If the angular speed relative error of all SMs be less than the allowed error for two consecutive iterations, the solution is converged, and can proceed to step 3.e. If not, the solution has not converged, and the next iteration should begin at step 3.a.
    e. Calculate the controllers' model of zero Fourier coefficient for the next time step
    f. Predict the SM quantities of rotor speed, rotor angle, *d*- and *q*- axes currents and go step 3.a for the next time-point

The prediction of variables in step 3.f reduces the number of iterations. Equation (2.163) represents the prediction relationship. In step 3.d, the relationship of relative error is given as (2.164)

2.5 Comparison of methods: TD, DP, 3pPD and PD

The test system used in this section is referred to as 118-GMD. The system voltage level is 345/138 kV at transmission, and 25 kV at distribution level. The total number of power transformers is 173, the saturation of transformers is excluded in this study. The model further embeds 20 power plants with a total installed capacity of 3800 MW and 91 electric loads. There are 177 transmission lines with a total length of 10063 km. The models of synchronous machines (SMs) include mechanical and electrical dynamics, turbine-governor, control system with automatic voltage regulator (AVR), power system stabilizer (PSS).

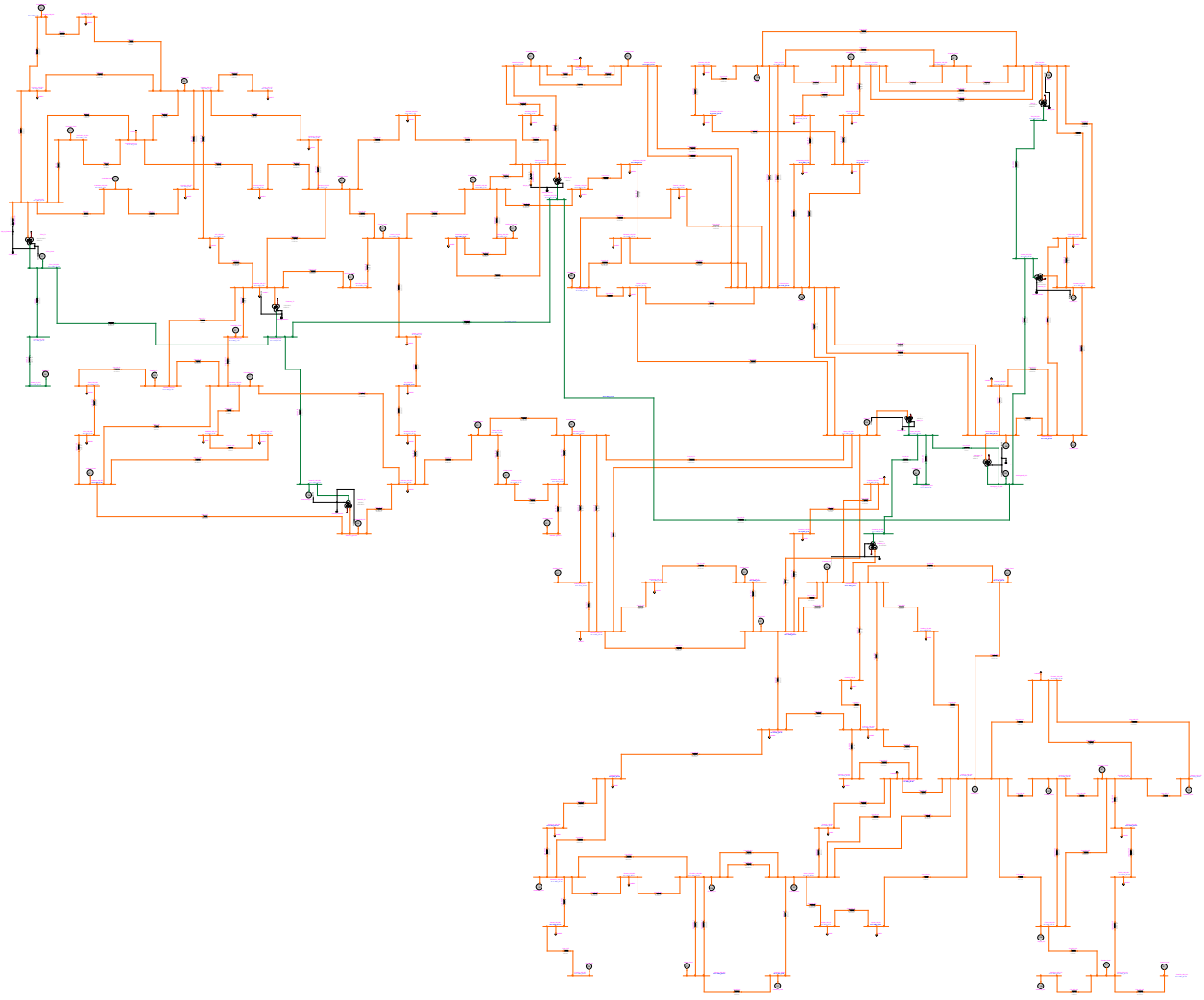

Figure 2.12 IEEE-118 benchmark

The same numerical integration procedures are utilised to make comparisons on the same premise. To discretize derivative equations, the Trapezoidal and backward-Euler numerical integration methods are used. The primary numerical solution is the Trapezoidal integration technique, with two halved time-steps of backward-Euler integration employed to reduce numerical oscillations after a discontinuity. To ensure a consistent computational environment for comparison, all techniques are coded in MATLAB. The developed TD technique is validated using EMTP. Since the traditional PD method does not simulate unbalanced events, a three-phase fault is applied to the study system and the simulation results obtained from different methods are compared. The fault occurs on Bus TwinBrch_138_012 at 0.1 second and is removed after 100ms. The simulation is performed for one second. The output waveform of DP, 3pPD, and PD approaches are in phasor-domain. At the end of the simulation, the phasor results are converted to TD independently.

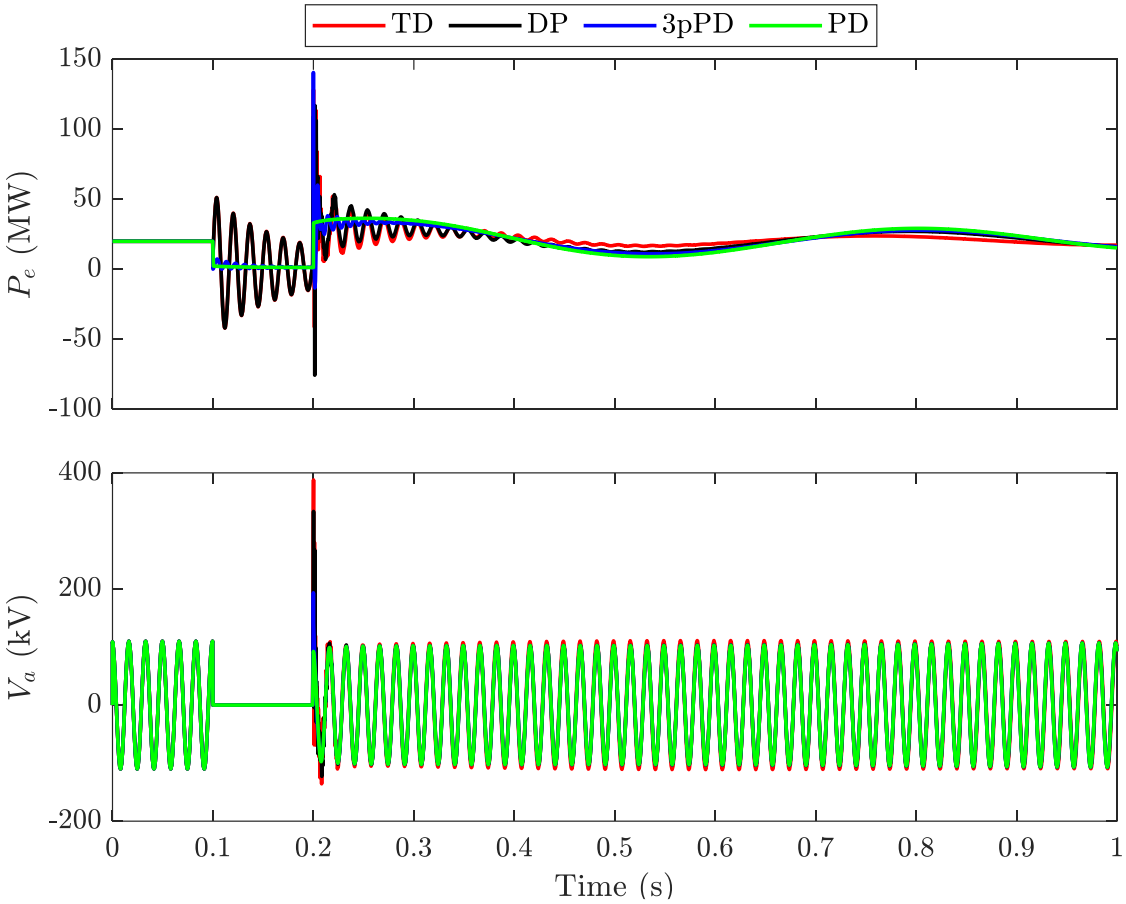

Figure 2.13 Electrical power and bus voltage waveforms, $\Delta t = 10\mu s$

The electrical power and bus voltage waveforms of the machine of the simulating techniques using $\Delta t = 10\mu s$ are shown in Figure 2.13. The results are comparable in the steady state, while there is considerable inconstancy during transient dynamics.

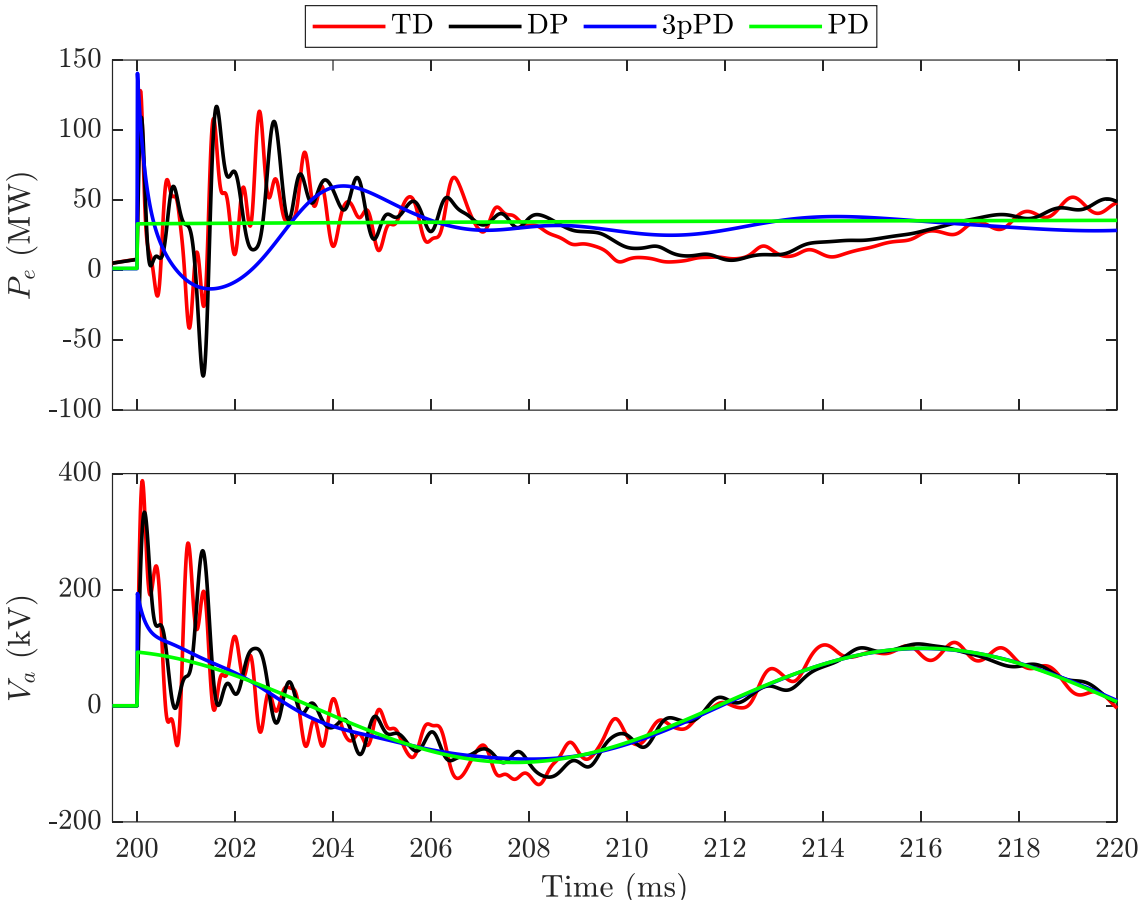

Figure 2.14 Electrical power and bus voltage waveforms, $\Delta t = 10\mu s$ (zoom)

The simulation results during the transient evolution using $\Delta t = 10\mu s$ are shown in

Figure 2.14. This section provides a visual examination; and, section 2.5.1 offers an analytical study to compare the results. The 3pPD performs better than the PD in presenting electrical power transients, even though both the 3pPD and the PD do not replicate fast transients. Furthermore, the DP technique does not produce the same outcomes as the TD method.

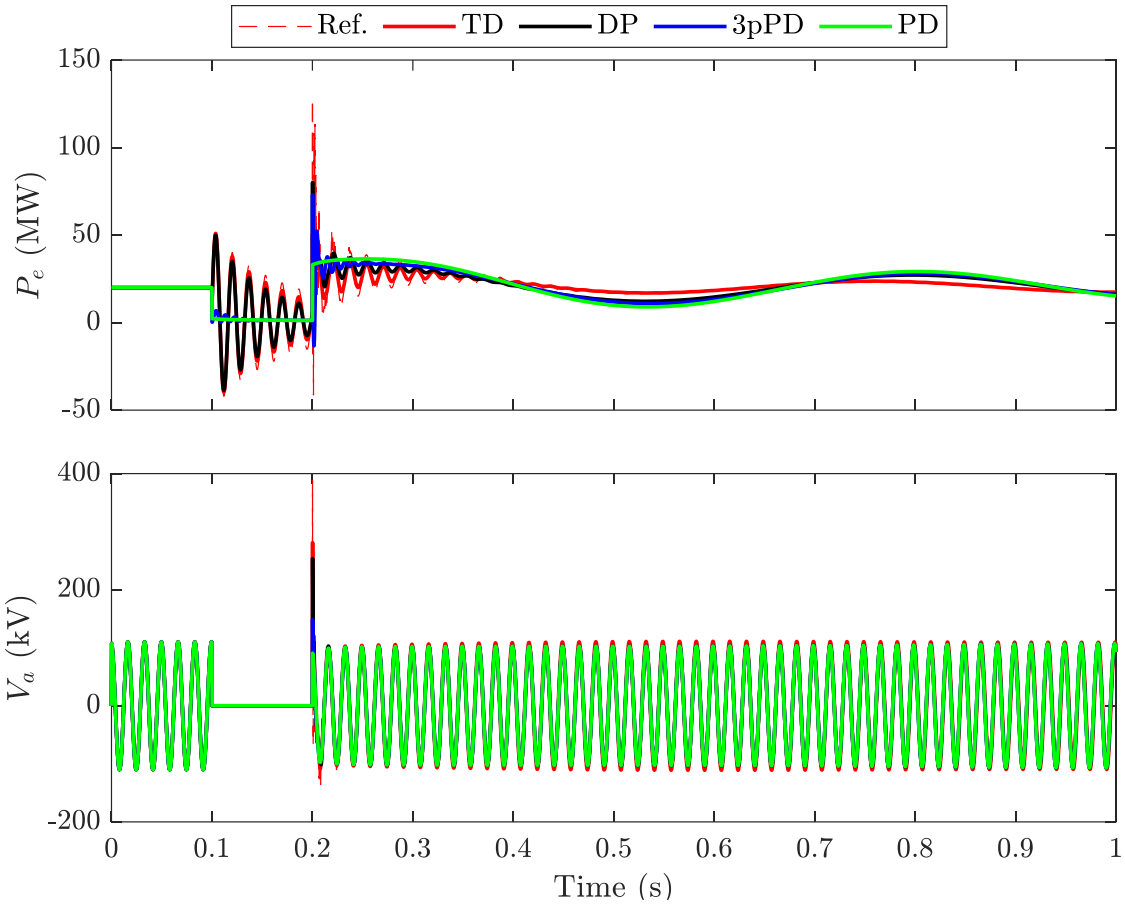

Figure 2.15 Electrical power and bus voltage waveform, $\Delta t = 500\mu s$

The electrical power and bus voltage waveforms of the machine are simulated with a larger time step of $\Delta t = 500\mu s$, and the results, as well as the reference, are shown in Figure 2.15. The result of TD with $\Delta t = 10\mu s$ is the reference. After damming the fast transient, the results are similar. It demonstrates that increasing the time step has no significant impact on the electromechanical transient.

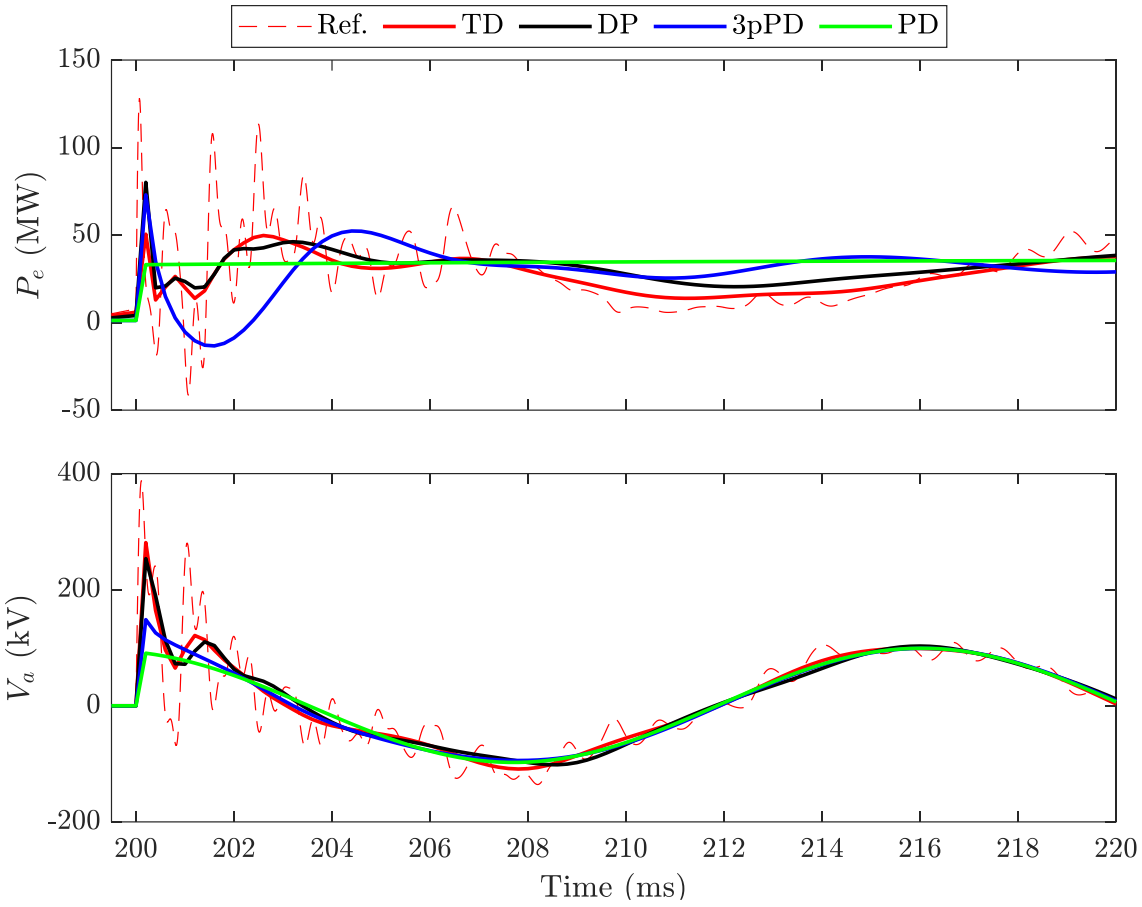

Figure 2.16 Electrical power and bus voltage waveform, $\Delta t = 500\mu s$ (zoom)

The simulation results during the transient evolution using $\Delta t = 500\mu s$ are shown in Figure 2.16. Even using large time steps, the 3pPD outperforms the PD in terms of displaying electrical power transients; and, the accuracy of both the TD and the DP diminishes, and the DP does not outperform the TD.

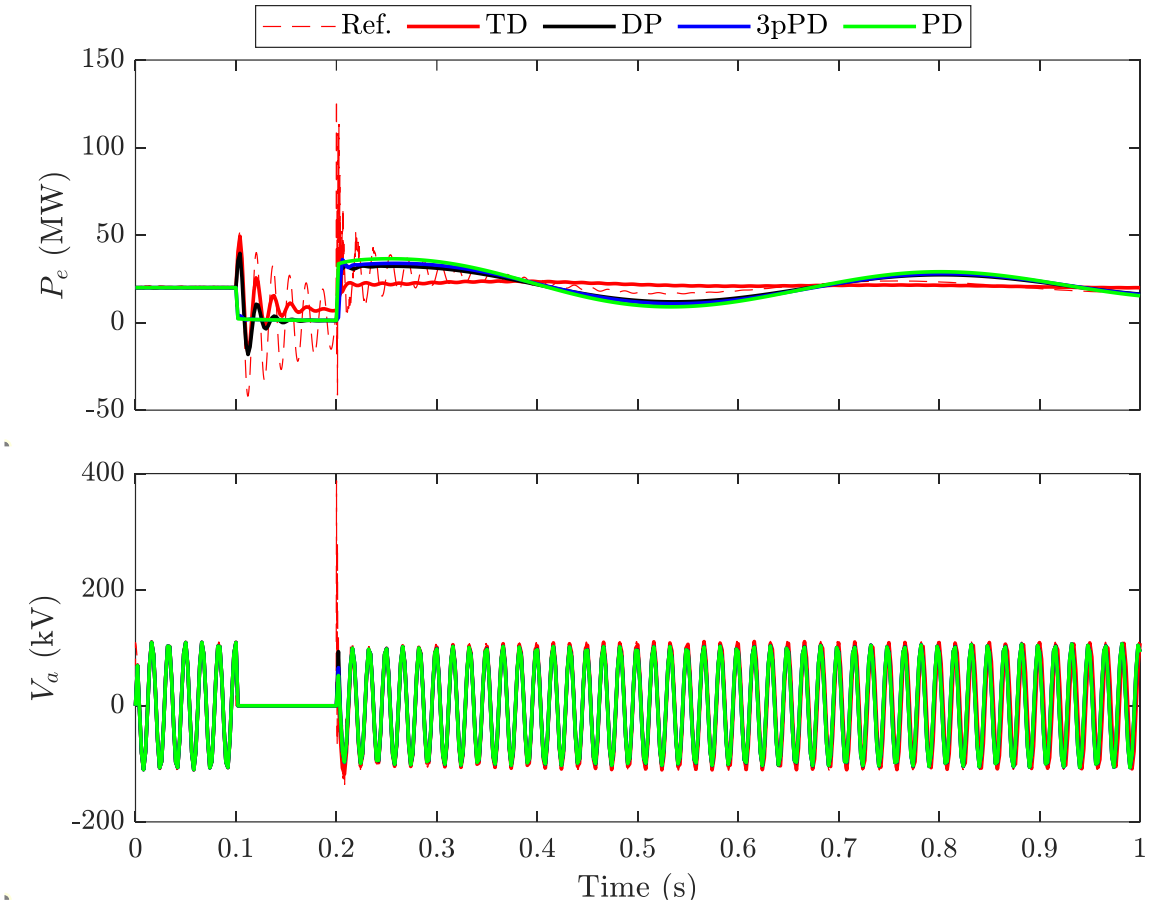

Figure 2.17 Electrical power and bus voltage waveform, $\Delta t = 2\text{ms}$

The electrical power and bus voltage waveforms of the machine are simulated with a very large time step of $\Delta t = 2\text{ms}$, and the results, as well as the reference, are shown in Figure 2.17. The result of TD with $\Delta t = 10\mu\text{s}$ is the reference. The result accuracy of the approaches, particularly the TD, falls when a very large time step is used.

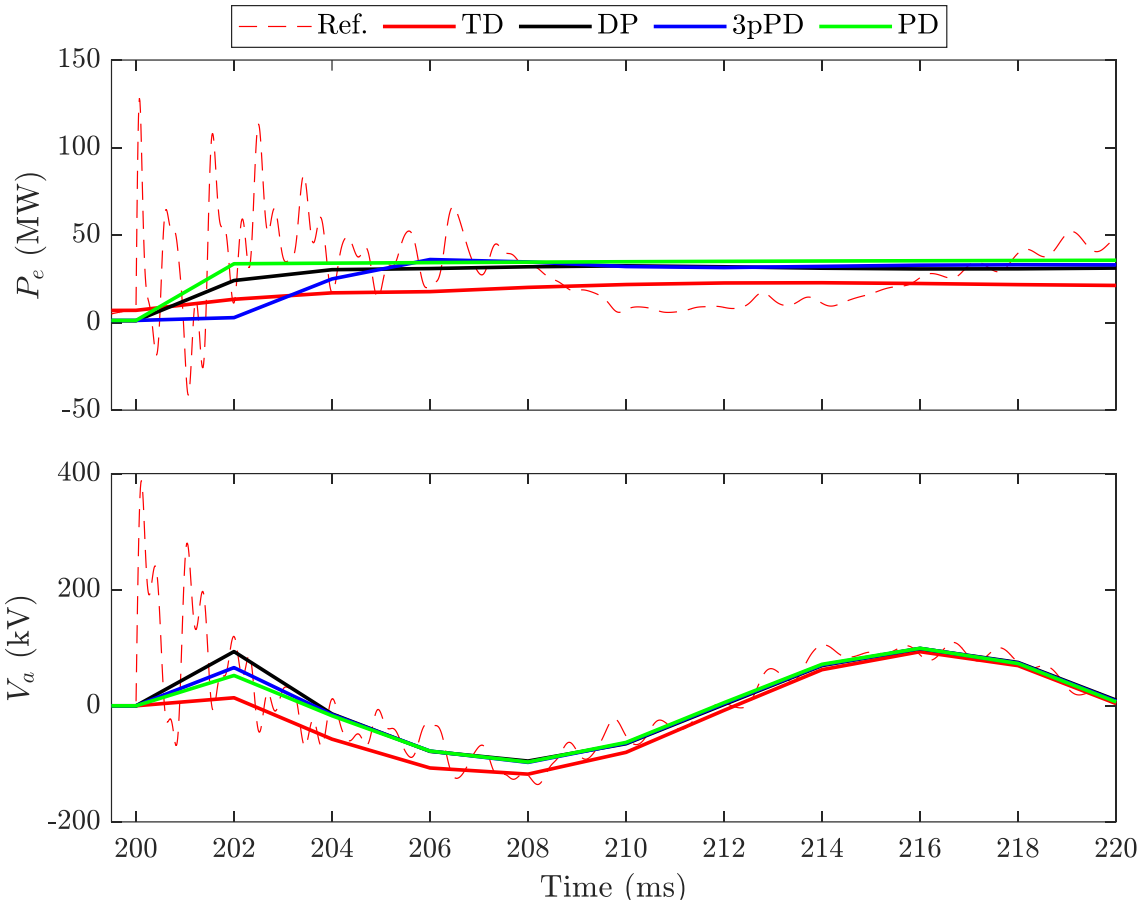

Figure 2.18 Electrical power and bus voltage waveform, $\Delta t = 2\text{ms}$ (zoom)

The simulation results during the transient evolution using $\Delta t = 2\text{ms}$ are shown in Figure 2.18. The accuracy of techniques for modelling transient evolution drops considerably when a very large time step is applied, and the results become extremely similar.

2.5.1 Accuracy evaluation

Although the presented waveforms in Section 2.5 determine the differences between the solution approaches, in this section the error of methods are measured. The percentage of 2-norm relative error [39] is employed to compare the results:

$$\varepsilon = \sqrt{\frac{\sum_{i=1}^{N}\left(x_i - \tilde{x}_i\right)^2}{\sum_{i=1}^{N}\left(x_i\right)^2}} \times 100 \tag{2.363}$$

where x_i is the reference result which is the TD response with $\Delta t = 10\mu s$. $\tilde{x}_i$ is the result from the evaluated.

To compare phasor domain results with the reference, the results of DP, 3pPD, and PD are converted to time domain. In this section, the simulations are performed using different numerical integration time-steps to evaluate accuracy as a function of time-step.

Table 2.1 Error % of electrical power/voltage

$\Delta t\ (\mu s)$	TD	DP	3pPD	PD
10	-	2.78/1.95	3.85/3.17	4.92/3.45
100	1.10/0.17	2.84/2.23	4.01/3.22	4.97/3.53
200	2.03/0.23	2.90/2.36	4.13/3.26	4.93/3.55
500	3.20/0.77	2.86/2.54	4.13/3.56	4.91/3.87
1000	2.57/1.97	2.60/3.54	3.78/4.44	4.86/4.85
2000	3.05/6.55	2.64/6.15	3.48/7.58	4.77/8.4
5000	6.39/24.53	2.71/27.75	4.04/28.65	4.38/28.08

Table 2.1 illustrates electrical power and bus voltage errors as a function of simulation time-step. The relative error is computed at a time frame of 200 to 250 ms. The DP approach is more successful when the time-step is significantly increased, but it is less accurate in the interval where the transient is concentrated.

2.5.2 Computing time

This section compares the time efficiency of TD, DP, 3pPD, and PD methods on the given benchmark. The DP, 3pPD, and PD methods use phasor for calculating the simulation. To compare computing time, only the time of dynamic simulation is calculated, in other word the time of load flow, initialization, and the result converting time of phasor domain methods is not considered. The Table 2.2 and

Table 2.3 show the computation time of event at Section 2.5 using different time steps for the implemented methods.

The TD approach is 5.58 times quicker than the DP technique in the non-iterative solution and 2.31 times quicker than the 3pPD approach. In addition, the TD approach simulates 0.7 times slower than the PD approach.

Table 2.2 Computing times for non-iterative solution

Δt (**μs**)	**TD** (**s**)	**DP** (**s**)	**3pPD** (**s**)	**PD** (**s**)
10	286.00	1611.17	674.19	199.70
100	28.27	162.03	66.47	20.08
200	14.49	81.34	33.56	10.19
500	5.85	32.45	13.53	4.19
1000	2.89	16.50	6.75	2.07
2000	1.45	8.28	3.39	1.02
5000	0.64	3.28	1.37	0.42

Table 2.3 Computing time for iterative solution

Δt (**μs**)	**TD** (**s**)	**DP** (**s**)	**3pPD** (**s**)	**PD** (**s**)
10	698.90	2114.46	1115.98	252.64
100	71.87	222.05	112.23	31.65
200	36.53	115.13	63.97	17.21
500	17.64	50.01	25.93	6.92
1000	8.75	24.12	13.40	3.89
2000	4.43	13.57	7.28	2.05
5000	2.28	5.76	3.21	0.95

The TD approach is 2.92 times quicker than the DP method and 1.57 times quicker than the 3pPD technique when employing the iterative approach. In addition, the TD approach simulates 0.43 times slower than the PD approach.

The number of equations representing the network with SMs is the same for the TD, DP, and 3pPD methods. Since the 3pPD approach does not have derivative part in representing equations of inductors and capacitors, it does not have a historic term. As a result, it runs faster than the DP method. Unlike the TD method which uses real numbers in all calculations, the phasor domain approaches employ complex numbers, which makes the computation heavy for the DP, 3pPD, and DP methods.

Considering the mentioned reasons, when using the same time-step, the DP and 3pPD methods run simulation slower than the TD method.

2.6 Conclusion

The section of the thesis described the EMT-type and phasor domain simulation methods with emphasis on the SM model. Based on the presented simulations, it is shown that the DP method due to its dual (TD and phasor-domain) nature is more accurate than the pure phasor domain methods (3pPD and DP). The accuracies and limitations of 3pPD and DP methods are compared, and the differences are explained.

Although the DP method can capture faster EMT-type transients, it does not deliver the same accuracy as the pure TD method. Moreover, it is shown that for larger time steps, the accuracy of the DP method deteriorates, and its computational performance does not surpass the TD method for the same numerical integration time-step. It is also demonstrated that the TD method can maintain sufficient accuracy at very high numerical time steps if it employs a fully iterative process for the solution of its synchronous machine equations. It appears that despite its theoretical advantages, the DP method remains on average 2.9 times slower than the full TD method. This conclusion is based on comparing codes in the same development environment and for different network conditions and fault cases.

Chapter 3 DP SYNCHRONOUS MACHINE IMPROVED MODEL

The SM model presented in Section 2.2 models zero and second harmonics, and the SM controllers include zero harmonic. Section 2.5 indicates that the DP model does not deliver the same transient result as the TD technique despite using a very small-time step. This chapter proposes an improved synchronous machine model based on the DP method. The model employs harmonics to presents an accurate simulation. The first step is obtaining the relation of harmonics on the power system and synchronous machines.

3.1 Transformation symmetrical components to *dq*0-frame

A three-phase set of unbalanced current or voltage with harmonics can be presented as:

$$x_{abc} = \frac{1}{2}\begin{bmatrix} x_{a_0} \\ x_{b_0} \\ x_{c_0} \end{bmatrix} + \sum_{k=1}^{\infty} \begin{bmatrix} x_{a_k} \cos\left(k\omega_s t + \theta_{a_k}\right) \\ x_{b_k} \cos\left(k\omega_s t + \theta_{b_k}\right) \\ x_{c_k} \cos\left(k\omega_s t + \theta_{c_k}\right) \end{bmatrix} \tag{3.1}$$

where x_{abc} is the vector of three-phase current or voltage, t is time, k is the harmonic number, ω_s is synchronous rotating speed, $x_{a,k}$ and $\theta_{a,k}$ are *k*-th Fourier coefficient and angle of phase "a" variable, respectively.

Equation (3.1) can be rewritten with exponential Fourier series as:

$$x_{abc} = \sum_{k=-\infty}^{\infty} \begin{bmatrix} \mathrm{X}_{a_k} \\ \mathrm{X}_{b_k} \\ \mathrm{X}_{c_k} \end{bmatrix} e^{jk\omega_s t} \tag{3.2}$$

where $\mathrm{X}_{a,k}$ is *k*-th exponential Fourier coefficient of phase "a" current or voltage.

$$\begin{bmatrix} \mathrm{X}_{a_k} \\ \mathrm{X}_{b_k} \\ \mathrm{X}_{c_k} \end{bmatrix} = \frac{1}{2}\begin{bmatrix} x_{a_k} e^{j\theta_{a_k}} \\ x_{b_k} e^{j\theta_{b_k}} \\ x_{c_k} e^{j\theta_{c_k}} \end{bmatrix} \text{ for } k \geq 0 \tag{3.3}$$

and the below equation gives the negative Fourier coefficients, where * is the conjugation of a phasor.

$$\begin{bmatrix} \mathrm{X}_{a_k} \\ \mathrm{X}_{b_k} \\ \mathrm{X}_{c_k} \end{bmatrix} = \begin{bmatrix} \mathrm{X}^*_{a_{-k}} \\ \mathrm{X}^*_{a_{-k}} \\ \mathrm{X}^*_{a_{-k}} \end{bmatrix} = \frac{1}{2} \begin{bmatrix} x_{a_{-k}} e^{-j\theta_{a_{-k}}} \\ x_{b_{-k}} e^{-j\theta_{b_{-k}}} \\ x_{c_{-k}} e^{-j\theta_{c_{-k}}} \end{bmatrix} \text{ for } k < 0 \tag{3.4}$$

The following equation expresses the relationship between three-phase and symmetrical component variables:

$$\begin{bmatrix} x_a \\ x_b \\ x_c \end{bmatrix} = \begin{bmatrix} 1 & 1 & 1 \\ e^{-j\frac{2\pi}{3}} & e^{j\frac{2\pi}{3}} & 1 \\ e^{j\frac{2\pi}{3}} & e^{-j\frac{2\pi}{3}} & 1 \end{bmatrix} \begin{bmatrix} \sum_{k=-\infty}^{\infty} \mathrm{X}_{p_k} e^{jk\omega_s t} \\ \sum_{k=-\infty}^{\infty} \mathrm{X}_{n_k} e^{jk\omega_s t} \\ \sum_{k=-\infty}^{\infty} \mathrm{X}_{z_k} e^{jk\omega_s t} \end{bmatrix} \tag{3.5}$$

where subscripts *p*, *n*, and *z* are positive, negative, and zero sequence components.

Replacing equation (3.5) into (2.18) gives the relation between *dq0*-frame and symmetrical components for a Fourier series:

$$\begin{bmatrix} x_d \\ x_q \\ x_0 \end{bmatrix} = \frac{2}{3} \begin{bmatrix} \cos(\theta) & \cos\left(\theta - \frac{2\pi}{3}\right) & \cos\left(\theta + \frac{2\pi}{3}\right) \\ -\sin(\theta) & -\sin\left(\theta - \frac{2\pi}{3}\right) & -\sin\left(\theta + \frac{2\pi}{3}\right) \\ \frac{1}{2} & \frac{1}{2} & \frac{1}{2} \end{bmatrix} \begin{bmatrix} 1 & 1 & 1 \\ e^{-j\frac{2\pi}{3}} & e^{j\frac{2\pi}{3}} & 1 \\ e^{j\frac{2\pi}{3}} & e^{-j\frac{2\pi}{3}} & 1 \end{bmatrix} \begin{bmatrix} \sum_{k=-\infty}^{\infty} \mathrm{X}_{p_k} e^{jk\omega_s t} \\ \sum_{k=-\infty}^{\infty} \mathrm{X}_{n_k} e^{jk\omega_s t} \\ \sum_{k=-\infty}^{\infty} \mathrm{X}_{z_k} e^{jk\omega_s t} \end{bmatrix} \tag{3.6}$$

where $\theta = \omega_s t + \delta - \frac{\pi}{2}$.

The equation (3.6) is simplified as follows:

$$\begin{bmatrix} x_d \\ x_q \\ x_0 \end{bmatrix} = \sum_{k=-\infty}^{\infty} \left(\begin{bmatrix} e^{-j\left((1-k)\omega_s t+\delta-\frac{\pi}{2}\right)} & e^{j\left((1+k)\omega_s t+\delta-\frac{\pi}{2}\right)} & 0 \\ e^{-j\left((1-k)\omega_s t+\delta\right)} & e^{j\left((1+k)\omega_s t+\delta\right)} & 0 \\ 0 & 0 & e^{jk\omega_s t} \end{bmatrix} \begin{bmatrix} \mathrm{X}_{p_k} \\ \mathrm{X}_{n_k} \\ \mathrm{X}_{z_k} \end{bmatrix} \right) \tag{3.7}$$

The *dq*0-axes variables can be expressed separately using equation (3.7):

$$x_d = \sum_{k=-\infty}^{\infty} \mathrm{X}_{p_k} e^{-j\left((1-k)\omega_s t+\delta-\frac{\pi}{2}\right)} + \sum_{k=-\infty}^{\infty} \mathrm{X}_{n_k} e^{j\left((1+k)\omega_s t+\delta-\frac{\pi}{2}\right)} \tag{3.8}$$

$$x_q = \sum_{k=-\infty}^{\infty} \mathrm{X}_{p_k} e^{-j\left((1-k)\omega_s t+\delta\right)} + \sum_{k=-\infty}^{\infty} \mathrm{X}_{n_k} e^{j\left((1+k)\omega_s t+\delta\right)} \tag{3.9}$$

$$x_0 = \sum_{k=-\infty}^{\infty} \mathrm{X}_{z_k} e^{jk\omega_s t} \tag{3.10}$$

Equations (3.8) and (3.9) illustrates that the variables on both *d*- and *q*- axes have relation with the Fourier coefficients of both positive and negative sequence components. Equation (3.10) shows the variables on 0-axis has relation with the Fourier coefficients of zero-sequence component.

Rearranging equations (3.8) and (3.9) gives:

$$x_d = \sum_{k=-\infty}^{\infty} \left(\mathrm{X}_{p_{k+1}} e^{-j\left(\delta-\frac{\pi}{2}\right)} + \mathrm{X}_{n_{k-1}} e^{j\left(\delta-\frac{\pi}{2}\right)} \right) e^{jk\omega_s t} \tag{3.11}$$

$$x_q = \sum_{k=-\infty}^{\infty} \left(\mathrm{X}_{p_{k+1}} e^{-j\delta} + \mathrm{X}_{n_{k-1}} e^{j\delta} \right) e^{jk\omega_s t} \tag{3.12}$$

According to equation (3.11), the *k*-th exponential Fourier coefficient on *d*-axis is:

$$\mathrm{X}_{d_k} = \mathrm{X}_{p_{k+1}} e^{-j\left(\delta-\frac{\pi}{2}\right)} + \mathrm{X}_{n_{k-1}} e^{j\left(\delta-\frac{\pi}{2}\right)} \tag{3.13}$$

The *k*-th exponential Fourier coefficient on the *q*-axis, according to equation (3.12), is:

$$\mathrm{X}_{q_k} = \mathrm{X}_{p_{k+1}} e^{-j\delta} + \mathrm{X}_{n_{k-1}} e^{j\delta} \tag{3.14}$$

The *k*-th exponential Fourier coefficient on the 0-axis, according to equation (3.10), is:

$$\mathrm{X}_{0_k} = \mathrm{X}_{z_k} \tag{3.15}$$

Equations (3.13), (3.14), and (3.15) can be summed in one set of equations to find relation of the *dq0*-frame and symmetrical components for *k*-th Fourier coefficient.

$$\begin{bmatrix} \mathrm{X}_{d_k} \\ \mathrm{X}_{q_k} \\ \mathrm{X}_{0_k} \end{bmatrix} = \begin{bmatrix} je^{-j\delta} & -je^{j\delta} & 0 \\ e^{-j\delta} & e^{j\delta} & 0 \\ 0 & 0 & 1 \end{bmatrix} \begin{bmatrix} \mathrm{X}_{p_{k+1}} \\ \mathrm{X}_{n_{k-1}} \\ \mathrm{X}_{z_k} \end{bmatrix} \tag{3.16}$$

The transformation from symmetrical components to *dq0*-frame for *k*-th Fourier coefficient, the inverse of transformation in equation (3.16), is:

$$\begin{bmatrix} \mathrm{X}_{p_{k+1}} \\ \mathrm{X}_{n_{k-1}} \\ \mathrm{X}_{z_k} \end{bmatrix} = \frac{1}{2} \begin{bmatrix} -je^{j\delta} & e^{j\delta} & 0 \\ je^{-j\delta} & e^{-j\delta} & 0 \\ 0 & 0 & 2 \end{bmatrix} \begin{bmatrix} \mathrm{X}_{d_k} \\ \mathrm{X}_{q_k} \\ \mathrm{X}_{0_k} \end{bmatrix} \tag{3.17}$$

According to equation (3.17), the positive and negative sequences of the *k*-th Fourier coefficient can be written as:

$$\mathrm{X}_{p_k} = \frac{1}{2} \left(\mathrm{X}_{d_{k-1}} e^{j\left(\delta - \frac{\pi}{2}\right)} + \mathrm{X}_{q_{k-1}} e^{j\delta} \right) \tag{3.18}$$

$$\mathrm{X}_{n_k} = \frac{1}{2} \left(\mathrm{X}_{d_{k+1}} e^{-j\left(\delta - \frac{\pi}{2}\right)} + \mathrm{X}_{q_{k+1}} e^{-j\delta} \right) \tag{3.19}$$

or

$$\mathrm{X}_{p_k} = \frac{1}{2} \left(\mathrm{X}_{d_{k-1}} + j\mathrm{X}_{q_{k-1}} \right) e^{j\left(\delta - \frac{\pi}{2}\right)} \tag{3.20}$$

$$\mathrm{X}_{n_k} = \frac{1}{2} \left(\mathrm{X}_{d_{k+1}} - j\mathrm{X}_{q_{k+1}} \right) e^{-j\left(\delta - \frac{\pi}{2}\right)} \tag{3.21}$$

In case of having an unbalanced system, the negative sequence of fundamental frequency causes second harmonic on the *d*- and *q*- axes (equation (3.21)), then the second harmonic on *d*- and *q*- axes produce the positive and negative symmetrical components of third harmonic in the network (equations (3.13)–(3.14)). Subsequently, the negative sequence of third harmonic makes the fourth harmonic on the *d*- and *q*- axes (equation (3.21)). This circle continues for the odd harmonics of symmetrical components and the even harmonics of *d*- and *q*- axes.

3.1.1 Discretized equations

The *k*-th Fourier coefficient of positive sequence voltage according to equations (3.20), (2.194), and (2.195) is:

$$\begin{aligned} \mathrm{V}_{p_{k,n}} = & \frac{1}{2}\left(-\mathrm{Z}_{dd_{k-1}}\,\mathrm{I}_{d_{k-1,n}} + \mathrm{Z}_{dq_{k-1,n}}\,\mathrm{I}_{q_{k-1,n}} - j\left(\mathrm{Z}_{qd_{k-1,n}}\,\mathrm{I}_{d_{k-1,n}} + \mathrm{Z}_{qq_{k-1}}\,\mathrm{I}_{q_{k-1,n}}\right)\right)e^{j\left(\delta_n-\frac{\pi}{2}\right)} \\ & + \frac{1}{2}\left(\mathrm{E}_{hd_{k-1,n-1}} + j\,\mathrm{E}_{hq_{k-1,n-1}}\right)e^{j\left(\delta_n-\frac{\pi}{2}\right)} \end{aligned} \tag{3.22}$$

The *k*-th Fourier coefficient of negative sequence voltage according to equation (3.21), (2.194), and (2.195) is:

$$\begin{aligned} \mathrm{V}_{n_{k,n}} = & \frac{1}{2}\left(-\mathrm{Z}_{dd_{k+1}}\,\mathrm{I}_{d_{k+1,n}} + \mathrm{Z}_{dq_{k+1,n}}\,\mathrm{I}_{q_{k+1,n}} + j\left(\mathrm{Z}_{qd_{k+1,n}}\,\mathrm{I}_{d_{k+1,n}} + \mathrm{Z}_{qq_{k+1}}\,\mathrm{I}_{q_{k+1,n}}\right)\right)e^{-j\left(\delta_n-\frac{\pi}{2}\right)} \\ & + \frac{1}{2}\left(\mathrm{E}_{hd_{k+1,n-1}} - j\,\mathrm{E}_{hq_{k+1,n-1}}\right)e^{-j\left(\delta_n-\frac{\pi}{2}\right)} \end{aligned} \tag{3.23}$$

To have *k*-th harmonic of SM's DP model by symmetrical components, equation (3.22) needs to be rewritten as:

$$\mathrm{V}_{p_{k,n}} = -\mathrm{Z}_{p_{k,n}}\,\mathrm{I}_{p_{k,n}} + \mathrm{V}_{hp_{k,n-1}} \tag{3.24}$$

and equation (3.23) needs to be rewritten as:

$$\mathrm{V}_{n_{k,n}} = -\mathrm{Z}_{n_{k,n}}\,\mathrm{I}_{n_{k,n}} + \mathrm{V}_{hn_{k,n-1}} \tag{3.25}$$

The possible solution of finding parameters of equations (3.24) and (3.25) is to define equivalent impedance and history term as below. The equivalent impedance is:

$$\mathrm{Z}_{p_{k,n}} = \frac{\mathrm{Z}_{dd_{k-1}} + \mathrm{Z}_{qq_{k-1}} + j\left(\mathrm{Z}_{dq_{k-1,n}} + \mathrm{Z}_{qd_{k-1,n}}\right)}{2} \tag{3.26}$$

$$\mathrm{Z}_{n_{k,n}} = \frac{\mathrm{Z}_{dd_{k+1}} + \mathrm{Z}_{qq_{k+1}} - j\left(\mathrm{Z}_{dq_{k+1,n}} + \mathrm{Z}_{qd_{k+1,n}}\right)}{2} \tag{3.27}$$

and history term is:

$$\begin{aligned}\mathrm{V}_{hp_{k,n-1}} = &-\frac{\mathrm{Z}_{dd_{k-1}} - \mathrm{Z}_{qq_{k-1}} - j\left(\mathrm{Z}_{dq_{k-1,n}} - \mathrm{Z}_{qd_{k-1,n}}\right)}{2}\left(\mathrm{I}_{d_{k-1,n}} - j\,\mathrm{I}_{q_{k-1,n}}\right)e^{j\left(\delta_n - \frac{\pi}{2}\right)} \\ &+\left(\mathrm{E}_{hd_{k-1,n-1}} + j\,\mathrm{E}_{h\mathrm{q}_{k-1,n-1}}\right)e^{j\left(\delta_n - \frac{\pi}{2}\right)}\end{aligned} \tag{3.28}$$

$$\begin{aligned}\mathrm{V}_{hn_{k,n-1}} = &-\frac{\mathrm{Z}_{dd_{k+1}} - \mathrm{Z}_{qq_{k+1}} + j\left(\mathrm{Z}_{dq_{k+1,n}} - \mathrm{Z}_{qd_{k+1,n}}\right)}{2}\left(\mathrm{I}_{d_{k+1,n}} + j\,\mathrm{I}_{q_{k+1,n}}\right)e^{-j\left(\delta_n - \frac{\pi}{2}\right)} \\ &+\left(\mathrm{E}_{d_{k+1,n-1}} - j\,\mathrm{E}_{hq_{k+1,n-1}}\right)e^{-j\left(\delta_n - \frac{\pi}{2}\right)}\end{aligned} \tag{3.29}$$

The history term depends on not only the quantities in the previous time step, but also the quantities in the current time step. Therefore, an iterative solve is required to solve the model.

Equation (2.196), 0-axis voltage, is discretized as follows:

$$\mathrm{V}_{0_{k,n}} = -\mathrm{Z}_{00_k}\,\mathrm{I}_{0_{k,n}} + \mathrm{E}_{h0_{k,n-1}} \tag{3.30}$$

where Z_{00_k} is given by:

$$\mathrm{Z}_{00_k} = \frac{X_l + 3X_n}{\omega_s}\left(\frac{2}{\Delta t} + jk\omega_s\right) + R_a + 3R_n \tag{3.31}$$

and the history term of 0-axis voltage in equation (2.241) is:

$$\mathrm{E}_{h0_{k,n-1}} = -\mathrm{V}_{0_{k,n-1}} + \left(\frac{X_l + 3X_n}{\omega_s}\left(\frac{2}{\Delta t} - jk\omega_s\right) - \left(R_a + 3R_n\right)\right)\mathrm{I}_{0_{k,n-1}} \tag{3.32}$$

3.1.2 Norton equivalent circuit of SM

The *k*-th harmonic of SM's DP model by symmetrical components is expressed as follows using equations (3.24), (3.25), and (3.30):

$$\mathrm{V}_{pnz_{k,n}} = -\mathrm{Z}_{pnz_{k,n}} \mathrm{I}_{pnz_{k,n}} + \mathrm{E}_{hpnz_{k,n-1}} \tag{3.33}$$

where the $\mathrm{Z}_{pnz_{k,n}}$ matrix is the *k*-th harmonic SM equivalent impedance by symmetrical components. It should be noted that the *dq0* impedance is not constant and is a function of rotor speed.

$$\mathrm{Z}_{pnz_{k,n}} = \begin{bmatrix} \mathrm{Z}_{p_{k,n}} & 0 & 0 \\ 0 & \mathrm{Z}_{n_{k,n}} & 0 \\ 0 & 0 & \mathrm{Z}_{z_{k,n}} \end{bmatrix} \tag{3.34}$$

and $\mathrm{E}_{hpnz_{k,n-1}}$, vector of history term, is:

$$\mathrm{E}_{hdq0_{k,n-1}} = \begin{bmatrix} \mathrm{E}_{hp_{k,n-1}} & \mathrm{E}_{hn_{k,n-1}} & \mathrm{E}_{hz_{k,n-1}} \end{bmatrix}^T \tag{3.35}$$

To add equivalent *k*-th harmonic SM model to the MANA matrix, the symmetrical components model expressed in equation (3.33) needs to transform to *abc* frame.

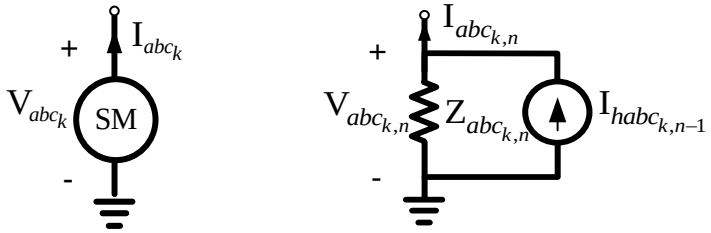

a) b)

Figure 3.1 a) Synchronous machine, b) Equivalent SM circuit, DP models

Figure 3.1 shows the Norton equivalent circuit by for the *k*-th harmonic.

The equivalent impedance and history term in Figure 3.1 are:

$$\mathrm{Z}_{abc_{k,n}} = \mathbf{A}^{-1}\mathrm{Z}_{pnz_{k,n}}\mathbf{A} \tag{3.36}$$

$$\mathrm{I}_{habc_{k,n}} = \mathbf{A}^{-1}\mathrm{Z}^{-1}_{pnz_{k,n}}\mathrm{E}_{hpnz_{k,n}} \tag{3.37}$$

Unlike equivalent circuit of inductor and capacitor, the equivalent impedance and history term of SM model are a function of state of the network at current state of the network. Thus, an iterative method is needed to solve a system includes SM models.

3.1.3 Simulation steps

The following are the steps in a DP simulation approach using harmonics:

1. Three phase Load-flow
2. Initialization
    a. Convert the loads to constant impedances
    b. Calculate equivalent circuit of elements by discretized method for network harmonics
    c. Build the MANA matrix (equation (1.8)) for network harmonics (exclude the SMs)
    d. Calculate the history terms for the first time-step based on the load flow results, compute the history term for the fundamental frequency, whereas the history term for the other harmonics is zero.
3. Dynamic simulation
    a. Calculate unknowns for all harmonic (start from fundamental frequency ($k = 1$))
        i. Calculate equivalent impedance and injection current using equations (3.36) and (3.37) for all SMs
        ii. Add equivalent impedance of SMs to the admittance submatrix of MANA, add injection current of SMs to the $\mathrm{B}_{k,n}$ vector, and solve $\mathrm{A}_{k,n}\mathrm{X}_{k,n} = \mathrm{B}_{k,n}$

iii. Update *dq*0-axes currents (equations (2.235), (2.236), and (2.241)), rotor speed (equation (2.244)), and rotor angle (equation (2.246)) for all SMs

iv. If steps 3.a.i to 3.a.iii are done for all harmonics, then go step 3.b; if not, go to 3.a.i for the next harmonic

b. If the relative error of rotor speed for all SMs be less than accepted error, then the solution is converged and go to step 3.f. If the relative error of rotor speed of one or more SM(s) be more than accepted error then the solution is not converged, so go to step 3.a for the next iteration

c. Calculate controllers' model of all harmonics for the next time step

d. Predict SM quantities of rotor speed, rotor angle, *d*- and *q*- axes currents of all Fourier coefficients corresponding to harmonics

e. For all Fourier coefficients corresponding harmonics, calculate the history terms of all elements except SMs (the history term of an inductor, for example, as indicated in equation (1.19)) and update the $B_{k,n}$ vector. Then proceed to step 3.a for the next time step

The prediction of variables in step 3.e reduces the number of iterations. Equation (2.163) represents the prediction relationship. In step 3.d, the relationship between the relative error is given as equation (2.164).

3.2 Dynamic phasor model of synchronous machine controller

The SM's control devices regulate the machine's terminal voltage and electrical output power in order to maintain system stability. The SM variables determine the input of the controllers. The output of the exciter and turbine controller affects the field voltage and mechanical power of the SM. As a result, the SM's harmonics cause harmonics in the controllers, and the controller's harmonics induce harmonics in the SM's field voltage and mechanical power. Section 3.1 presents the model of harmonic for the SM's variables. In this section the importance of SM controller model considering harmonic is presented.

The exciter output is controlled by adjusting the exciter's field current. The exciter's output then regulates the rotor's magnetic field, resulting in a constant voltage output from the generator. The magnitude of the generator's terminal voltage and the output of the power system stabiliser are the exciter's inputs. The terminal voltage, input of exciter controller, is the root sum square of *d*- and *q*- axis voltages.

$$v_t = \sqrt{v_d^2 + v_q^2} \tag{3.38}$$

where v_t is the terminal voltage, v_d and v_q are voltages on *d*- and *q*- axes, respectively. In TD calculations, v_d and v_q are obtained from equations (2.88) and (2.89), respectively.

Although high-gain, fast-response-time excitation controller substantially helps transient stability, it can compromise small-signal stability (damping torque). The power system stabiliser (PSS) makes a beneficial contribution by dampening generator rotor angle swings that occur over a wide frequency range. Generator rotor angle swings or generator electrical power can both be used as PSS inputs. The excitation system can receive a control signal from the output of PSS controller. Several types of controllers are available, and in general the input of exciter and PSS collection is *d*- and *q*- axis voltages and rotational angular speed, and the output is field voltage on the *d*-axis.

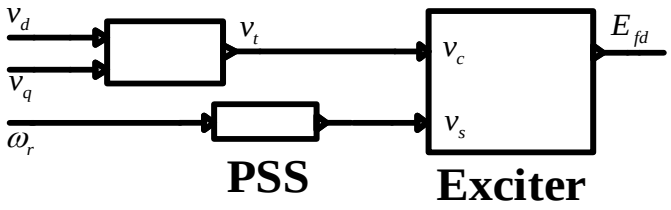

Figure 3.2 TD exciter with PSS input

A TD excitation controller with terminal voltage and PSS inputs is shown in Figure 3.2. ω_r is the rotor angular speed, E_{fd} is the field voltage on the *d*-axis, v_s and v_c are exciter inputs, with v_s being connected to the PSS output signal and v_c being connected to the measured terminal voltage. ω_r is obtained from equation (2.107), and E_{fd} is used in equation (2.91).

The DP model of SM controller has input/output phasors according to the calculating Fourier coefficients and is computed for all available harmonics.

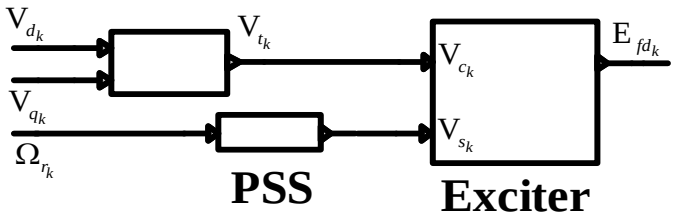

Figure 3.3 DP exciter with PSS

Figure 3.3 shows a dynamic-phasor excitation controller with terminal voltage and PSS inputs. The subscript k indicates the number of Fourier coefficient. In DP calculations of the *k*-th Fourier coefficients, V_{d_k}, V_{q_k}, and Ω_{r_k} are respectively obtained from equations (2.194), (2.195), and (2.201). The *k*-th Fourier coefficient of *d*-axis field voltage, E_{fd_k}, is used in equation (2.197). V_{s_k} and V_{c_k} are *k*-th Fourier coefficient of exciter inputs, with V_{s_k} being the PSS output signal and V_{c_k} being the measured terminal voltage.

3.2.1 Controller model without harmonics

Fundamental frequency of positive sequence is the basic component in the power system. The network main component cause zero Fourier coefficient on *d*- and *q*- axes. To reduce calculation for the DP method, the controller model without harmonics computes the zero Fourier coefficient and ignores harmonics on controller devices. Therefore, the output of exciter has the term with the zero Fourier coefficient and all other coefficients have zero amplitude. The mechanical torque in equation (2.201) and electrical field voltage on *d*-axis in equation (2.197) are equal zero for $k \neq 0$.

3.2.2 Controller model with harmonics

Harmonics occur in the SM when the network contains harmonics or is unbalanced. To improve accuracy of DP model, the nonzero Fourier coefficients are calculated for the controllers. For $k \neq 0$, the mechanical torque in equation (2.201) and electrical field voltage on the *d*-axis in equation (2.197) are known, and the controller is modelled for all simulated harmonics.

The terminal voltage, equation (3.38), is a nonlinear relation which exists in all exciter models. The DP method is challenging for modelling nonlinear elements. The next procedures attempt to determine the terminal voltage's Fourier coefficients.

The voltages on the *d*- and *q*- axes are represented by the Fourier series:

$$v_d = \sum_{k=-\infty}^{\infty} \mathrm{V}_{d_k} e^{jk\omega_s t} \tag{3.39}$$

$$v_q = \sum_{k=-\infty}^{\infty} \mathrm{V}_{q_k} e^{jk\omega_s t} \tag{3.40}$$

The square of *d*-axis voltage, $v_d{}^2$, is:

$$v_d{}^2 = \left(\sum_{k=-\infty}^{\infty} \mathrm{V}_{d_k} e^{jk\omega_s t} \right) \left(\sum_{k=-\infty}^{\infty} \mathrm{V}_{d_k} e^{jk\omega_s t} \right)^* \tag{3.41}$$

Expanding equation (3.41) gives:

$$v_d{}^2 = \sum_{k=-\infty}^{\infty} \sum_{l=-\infty}^{\infty} \mathrm{V}_{d_k} \mathrm{V}_{d_{-l}} e^{jk\omega_s t} e^{-jl\omega_s t} \tag{3.42}$$

or:

$$v_d{}^2 = \sum_{k=-\infty}^{\infty} \sum_{l=-\infty}^{\infty} \mathrm{V}_{d_k} \mathrm{V}_{d_{-l}} e^{j(k-l)\omega_s t} \tag{3.43}$$

Resorting equation (3.43) gives:

$$v_d{}^2 = \sum_{k=-\infty}^{\infty} \sum_{l=-\infty}^{\infty} \mathrm{V}_{d_k} \mathrm{V}_{d_{l-k}} e^{jl\omega_s t} \tag{3.44}$$

In equation (3.44), the Fourier coefficients are separated as follows:

$$v_d{}^2 = \mathrm{V}_{d_0}^2 + 2\sum_{k=1}^{\infty} \mathrm{V}_{d_k}^2 + \sum_{k=-\infty}^{\infty} \sum_{\substack{l=-\infty \\ l\neq 0}}^{\infty} \left(\mathrm{V}_{d_{l-k}} \mathrm{V}_{d_k} e^{jl\omega_s t} \right) \tag{3.45}$$

Then, rearrange equation (3.45) as follows:

$$v_d{}^2 = \mathrm{V}_{d_0}^2 + 2\sum_{k=1}^{\infty}\mathrm{V}_{d_k}^2 + 2\mathrm{V}_{d_0}\sum_{\substack{k=-\infty \\ k\neq 0}}^{\infty}\mathrm{V}_{d_k}e^{jk\omega_s t} + \sum_{\substack{k=-\infty \\ k\neq l \\ k\neq 0}}^{\infty}\sum_{\substack{l=-\infty \\ l\neq 0}}^{\infty}\mathrm{V}_{d_{l-k}}\mathrm{V}_{d_k}e^{jl\omega_s t} \tag{3.46}$$

The same procedure can be done to find square of *q*-axis voltage. Therefore, Fourier series of terminal voltage is:

$$\begin{aligned} v_t^2 = {} & \mathrm{V}_{d_0}^2 + \mathrm{V}_{q_0}^2 + 2\sum_{k=1}^{\infty}\left(\mathrm{V}_{d_k}^2 + \mathrm{V}_{q_k}^2\right) + 2\sum_{\substack{k=-\infty \\ k\neq 0}}^{\infty}\left(\mathrm{V}_{d_0}\mathrm{V}_{d_k} + \mathrm{V}_{q_0}\mathrm{V}_{q_k}\right)e^{jk\omega_s t} \\ & + \sum_{\substack{k=-\infty \\ k\neq l \\ k\neq 0}}^{\infty}\sum_{\substack{l=-\infty \\ l\neq 0}}^{\infty}\left(\mathrm{V}_{d_{l-k}}\mathrm{V}_{d_k} + \mathrm{V}_{q_{l-k}}\mathrm{V}_{q_k}\right)e^{jl\omega_s t} \end{aligned} \tag{3.47}$$

To find root of equation (3.47), the following relation is used.

$$\sqrt{a+b+c} \approx \sqrt{a} + \frac{b}{2\sqrt{a}} \tag{3.48}$$

The equation (3.48) can be utilised when term c is substantially smaller than term b, and term a is significantly greater than term b. The amplitude of harmonics in the system are smaller than the fundamental frequency. Therefore, using approximate equation (3.48), the Fourier series of terminal voltage, equation (3.47), can be written as follows:

$$v_t \simeq \mathrm{V}_{t_0} + \sum_{\substack{l=-\infty \\ l\neq 0}}^{\infty}\mathrm{V}_{t_l}e^{jl\omega_s t} \tag{3.49}$$

where V_{t_0} in equation (3.49) is:

$$\mathrm{V}_{t_0} \simeq \sqrt{\mathrm{V}_{d_0}^2 + \mathrm{V}_{q_0}^2 + 2\sum_{k=1}^{\infty}\left(\mathrm{V}_{d_k}^2 + \mathrm{V}_{q_k}^2\right)} \tag{3.50}$$

and V_{t_k} in equation (3.49) is:

$$\mathrm{V}_{t_k} \simeq \frac{\mathrm{V}_{d_0}\mathrm{V}_{d_k} + \mathrm{V}_{q_0}\mathrm{V}_{q_k}}{\mathrm{V}_{t_0}} \tag{3.51}$$

3.3 Simulation results

In this section, the two-area system [34] is used to evaluate impact of simulation harmonics in synchronous machines. The network has four synchronous machines, four transformers, two loads, and eight lines. A line-to-line fault, phase “a” to “b”, occurs on bus number 6 at 0.05 second and is removed after 100 ms. The simulations are run on the same platform using 10 μs integration time step. To distinguish between the proposed DP method that considers harmonics and the approach that does not, the proposed method is referred to as Harmonic Dynamic Phasor (DPH), while the method that does not consider harmonics is referred to as DP. To validate the proposed method, the results are compared to the TD method. Fundamental, third, and fifth harmonics are used to simulate the power system. For the SM and controllers, the zero frequency and second, fourth, and sixth harmonics are simulated in accordance with the system harmonics.

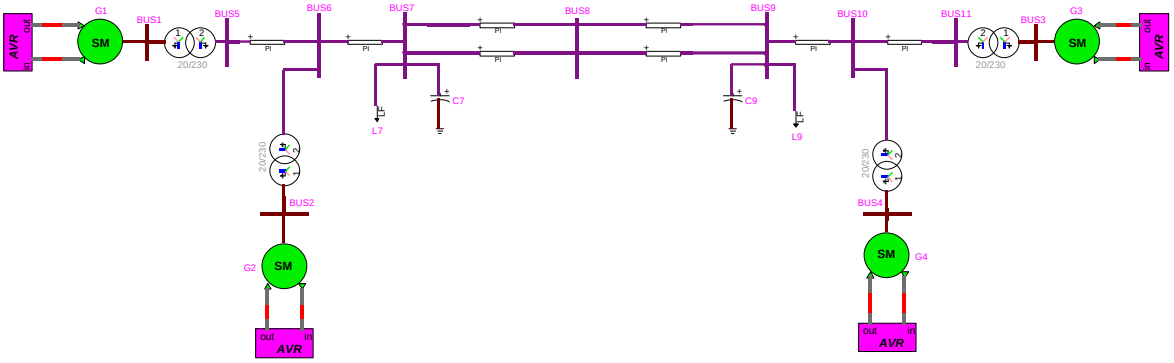

Figure 3.4 Two area test case

The following figure shows the model of exciter and PSS used in the two-area test case. The same model is used for the four SM in the test case.

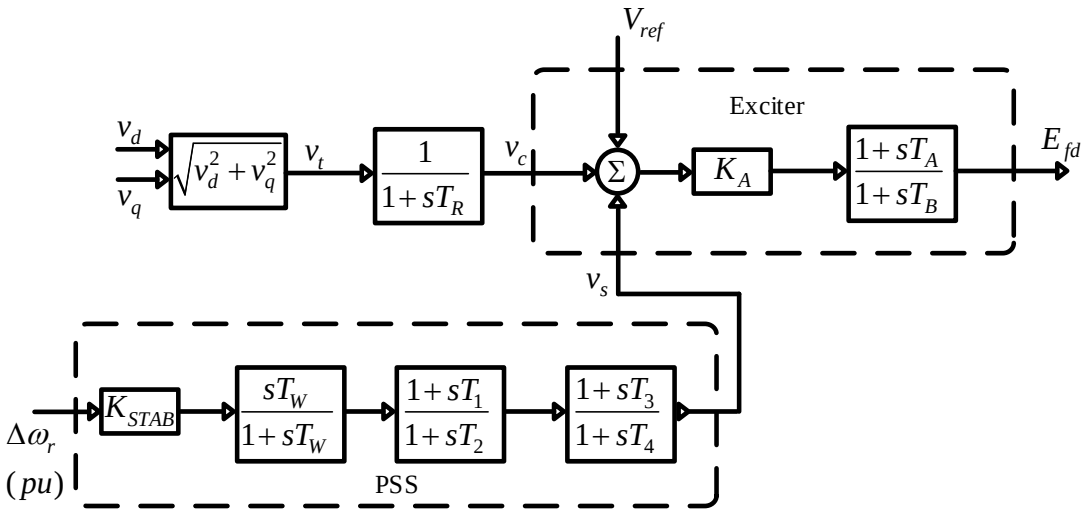

Figure 3.5 TD exciter and PSS model of the test case

In Figure 3.5, V_{ref} is the terminal voltage reference, $\Delta\omega_r$ is the deviation of rotor angular speed, and s is the Laplace variable. K is the gain of controller, and T is the constant coefficient of transfer function. The parameters of the controller are defined in reference [34].

The control models consist of transfer functions connected to each other. The simulators discretize the differential relation to calculate output of each transfer function. The following process demonstrates how to compute a transfer function.

$$y = \frac{1+sT_1}{1+sT_2}u \tag{3.52}$$

Equation (3.52) is an example of a transfer function, where u and y are respectively the input and the output of a first order transfer function.

$$y + T_2\frac{dy}{dt} = u + T_1\frac{du}{dt} \tag{3.53}$$

The converted relation of equation (3.52) from the transfer function to the differential relation is equation (3.53). The same integration rule used to discretize relation of the network elements and SM employed to compute controller models.

$$y_n = \frac{\left(1+\frac{2T_1}{\Delta t}\right)u_n + \left(1-\frac{2T_1}{\Delta t}\right)u_{n-1} - \left(1-\frac{2T_2}{\Delta t}\right)y_{n-1}}{1+\frac{2T_2}{\Delta t}} \tag{3.54}$$

Equation (3.54) is the discretized of equation (3.53) using the Trapezoidal integration rule.

The DP relation of equation (3.53) using DP property of equation (1.12) is:

$$\mathrm{Y}_k + T_2\frac{d\mathrm{Y}_k}{dt} + jk\omega_s\mathrm{Y}_k = \mathrm{U}_k + T_1\frac{d\mathrm{U}_k}{dt} + jk\omega_s\mathrm{U}_k \tag{3.55}$$

where k means the number of Fourier coefficient.

The discretized equation (3.55) using the Trapezoidal integration rule is:

$$\mathrm{Y}_{k,n} = \frac{\left(1+jk\omega_s+\frac{2T_1}{\Delta t}\right)\mathrm{U}_{k,n} + \left(1+jk\omega_s-\frac{2T_1}{\Delta t}\right)\mathrm{U}_{k,n-1} - \left(1+jk\omega_s-\frac{2T_2}{\Delta t}\right)\mathrm{Y}_{k,n-1}}{1+jk\omega_s+\frac{2T_2}{\Delta t}} \tag{3.56}$$

Initializing calculations are used to start the simulation. The initial value of the variables in a power system simulation is determined by load flow calculations. The SM controller, like the model of power system elements, must be initialised to begin simulation from a steady state.

Because the two-area system is a balanced network, there is no negative component at steady state, and hence no harmonic in the SM and network at the system's starting condition. As a result, the amplitude of nonzero Fourier coefficient variables is equal to zero in this scenario. Initialization is required for the zero Fourier coefficient model of controllers.

The value of a variable at the first moment of simulation is:

$$x_0 = x_{-1} \tag{3.57}$$

where x_0 is value of variable at the simulation beginning, and x_{-1} means value of variable at one step before starting the simulation.

The output's zero Fourier coefficient of the output of equation (3.56) is:

$$\mathrm{Y}_{0,0} = \mathrm{U}_{0,0} \tag{3.58}$$

where $U_{0,0}$ and $Y_{0,0}$ are respectively the zero Fourier coefficients of the transfer function's input and output at the start of the simulation.

3.3.1 Control modeller without harmonics

This section shows the result of the TD, DP, and DPH methods for the scenario described in Section 3.3. The DPH method simulates network and SM harmonics. Harmonics are not used to model the controllers; instead, only the zero Fourier coefficient is used.

The angular speed and field voltage results are shown in Figure 3.4 for SM number 3. The SM number 3 is connected to bus number 3, which has the most severe transient in the system.

The output of DP and DPH is in phasor domain. To compare TD, DP, and DPH results, phasor-domain results are converted to TD as follows:

$$x = \mathrm{X}_0 + 2\sum_{k=1}^{\infty} \Re\left(\mathrm{X}_k e^{jk\omega_s t}\right) \tag{3.59}$$

where x is TD variable, and X_k is phasor-domain variable of k-th Fourier coefficient.

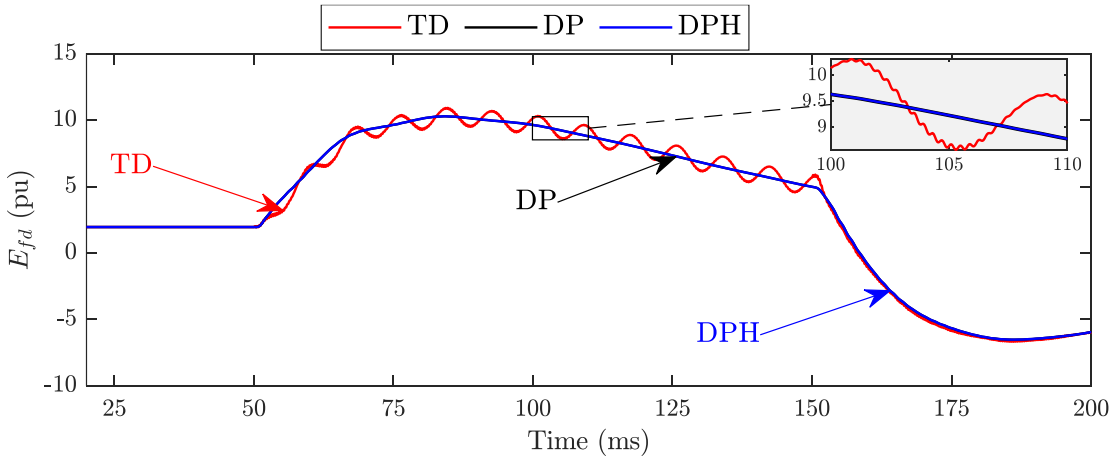

Figure 3.6 Field voltage on *d*-axis

Figure 3.6 shows the simulation of field voltage using TD, DP, and DPH methods. For DPH, the harmonics are not modeled in controllers. During occurring the fault (from 50ms to 150ms), the filed voltage of TD has a second harmonic component which is not simulated by DP and DPH methods.

To show the accuracy of a method, the absolute error is used:

$$\epsilon_x = \left| x_E - x_A \right| \tag{3.60}$$

where x_E is the exact value and x_A is the approximation value.

The absolute error of DP and DPH are calculated using equation (3.60). The result of TD is used as exact value.

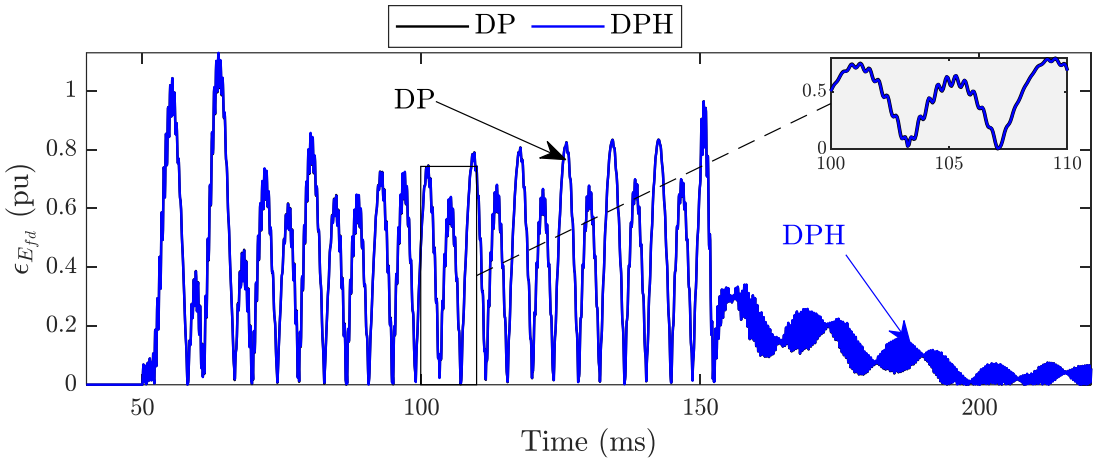

Figure 3.7 Error of field voltage on *d*-axis

Modeling harmonics in synchronous machines without taking controllers into consideration offers minimal advantage, as shown in Figure 3.7. The absolute errors of the DP and DPH techniques for field voltage are similar.

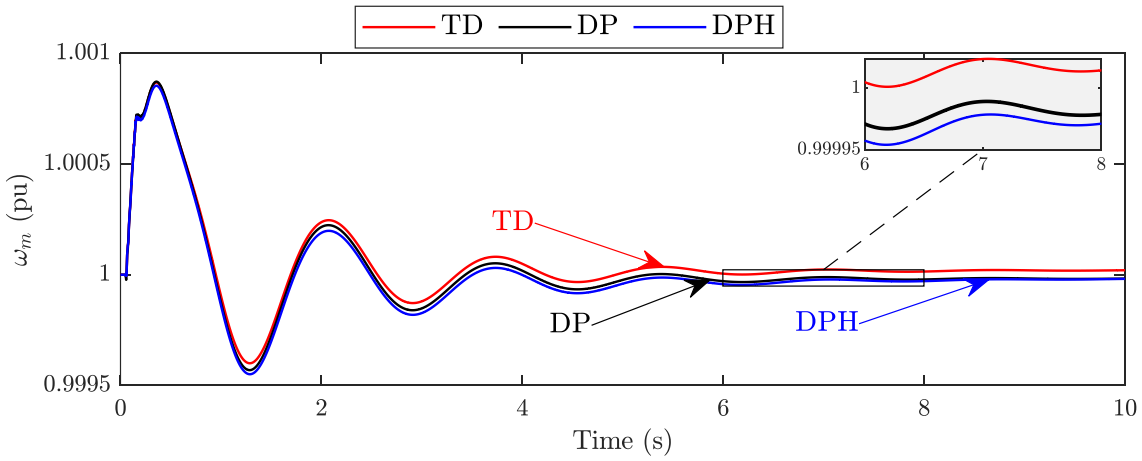

Figure 3.8 Angular speed

Figure 3.8 depicts the machine's angular speed as simulated by the methods. Both the DP and DPH approaches exhibit considerable inconsistencies, especially as the system stabilizes.

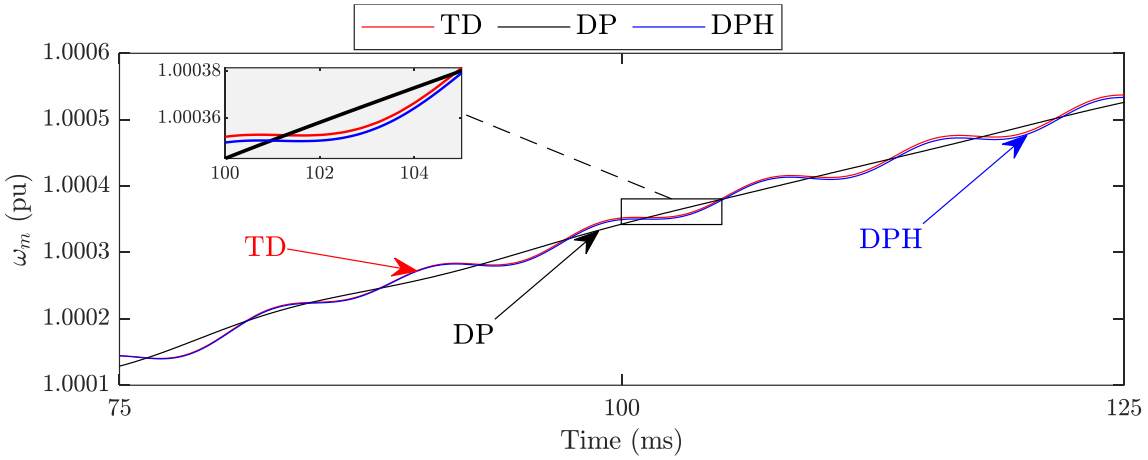

Figure 3.9 Angular speed (zoom)

Figure 3.9 shows the angular speed of the machine when a fault is applied. There is a second harmonic on the TD result which DPH simulated satisfactorily, but the DP is not able to model the second harmonic.

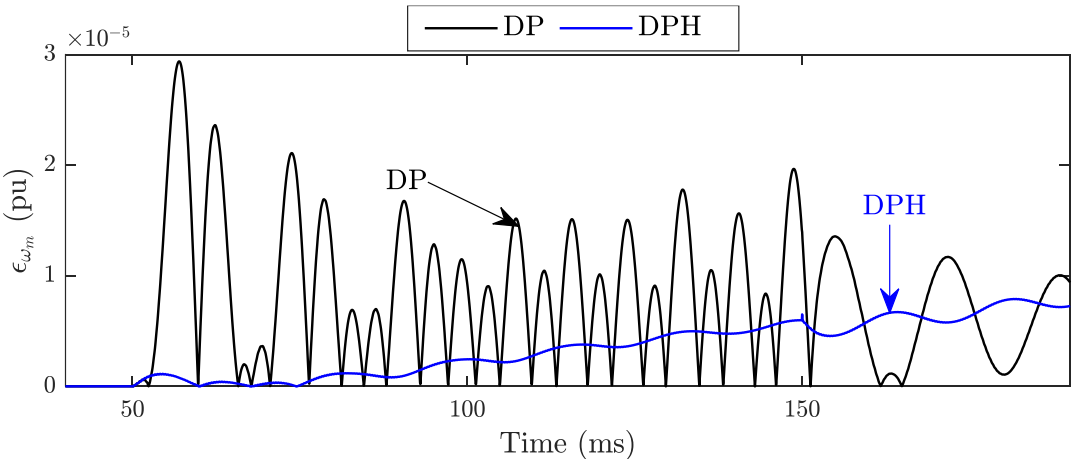

Figure 3.10 Error of angular speed (zoom)

The DPH approach has more accuracy than the DP method to simulate the angular speed error when the fault is applied, shown in Figure 3.10. It is because DPH models the second harmonic of the angular speed.

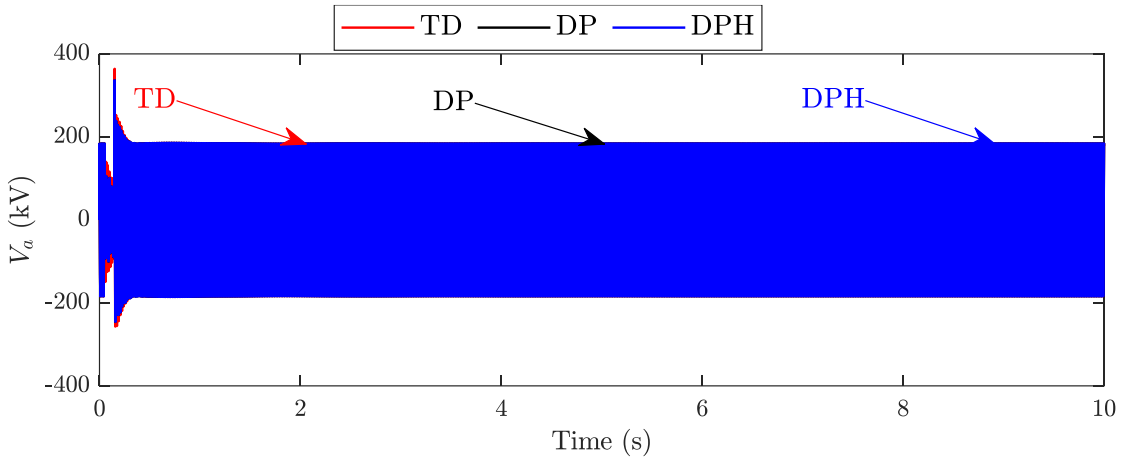

Figure 3.11 Bus voltage

The bus voltage waveforms of the machine of the DP and DPH are shown in Figure 3.11. The inconstancy during transient dynamics is considerable.

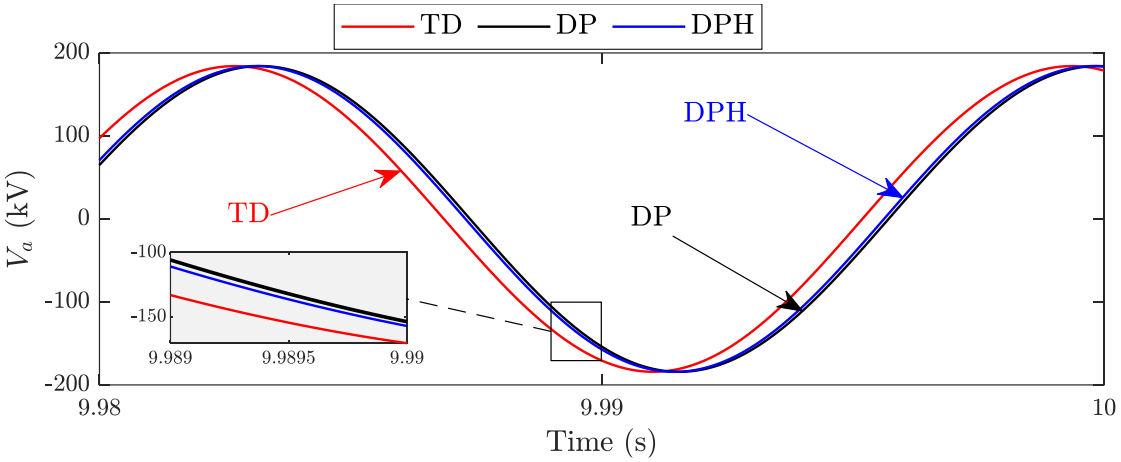

Figure 3.12 Bus voltage (semi-steady-state zoom)

The bus voltage waveforms of the machine during semi-steady-state are shown in Figure 3.12. Because of the error in the angular speed, a shift of phase appears in voltage terminal of the machine.

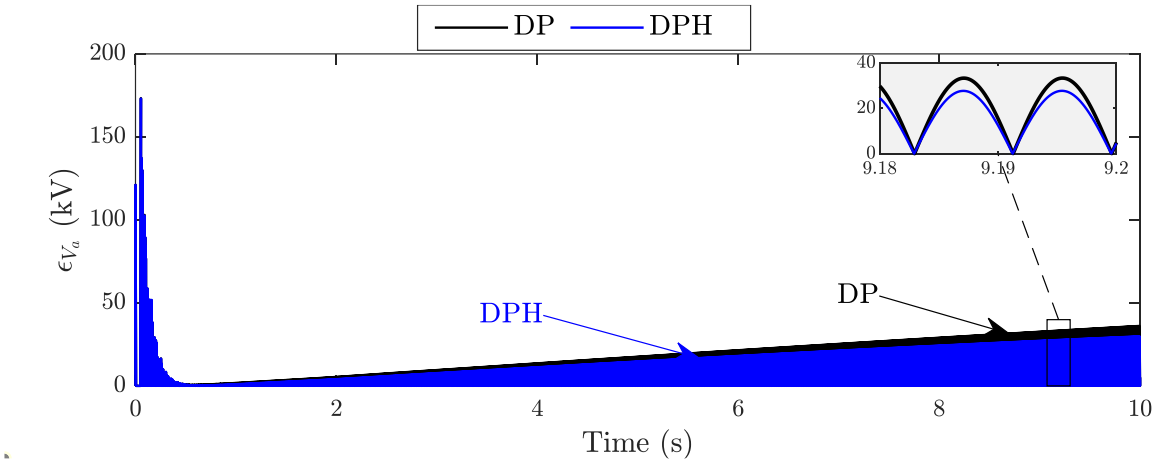

Figure 3.13 Error of bus voltage

The error of the voltage bus is presented in Figure 3.13. The applying the harmonics to the model of the machine a little improved the accuracy of the DP method.

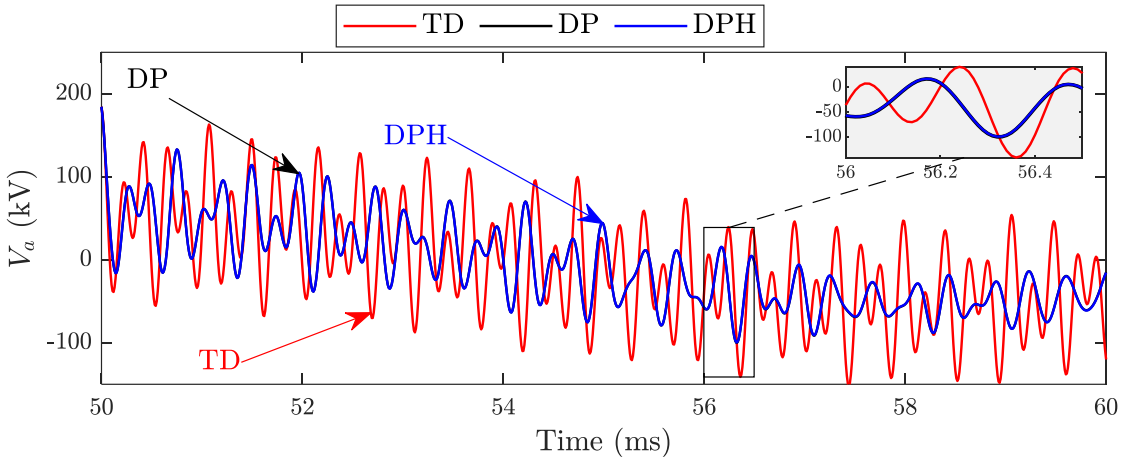

Figure 3.14 Bus voltage (transient zoom)

During the fault, the bus voltages simulated by the DP and DPH are identical (Figure 3.14); nevertheless, when compared to the TD technique, the DP and DPH exhibit considerable errors.

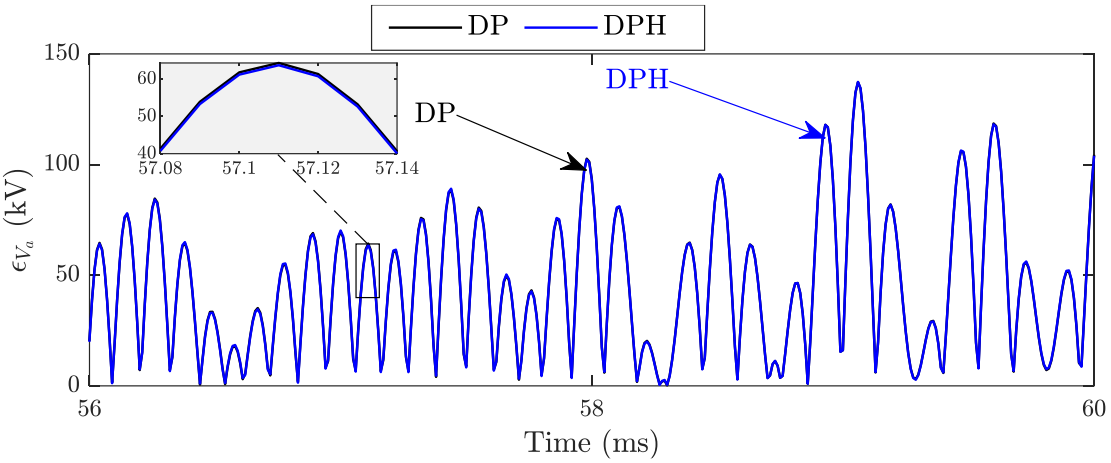

Figure 3.15 Error of bus voltage (transient zoom)

During the fault evolution, Figure 3.15 illustrates that the DPH does not provide a more accurate result than the DP.

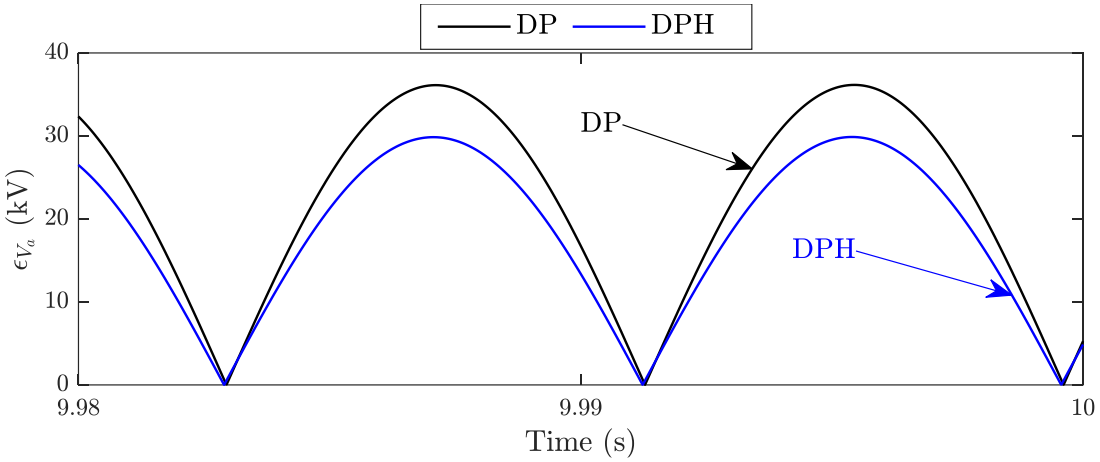

Figure 3.16 Error of bus voltage (semi-steady-state zoom)

Figure 3.16 indicates that the DPH approach improves bus voltage slightly when compared to the DP method in semi-steady-state.

Although DPH models harmonics generated in the system and the SM, simulation results demonstrate that the DPH model is inaccurate.

3.3.2 Control modeller with harmonics

In this section, harmonics are modeled in both SM and controllers for DPH method. The method explained in Section 3.2.2 is used to model harmonics of the SM controllers (DPH method). To demonstrate the influence of the suggested approach, the results of DPH method calculating harmonics in network and SM and controller, DP method utilising just fundamental frequency, and time domain are shown.

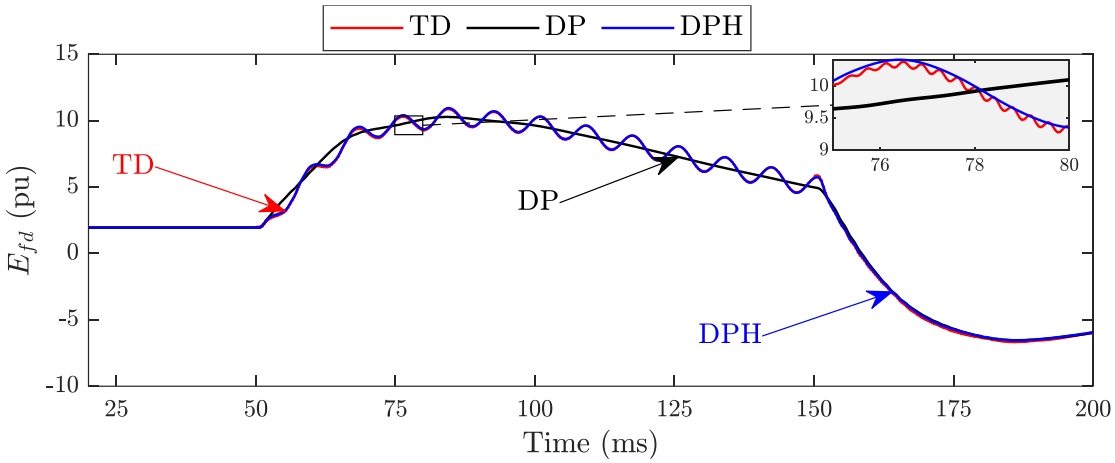

Figure 3.17 Field voltage on *d*-axis

Figure 3.17 shows field voltage evolution during fault. Comparing simulated field voltages shows that modeling harmonics in exciter cause more accurate result for DPH method.

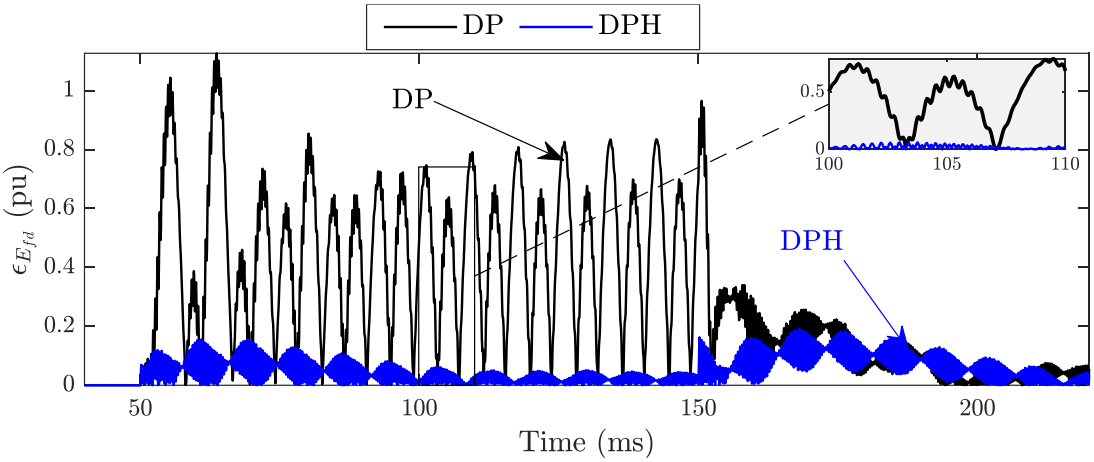

Figure 3.18 Error of Field voltage on *d*-axis

Figure 3.18 shows the absolute error of field voltage obtained from DPH and DP comparing to TD method. The absolute error of DP and DPH are calculated using equation (3.60). The result of TD is used as the exact value.

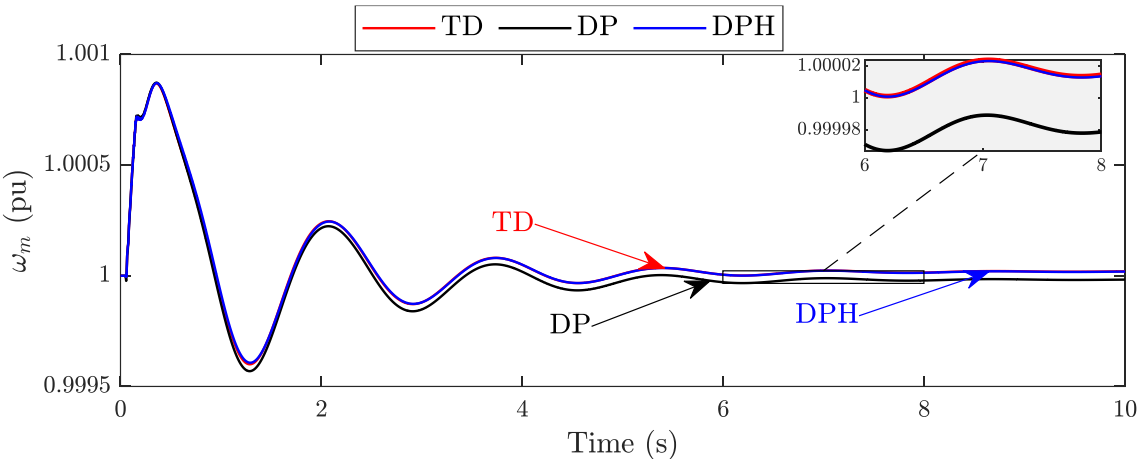

Figure 3.19 Angular speed

Figure 3.19 shows that the DPH method delivers a more accurate angular speed than the DP method.

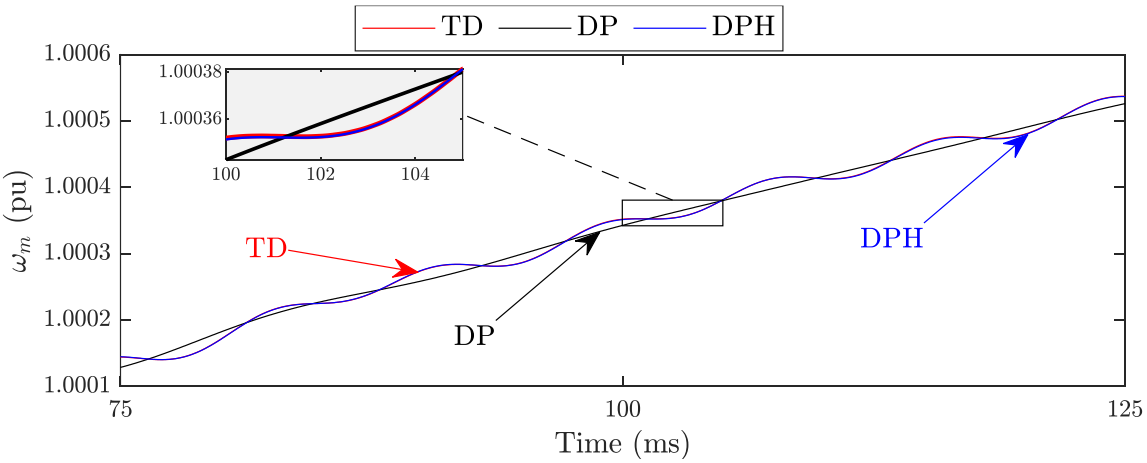

Figure 3.20 Angular speed (zoom)

When a fault is imposed, Figure 3.20 represents the machine's angular speed. On the TD result, there is a second harmonic that DPH successfully modelled, but the DP is unable to model the second harmonic.

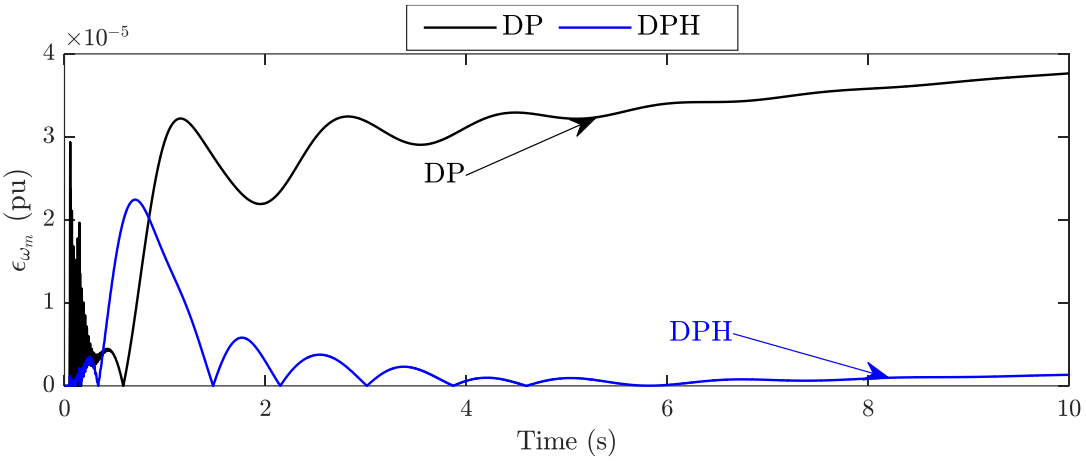

Figure 3.21 Error of angular speed

Figure 3.21 shows that applying harmonic on both machine and controller significantly improves the accuracy of the DPH method.

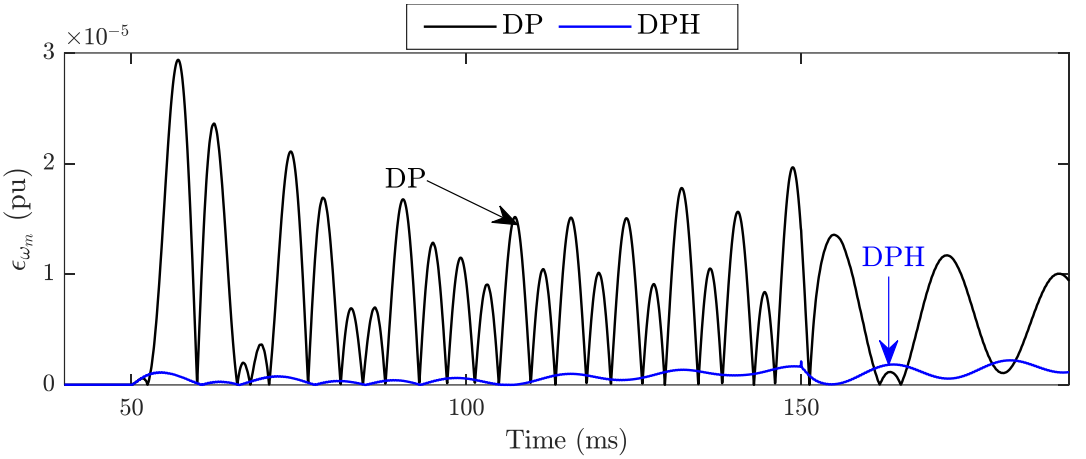

Figure 3.22 Error of angular speed (zoom)

Figure 3.22 depicts the angular speed error of the DP and DPH results during fault evolution. The accuracy of the DPH approach is greatly enhanced by the suggested method.

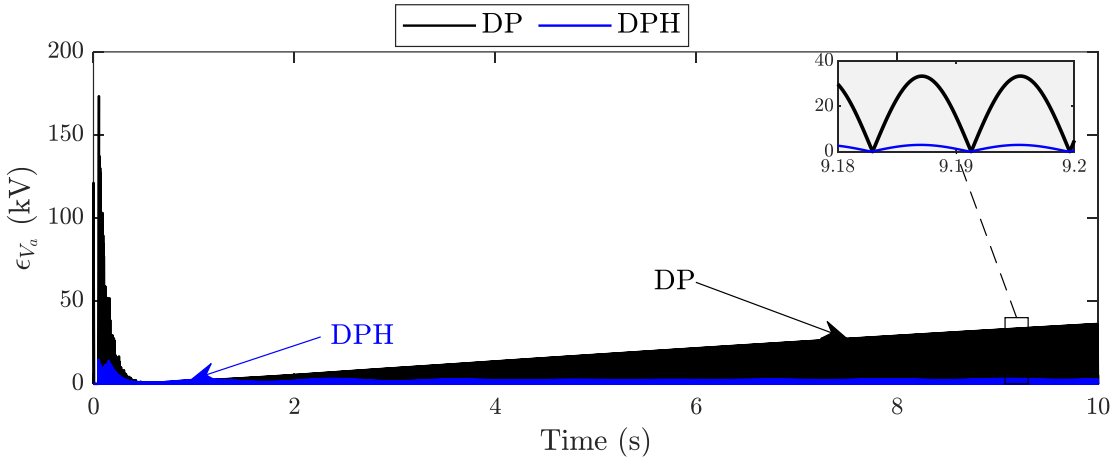

Figure 3.23 Error of bus voltage

The bus voltage error of the DP and DPH methods are presented in Figure 3.23. The DP technique has a persistent error in the machine's angular speed, the phase of terminal voltage increases with time, and as a consequence, the DP method's error increases gradually.

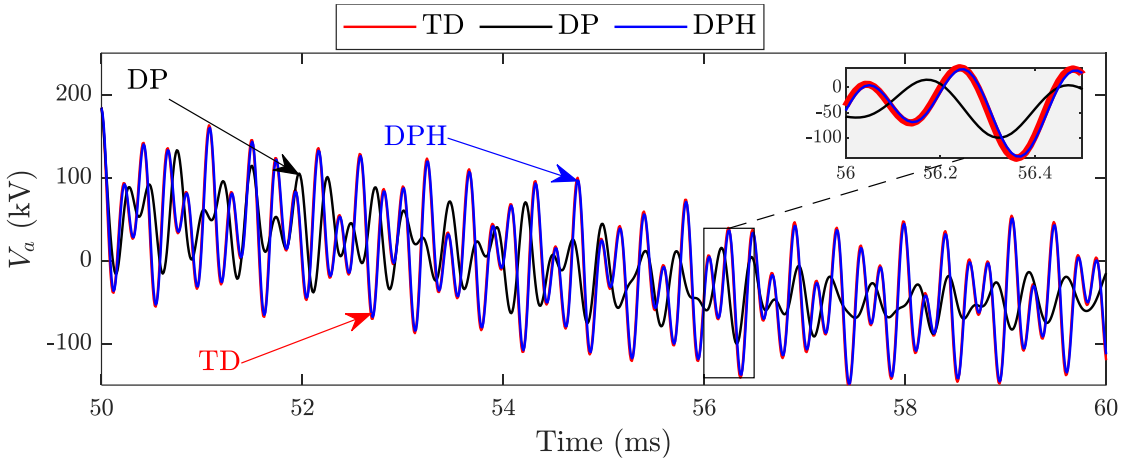

Figure 3.24 Bus voltage (transient zoom)

Figure 3.25 presents the bus voltage of the TD, DP, and DPH methods. Applying harmonics to the machine's controller produces an accurate field voltage, allowing the DPH approach to appropriately represent the machine's terminal voltage.

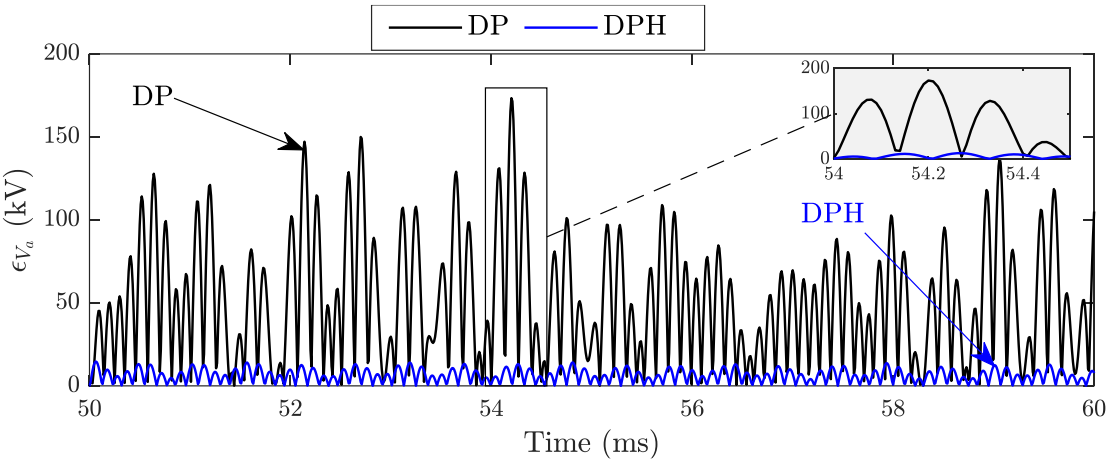

Figure 3.25 Error of bus voltage (transient zoom)

Figure 3.25 demonstrates that the DPH approach performs much better than the DP method in modeling bus voltage during fast transient dynamics.

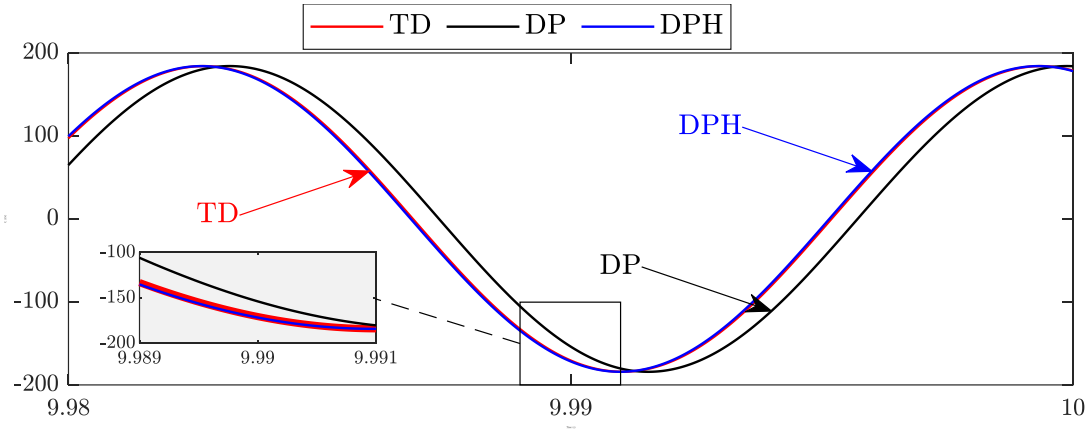

Figure 3.26 Bus voltage (semi-steady-state zoom)

In Figure 3.26, the DP has a voltage shift of phase after the removing the fault. The proposed DPH, on the other hand, properly models the voltage.

3.4 Conclusion

This chapter covers the approach for computing harmonics in the SM as well as controllers for the dynamic phasor method. Initially, the findings show that using the fundamental frequency of SM in the DP model alone does not produce the same results as using the TD approach. Furthermore,

while including harmonics into the SM model improves simulation results significantly, which is insufficient. The results are then greatly improved by introducing harmonics to the controllers using the proposed idea of computing the nonlinear component of the exciter.

Chapter 4 DYNAMIC PHASOR-BASED SIMULATION OF GEOMAGNETIC DISTURBANCES

This chapter proposes a dynamic phasor (DP)-based technique for simulation of geomagnetic disturbance (GMD) impact on a power system. GMD allows quasi-dc geomagnetically-induced currents to circulate through transmission lines and grounded high-voltage transformers, causing transformer saturation, increased reactive power losses, and potential voltage control issues. Nonlinear effects and the dynamic interplay of fundamental frequency, quasi-dc, and low-order harmonic components generate these phenomena. The solution of GMD system impacts needs advanced simulation tools and methodologies due to the complexity of these phenomena. In the literature, there are three types of approaches for simulating GMD system impacts [40]: electromagnetic transient-based (EMT) [41, 42], and load-flow-based (LF) [43-46], and transient stability (TS)-type methods [47, 48]. The EMT method provides an accurate solution. The phasor-based method is fast; however, it neglects to account for nonlinear effects and the dynamic interactions, making it is less accurate. The purpose of this section is to suggest a novel application for the DP technique. In comparison to the phasor-based method, the suggested DP-based methodology allows modelling of GMD effects, providing a more accurate solution. It also allows for a large simulation time-step, which reduces simulation time. Conducted simulations demonstrates that the proposed DP-method provides an accuracy comparable to that of the EMT method. Therefore, the proposed method offers an efficient solution method for GMD simulation.

4.1 Recall on Geomagnetic Disturbance

Solar mass energetic particles emitted from the sun's outer layer generate a Geoelectric Field (GEF) on transmission lines, resulting in Geomagnetic Disturbance (GMD). The GEF generates Geomagnetically Induced Currents (GICs) that flow through transmission lines and grounded transformers at low frequencies (0.1 Hz or lower). According to the flow of quasi-dc currents in the transformer winding, the operating point of the magnetisation characteristics shifts to one side, creating a lengthy uni-directional saturation of the transformer. The main negative effects of uni-directional saturation on the electric grid are: first, increased transformer magnetization currents and reactive power losses, which can cause voltage regulation issues or even voltage instability; second, transformer hotspot formation on windings and/or structural parts due to the extension of

the magnetic flux beyond the transformer core; and third, transformer hotspot formation on windings and/or structural parts due to the extension of the magnetic flux beyond the transformer core [40].

4.2 GMD Model

Modeling transformer saturation is required to simulate GMD.

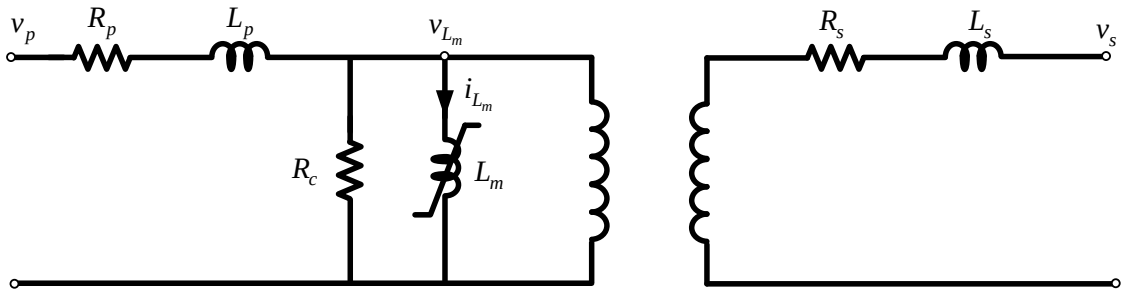

Figure 4.1 Transformer with saturation model

Figure 4.1 demonstrates a single-phase transformer with saturation model. The saturation is modeled by a nonlinear inductor in the magnetizing branch. v_p, v_s, and v_m are voltages of primary, secondary, and magnetization, respectively. R_p and R_s are equivalent resistance of copper loss on primary and secondary winding, respectively. L_p and L_s are equivalent inductance of flux leakage on primary and secondary winding, respectively. R_c is equivalent resistance of transformer core loss. L_m is equivalent inductance of transformer saturation.

Different sorts of 3-phase transformers can then be constructed utilising various winding connections. To depict saturation, the first step is to model the nonlinear inductor. The TD nonlinear inductor model is discussed in this section. The DP model is then produced by utilising the TD model.

4.2.1 Nonlinear inductor

The magnetizing branch of transformer can be modeled by a nonlinear inductor. The inductor is defined by a relation of current and magnetic flux.

$$\phi_{L_m} = f\left(i_{L_m}\right) \tag{4.1}$$

where ϕ_{L_m} and i_{L_m} are flux and current of magnetization branch. f is the function of flux by current variable.

Generally, this relation is given by piecewise segments and is symmetric with respect to the origin.

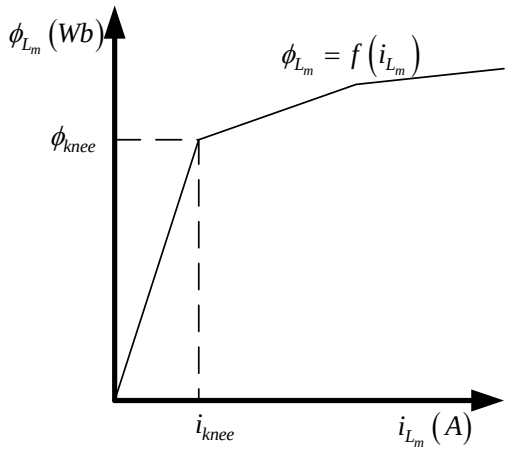

Figure 4.2 Current and magnetic flux relation of nonlinear inductor

Figure 4.2 shows current and magnetic flux relation of a nonlinear inductor. ϕ_{knee} and i_{knee} are flux and current at the knee point. Inductor is linear for flux and current less than the knee point.

The relation of voltage and flux is:

$$v_{L_m} = \frac{d\phi_{L_m}}{dt} \tag{4.2}$$

4.2.1.1 Time domain model

To simulate nonlinear inductance, the TD solution of reference [49] for nonlinear components is used. Assume that the flux-current are oscillating at a piecewise:

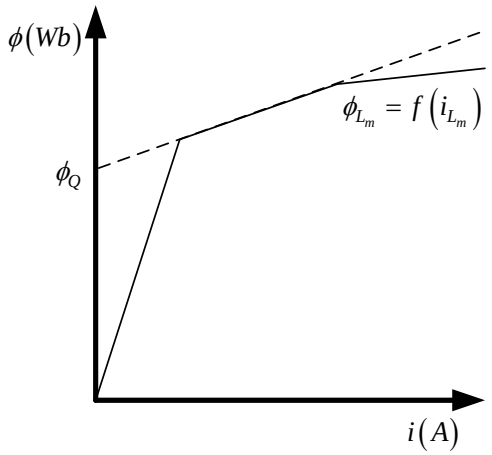

Figure 4.3 Linearizing relation of a flux-current at a segment

In Figure 4.3, ϕ_Q is flux of linearized equation at a segment when current is zero. Then relation of the piecewise can be written as:

$$\phi_{L_m} = K_Q i_{L_m} + \phi_Q \tag{4.3}$$

where K_Q is the slope of the flux-relation at the segment.

Assume that the flux-current are oscillating at a piecewise, then replacing equation (4.3) in equation (4.2) gives:

$$v_{L_m} = \frac{d\left(K_Q i_{L_m} + \phi_Q\right)}{dt} \tag{4.4}$$

Using Trapezoidal integration rule, equation (4.2) is discretized as:

$$i_{L_{m,n}} = \frac{1}{K_{Q_n}}\left(\frac{\Delta t}{2} v_{L_{m,n-1}} + K_{Q_{n-1}} i_{L_{m,n-1}} + \phi_{Q_{n-1}} - \phi_{Q_n}\right) + \frac{\Delta t}{2K_{Q_n}} v_{L_{m,n}} \tag{4.5}$$

The subscript n means the variable value at the *n*-th time-point ($x(t_n) = x_n$). The distance between the time-points is the numerical integration time-step (Δt).

Therefore, a TD nonlinear inductor and the Norton equivalent model using Trapezoidal rule can be shown as:

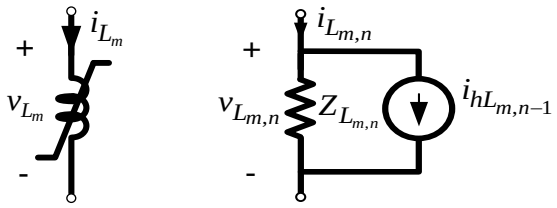

a) b)

Figure 4.4 Nonlinear inductor and equivalent circuit

where $i_{hL_{m,n-1}}$, the history term, is:

$$i_{hL_{m,n-1}} = \frac{1}{K_{Q_n}}\left(\frac{\Delta t}{2} v_{L_{m,n-1}} + K_{Q_{n-1}} i_{L_{m,n-1}} + \phi_{Q_{n-1}} - \phi_{Q_n}\right) \tag{4.6}$$

and $Z_{hL_{m,n}}$, the equivalent impedance, is:

$$Z_{L_{m,n}} = \frac{2K_{Q_n}}{\Delta t} \tag{4.7}$$

Unlike linear inductance (see equation (1.4)), the equivalent impedance of nonlinear inductance is not constant. The Newton iterative solution is used to determine the solution of the system containing nonlinear components. The matrix $\mathbf{A}_n$ becomes the Jacobian matrix of the Newton solution after linearizing nonlinear device equations at each solution time-point [30].

The properties of nonlinear components may be represented by piece-wise linear curves in most EMT simulations. The Newton–Raphson (NR) technique is highly efficient under this assumption, but it is prone to get stuck in an infinite loop, resulting in nonconvergence. First, the NR technique is changed to use the information from both axes of the nonlinear features, resulting in a biaxial NR approach. With more computing, the biaxial NR technique exhibits a substantial improvement in convergence performance. Following that, an iterative technique is presented that incorporates

the conventional NR, the biaxial NR [50, 51]. The suggested technique converges with some iterations.

The following are the steps in a GMD simulation using TD approach:

1. Three phase Load-flow: to simulate unbalanced network from initial state, a three-phase load flow is used.
2. Initialization
    a. Convert the loads to constant impedances: other load models like constant power or constant current can be used. In this thesis, the focus is on the modeling of SM and the simple load model, constant impedance is implemented.
    b. Calculate equivalent circuit of elements by discretized method
    c. Build the admittance submatrix of MANA (equation (1.8)) of the network (exclude the SMs and nonlinear inductances): During the simulation, the impedance of all components except SM and transformers remains constant. To avoid having repetitive computation, the constant portion of the admittance submatrix is computed during the initialization phase, and the variable part is added to the admittance submatrix during the simulation.
    d. Calculate the history terms for the first time-step based on the load-flow results
3. Dynamic simulation
    a. Calculate equivalent impedance and injection current for all SMs (using equations (2.161) and (2.162)) and all nonlinear inductances (using equations (4.6) and (4.7))
    b. Add equivalent impedance of SMs and nonlinear inductances to the admittance submatrix of MANA, add injection current of SMs and nonlinear inductances to the b_n vector, and solve $A_n x_n = b_n$
    c. Update working segment of nonlinear inductors and *dq*0-axes currents (equations (2.141), (2.147), and (2.151)), rotor speed (equation (2.154)), and rotor angle (equation (2.156)) for all SMs

d. If the root-mean-square error of bus voltage for two consecutive iterations be less than accepted error, then the solution is converged and go to step 3.e. If not then the solution is not converged, so go to step 3.a for the next iteration

e. Calculate controllers' model for the next time step

f. Predict the rotor speeds of all SMs and determine rotor angles based on the calculated rotor speeds

g. Calculate the history terms of all elements except SMs and nonlinear inductances (the history term of an inductor, for example, as indicated in equation (1.5)), then update the b_n vector and proceed to step 3.a for the next time step

4.2.1.2 Dynamic phasor model

The TD solution of reference [49] for nonlinear components is used, to find the DP model of a nonlinear inductor. The current based on the Fourier series having the zero and fundamental frequency components is:

$$i_{L_m} = \mathrm{I}_{L_{m,0}} + \mathrm{I}_{L_{m,1}} e^{j\omega t} + \mathrm{I}_{L_{m,-1}} e^{-j\omega t} \tag{4.8}$$

Assume that the flux-current are oscillating at a piecewise, then replacing equation (4.8) in equation (4.3) gives:

$$\phi_{L_m} = K_Q \mathrm{I}_{L_{m,0}} + K_Q \mathrm{I}_{L_{m,1}} e^{j\omega t} + K_Q \mathrm{I}_{L_{m,-1}} e^{-j\omega t} + \phi_Q \tag{4.9}$$

The relation of the flux and current for a segment (equation (4.3)) cannot be decoupled for the zero and fundamental frequency components. The proposes method is to assign ϕ_Q to the fundamental harmonic and assume the zero harmonic as a linear inductance with the parameter of the knee point. Therefore:

$$\Phi_{L_{m,0}} = L_{m,0} \mathrm{I}_{L_{m,0}} \tag{4.10}$$

$$\Phi_{L_{m,1}} = K_Q \mathrm{I}_{L_{m,1}} + \phi_{Q_1} e^{-j\omega t} \tag{4.11}$$

$$\Phi_{L_{m,-1}} = K_Q \mathrm{I}_{L_{m,-1}} + \phi_{Q_1} e^{j\omega t} \tag{4.12}$$

where $L_{m,0}$, the inductance of the zero harmonic, is:

$$L_{m,0} = \frac{\phi_{knee}}{i_{knee}} \tag{4.13}$$

According to the DP property of equation (1.14), the following relation can be written:

$$\phi_{Q_1} = \phi_{Q_{-1}} = \frac{\phi_Q}{2} \tag{4.14}$$

Therefore, voltage relation using Fourier series is:

$$v_{L_m} = \frac{d\left(L_{m,0}\mathrm{I}_{L_{m,0}} + K_Q\mathrm{I}_{L_{m,1}}e^{j\omega t} + \phi_{Q_1} + K_Q\mathrm{I}_{L_{m,-1}}e^{-j\omega t} + \phi_{Q_{-1}}\right)}{dt} \tag{4.15}$$

Separating harmonic coefficients gives:

$$\mathrm{V}_{L_{m,0}} = L_{m,0}\frac{d\mathrm{I}_{L_{m,0}}}{dt} \tag{4.16}$$

$$\mathrm{V}_{L_{m,1}} = j\omega K_Q\mathrm{I}_{L_{m,1}} + \frac{d\left(K_Q\mathrm{I}_{L_{m,1}}\right)}{dt} + \frac{d\left(\phi_{Q_1}\right)}{dt}e^{-j\omega t} \tag{4.17}$$

Using Trapezoidal integration rule, equations (4.16) and (4.17) are discretized as:

$$\mathrm{I}_{L_{m,0,n}} = \frac{\Delta t}{2L_{m,0}}\mathrm{V}_{L_{m,0,n-1}} + \mathrm{I}_{L_{m,0,n-1}} + \frac{\Delta t}{2L_{m,0}}\mathrm{V}_{L_{m,0,n}} \tag{4.18}$$

$$\mathrm{I}_{L_{m,1,n}} = \frac{\mathrm{V}_{L_{m,1,n-1}} + \left(\frac{2}{\Delta t} - j\omega\right)K_{Q_{n-1}}\mathrm{I}_{L_{m,1,n-1}} + \left(\phi_{Q_{n-1}} - \phi_{Q_n}\right)\left(\frac{1+e^{j\omega\Delta t}}{\Delta t}\right)e^{-j\omega t} + \mathrm{V}_{L_{m,1,n}}}{\left(j\omega + \frac{2}{\Delta t}\right)K_{Q_n}} \tag{4.19}$$

Therefore, a DP nonlinear inductor and the Norton equivalent model using Trapezoidal rule can be shown as:

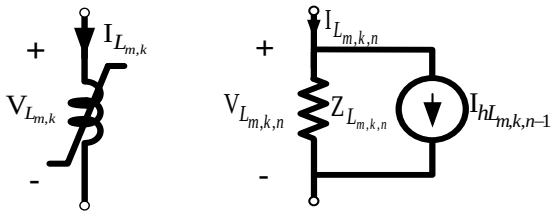

a) b)

Figure 4.5 Nonlinear inductor and Equivalent circuit

where $I_{hL_{m,0,n-1}}$ and $I_{hL_{m,1,n-1}}$, the history terms for the zero and fundamental harmonics, are:

$$I_{hL_{m,0,n-1}} = I_{L_{m,0,n-1}} + \frac{\Delta t}{2L_{m,0}} V_{L_{m,0,n-1}} \tag{4.20}$$

$$I_{hL_{m,1,n-1}} = \frac{V_{L_{m,1,n-1}} + \left(\frac{2}{\Delta t} - j\omega\right) K_{Q_{n-1}} I_{L_{m,1,n-1}} + \left(\phi_{Q_{n-1}} - \phi_{Q_n}\right)\left(\frac{1+e^{j\omega\Delta t}}{\Delta t}\right) e^{-j\omega t}}{\left(j\omega + \frac{2}{\Delta t}\right) K_{Q_n}} \tag{4.21}$$

and $Z_{hL_{m,0}}$ and $Z_{hL_{m,1,n}}$, the equivalent impedance for the zero and fundamental harmonics, are:

$$Z_{L_{m,0}} = \frac{2L_{m,0}}{\Delta t} \tag{4.22}$$

$$Z_{L_{m,1,n}} = \left(j\omega + \frac{2}{\Delta t}\right) K_{Q_n} \tag{4.23}$$

In simulation of GMD by DP method, the GEF impact is modeled by the zero-frequency harmonic. The solver models the system for the zero and the fundamental frequency. The superposition of the zero and fundamental frequency harmonics lead to transformation saturation. The following are the steps in a GMD simulation using DP approach:

1. Three phase Load-flow: to simulate unbalanced network from initial state, a three-phase load flow is used.

2. Initialization

    a. Convert the loads to constant impedances: other load models like constant power or constant current can be used. In this thesis, the fucus is on the modeling of SM and the simple load model, constant impedance is implemented.

    b. Calculate equivalent circuit of elements by discretized method

    c. Build the admittance submatrix of MANA (equation (1.8)) for zero and fundamental harmonics. The MANA admittance submatrix for the zero-frequency harmonic is constant. To calculate the fundamental frequency submatrix admittance of the network, the SMs and nonlinear inductances are excluded. During the simulation, the impedance of all components except SM and transformers remains constant. To avoid having repetitive computation, the constant portion of the admittance submatrix is computed during the initialization phase, and the variable part is added to the admittance submatrix during the simulation.

    d. Calculate the history terms for the first time-step based on the load-flow results

3. Dynamic simulation

    a. Calculate equivalent impedance and injection current for all SMs (using equations (2.335) and (2.336)) and all nonlinear inductances (using equations (4.20) to (4.23))

    b. Add equivalent impedance of SMs and nonlinear inductances to the admittance submatrix of MANA, add injection current of SMs and nonlinear inductances to the $\mathbf{B}_{1,n}$ vector, and solve both $\mathbf{A}_{0,n}\mathbf{X}_{0,n} = \mathbf{B}_{0,n}$ and $\mathbf{A}_{1,n}\mathbf{X}_{1,n} = \mathbf{B}_{1,n}$

    c. Update working segment of nonlinear inductors and *dq*0-axes currents (equations (2.319), (2.320), and (2.325)), rotor speed (equation (2.327)), and rotor angle (equation (2.330)) for all SMs

    d. If the root-mean-square error of bus voltage for two consecutive iterations be less than accepted error, then the solution is converged and go to step 3.e. If not then the solution is not converged, so go to step 3.a for the next iteration

e. Calculate controllers' model for the next time step

f. Predict the rotor speeds of all SMs and determine rotor angles based on the calculated rotor speeds

g. Calculate the history terms of all elements except SMs and nonlinear inductances (the history term of an inductor, for example, as indicated in equation (1.5)), then update the b_n vector and proceed to step 3.a for the next time step

4.3 Simulation results

This section contributes to a comparison of results obtained from time domain and dynamic phasor methods. All implemented methods use an iterative solution for saturation of transformers. To validate the methods, results are compared to TD method using an integration time step 100 μs.

Initially, the proposed DP method of transformer saturation modeling is validated. An overvoltage is applied to transformer connected bus 4 of IEEE-118 bus, and the magnetization currents of DP and TD methods are compared. In this test, there is no zero frequency harmonic and the simulation is done for the fundamental harmonic.

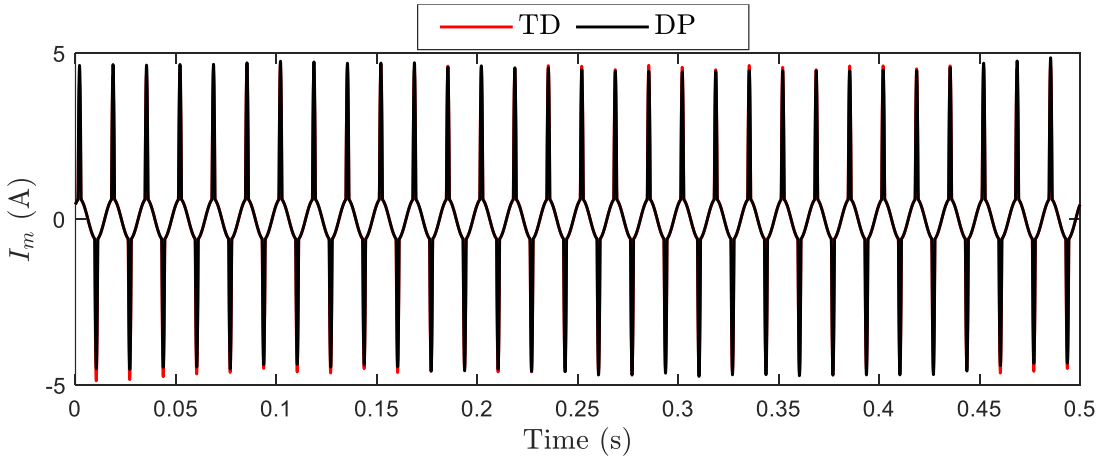

Figure 4.6 Magnetization current

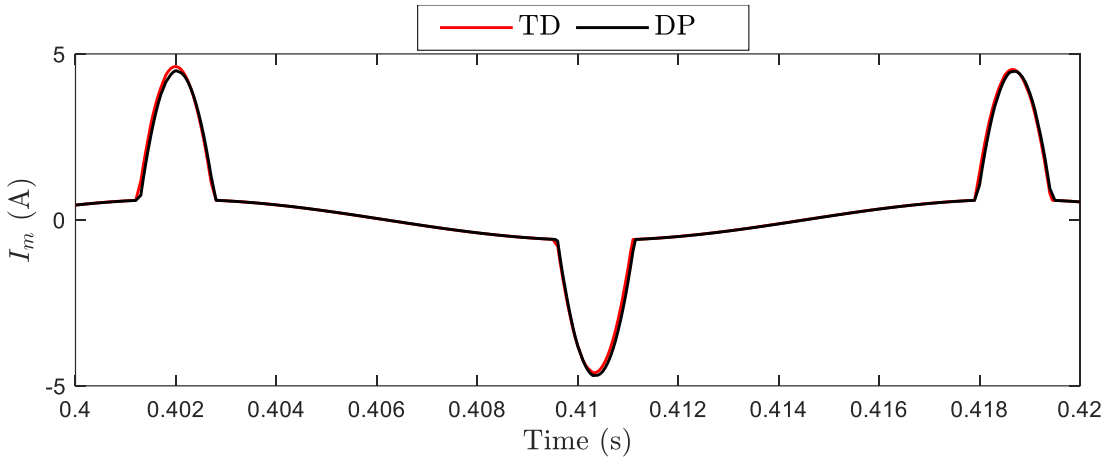

Figure 4.7 Magnetization current (zoom)

Figure 4.6 and Figure 4.7 show that the transformer saturation can be modeled by the DP method.

The proposed DP method of GMD modeling is validated. A GEF is applied to IEEE-118 bus system, and the magnetization currents of DP and TD methods are illustrated. In this test, the GEF is modeled at zero frequency harmonic system, and the transformer saturation is modeled at the fundamental frequency harmonic.

At $t = 100\mu s$, a GMD is applied to system creating an electric field with a constant amplitude of GEF = 5V/km positioned along an axis, which makes an angle $\theta_{GEF} = 35°$ with respect to the south–north axis. This constant GEF allows obtaining the system step response, illustrating saturation time delays, and performing future method-to-method comparison.

The test system is referred to as 118-GMD. The system voltage level is 345/138kV at transmission, 20kV at generation, and 25kV at distribution level. The total number of power transformers is 173 including the model of nonlinear iron core. The model further embeds 20 power plants with a total installed capacity of 3800 MW and 91 electric loads. There are 177 transmission lines with a total length of 10063 km. The models of synchronous machines (SMs) include mechanical and electrical dynamics, turbine-governor, control system with automatic voltage regulator (AVR), power system stabilizer (PSS). 118-GMD models GEFs as a lumped controllable dc voltage source in series with the transmission line model; the voltage is determined based on the GPS coordinates of line terminals and GEF amplitude and orientation specified by the user. Substation grounding has also

been incorporated. Further modeling data of 118-GMD can be found in [41]. Note that, the models of overexcitation limiter (OEL) for SM, and on-load-tapchanger (OLTC) of load transformers are excluded from the original benchmark.

The magnetizing branch voltage, current, and flux results are for generator transformer on NwCarlsl_138_004 for phase “a”. The simulations are performed by integration time steps of 100 μs.

To validate the DP result is compared to the TD method. shows magnetizing branch current during applying the GMD. The transformer saturates in one side according to GEF, and peak of current increases to about 50 A.

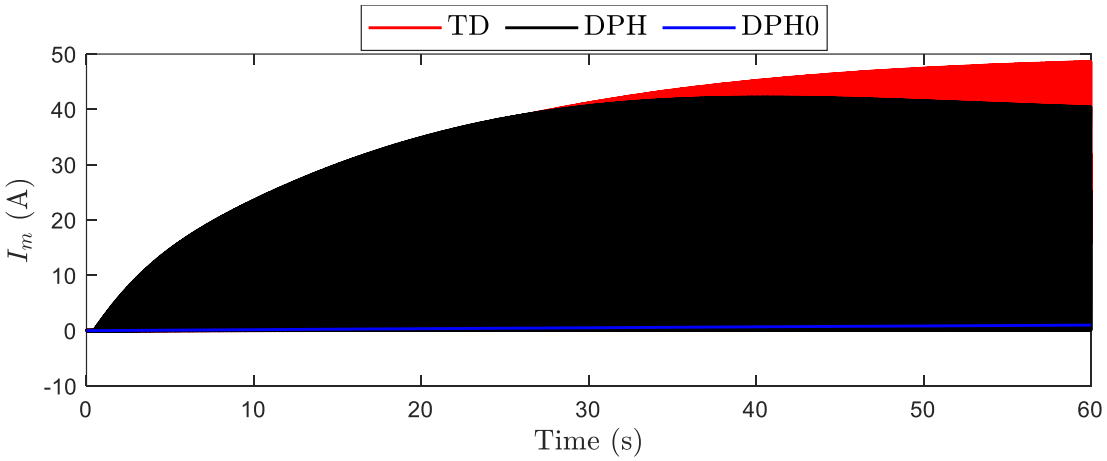

Figure 4.8 Magnetization current

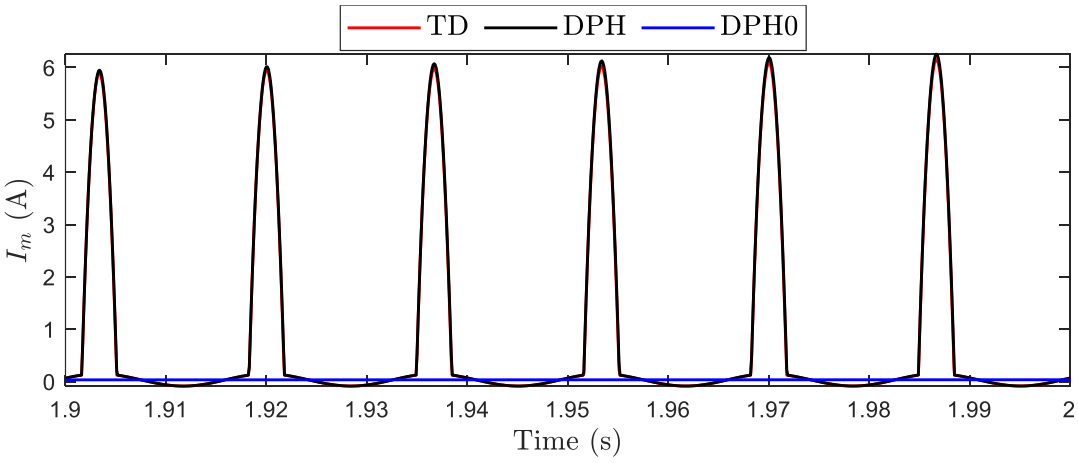

Figure 4.9 Magnetization current (zoom, low saturated)

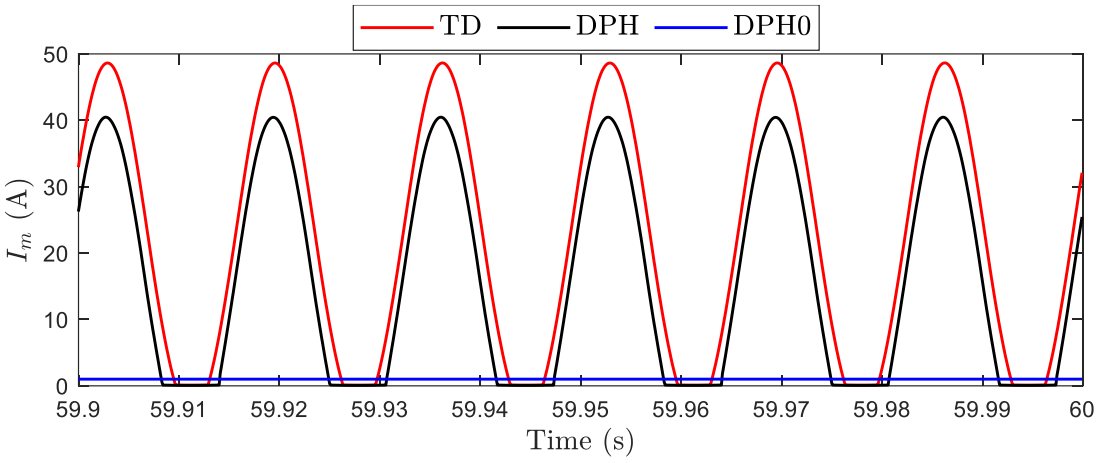

Figure 4.10 Magnetization current (zoom – high saturated)

Figure 4.8 shows magnetization current of TD and DP method. Figure 4.9 shows the magnetization current for interval of 1.9 to 2 seconds, when the transformer saturation current is increasing. In this stage of saturation, the DP method gives the same result as TD method.

Figure 4.10 shows magnetizing branch current when the transformer is deeply saturated. The DP has some error due to the assumption of considering the zero-frequency harmonic model of inductor as a linear inductor.

4.4 Conclusion

The proposed DP method gives a transformer saturation model, then the saturation model is used to simulate GMD impacts. To gain this aim, the system is modeled for the zero and fundamental frequency harmonic of DP method. The zero-frequency harmonic model of inductor is assumed linear, and the fundamental frequency uses the nonlinear model. The results show the DP is able to simulate GMD while its accuracy decreases for deep saturation modeling.

Also, the DP method has more equation than the TD method. Since the system is nonlinear, DP solves fundamental frequency and dc component dependently in each simulation time step. So that the number of equations of Newton solution for DP method is about three times to the number of equation that TD method has.

Chapter 5 CONCLUSION

5.1 Thesis summary

The dissertation describes the EMT-type and phasor domain simulators for power systems. Based on the presented simulations, it is shown that the DP method due to its dual (time domain and phasor domain) nature is more accurate than the pure phasor domain methods (3pPD and DP). The accuracies and limitations of 3pPD and DP methods are compared, and the differences are explained.

Although the DP method can capture faster EMT-type transients, it does not deliver the same accuracy as the pure TD method. Moreover, it is shown that for larger time steps, the accuracy of the DP method deteriorates, and its computational performance does not surpass the TD method for the same numerical integration time step. It is also demonstrated that the TD method can maintain sufficient accuracy at very high numerical time steps if it employs a fully iterative process for the solution of its synchronous machine equations. It appears that despite its theoretical advantages, the DP method remains on average 2.9 times slower than the full TD method. This conclusion is based on comparing codes in the same development environment and for different network conditions and fault cases.

In chapter 3 is shown that to have the same results of DP and TD methods, it is necessary to model harmonic in the power system as well as SM and controller. To simulate harmonics, the burden of computation increases by the number of implemented harmonics. As a result, the required memory and available hard drive space is several times more than the TD method.

To summarize, the DP method as well as TD can simulate EMT-type transients. And can employ large time steps to simulate low frequency transients. But to have accurate results, DP needs to model harmonics rather than fundamental frequency which increases the computation burden.

5.2 Publications

1- R. Hassani, J. Mahseredjian, T. Tshibungu, and U. Karaagac, "Evaluation of Time-Domain and Phasor-Domain Methods for Power System Transients," Electric Power Systems Research.

2- R. Pourramezan, R. Hassani, H. Karimi, M. Paolone, and J. Mahseredjian, "A Real-time Synchrophasor Data Compression Method Using Singular Value Decomposition," IEEE Transactions on Smart Grid, pp. 1-1, 2021.

3- A. Haddadi, R. Hassani, J. Mahseredjian, L. Gérin-Lajoie, and A. Rezaei-Zare, "Evaluation of Simulation Methods for Analysis of Geomagnetic Disturbance System Impacts," IEEE Transactions on Power Delivery, vol. 36, no. 3, pp. 1509-1516, 2021.

4- A. Haddadi, A. Rezaei-Zare, L. Gérin-Lajoie, R. Hassani, and J. Mahseredjian, "A Modified IEEE 118-Bus Test Case for Geomagnetic Disturbance Studies-Part I: Model Data," IEEE Transactions on Electromagnetic Compatibility, vol. 62, no. 3, pp. 955-965, 2020.

5- A. Haddadi, L. Gérin-Lajoie, A. Rezaei-Zare, R. Hassani, and J. Mahseredjian, "A Modified IEEE 118-Bus Test Case for Geomagnetic Disturbance Studies-Part II: Simulation Results," IEEE Transactions on Electromagnetic Compatibility, vol. 62, no. 3, pp. 966-975, 2020.

5.3 Future works

The main disadvantage of DP method is high computation burden. It makes the run of simulations slower than the TD method used for the same detail and time step. To increase simulation time, one possible method is parallel simulation. The computation of each harmonic can be done dependently at each time step point.

REFERENCES

[1] S. Henschel, "Analysis of electromagnetic and electromechanical power system transients with dynamic phasors," Ph.D. dissertation, University of British Colombia, 1999.

[2] Z. Miao, L. Piyasinghe, J. Khazaei, and L. Fan, "Dynamic Phasor-Based Modeling of Unbalanced Radial Distribution Systems," *IEEE Transactions on Power Systems*, vol. 30, no. 6, pp. 3102-3109, 2015.

[3] Z. Shuai, Y. Peng, J. M. Guerrero, Y. Li, and Z. J. Shen, "Transient Response Analysis of Inverter-Based Microgrids Under Unbalanced Conditions Using a Dynamic Phasor Model," *IEEE Transactions on Industrial Electronics*, vol. 66, no. 4, pp. 2868-2879, 2019.

[4] E. Karami, G. B. Gharehpetian, M. Madrigal, and J. d. J. Chavez, "Dynamic Phasor-Based Analysis of Unbalanced Three-Phase Systems in Presence of Harmonic Distortion," *IEEE Transactions on Power Systems*, vol. 33, no. 6, pp. 6642-6654, 2018.

[5] S. Zhu *et al.*, "Reduced-Order Dynamic Model of Modular Multilevel Converter in Long Time Scale and Its Application in Power System Low-Frequency Oscillation Analysis," *IEEE Transactions on Power Delivery*, vol. 34, no. 6, pp. 2110-2122, 2019.

[6] Ö. C. Sakinci and J. Beerten, "Generalized Dynamic Phasor Modeling of the MMC for Small-Signal Stability Analysis," *IEEE Transactions on Power Delivery*, vol. 34, no. 3, pp. 991-1000, 2019.

[7] J. Rupasinghe, S. Filizadeh, and L. Wang, "A Dynamic Phasor Model of an MMC With Extended Frequency Range for EMT Simulations," *IEEE Journal of Emerging and Selected Topics in Power Electronics*, vol. 7, no. 1, pp. 30-40, 2019.

[8] C. Guo, J. Yang, and C. Zhao, "Investigation of Small-Signal Dynamics of Modular Multilevel Converter Under Unbalanced Grid Conditions," *IEEE Transactions on Industrial Electronics*, vol. 66, no. 3, pp. 2269-2279, 2019.

[9] A. Bagheri-Vandaei and S. Filizadeh, "Generalised extended-frequency dynamic phasor model of LCC-HVDC systems for electromagnetic transient simulations," *IET Generation, Transmission & Distribution*, vol. 12, no. 12, pp. 3061-3069, 2018.

[10] P. Mattavelli, A. M. Stankovic, and G. C. Verghese, "SSR analysis with dynamic phasor model of thyristor-controlled series capacitor," *IEEE Transactions on Power Systems*, vol. 14, no. 1, pp. 200-208, 1999.

[11] Y. Xia, Y. Chen, H. Ye, and K. Strunz, "Multiscale Induction Machine Modeling in the dq0 Domain Including Main Flux Saturation," *IEEE Transactions on Energy Conversion*, vol. 34, no. 2, pp. 652-664, 2019.

[12] M. Berger, I. Kocar, H. Fortin-Blanchette, and C. Lavertu, "Hybrid Average Modeling of Three-Phase Dual Active Bridge Converters for Stability Analysis," *IEEE Transactions on Power Delivery*, vol. 33, no. 4, pp. 2020-2029, 2018.

[13] T. Yang, S. Bozhko, J. Le-Peuvedic, G. Asher, and C. I. Hill, "Dynamic Phasor Modeling of Multi-Generator Variable Frequency Electrical Power Systems," *IEEE Transactions on Power Systems*, vol. 31, no. 1, pp. 563-571, 2016.

[14] M. A. Elizondo, F. K. Tuffner, and K. P. Schneider, "Simulation of Inrush Dynamics for Unbalanced Distribution Systems Using Dynamic-Phasor Models," *IEEE Transactions on Power Systems,* vol. 32, no. 1, pp. 633-642, 2017.

[15] J. Song, J. Zhang, and H. Wen, "Accurate Dynamic Phasor Estimation by Matrix Pencil and Taylor Weighted Least Squares Method," *IEEE Transactions on Instrumentation and Measurement,* vol. 70, pp. 1-11, 2021.

[16] P. Zhang, J. R. Marti, and H. W. Dommel, "Synchronous Machine Modeling Based on Shifted Frequency Analysis," *IEEE Transactions on Power Systems,* vol. 22, no. 3, pp. 1139-1147, 2007.

[17] M. C. Chudasama and A. M. Kulkarni, "Dynamic Phasor Analysis of SSR Mitigation Schemes Based on Passive Phase Imbalance," *IEEE Transactions on Power Systems,* vol. 26, no. 3, pp. 1668-1676, 2011.

[18] S. Dambhare, S. A. Soman, and M. C. Chandorkar, "Adaptive Current Differential Protection Schemes for Transmission-Line Protection," *IEEE Transactions on Power Delivery,* vol. 24, no. 4, pp. 1832-1841, 2009.

[19] A. M. Stankovic and T. Aydin, "Analysis of asymmetrical faults in power systems using dynamic phasors," *IEEE Transactions on Power Systems,* vol. 15, no. 3, pp. 1062-1068, 2000.

[20] M. Daryabak *et al.*, "Modeling of LCC-HVDC Systems Using Dynamic Phasors," *IEEE Transactions on Power Delivery,* vol. 29, no. 4, pp. 1989-1998, 2014.

[21] X. Guo, Z. Lu, B. Wang, X. Sun, L. Wang, and J. M. Guerrero, "Dynamic Phasors-Based Modeling and Stability Analysis of Droop-Controlled Inverters for Microgrid Applications," *IEEE Transactions on Smart Grid,* vol. 5, no. 6, pp. 2980-2987, 2014.

[22] C. Liu, A. Bose, and P. Tian, "Modeling and Analysis of HVDC Converter by Three-Phase Dynamic Phasor," *IEEE Transactions on Power Delivery,* vol. 29, no. 1, pp. 3-12, 2014.

[23] Y. Peng, Z. Shuai, X. Liu, Z. Li, J. M. Guerrero, and Z. J. Shen, "Modeling and Stability Analysis of Inverter-Based Microgrid Under Harmonic Conditions," *IEEE Transactions on Smart Grid,* vol. 11, no. 2, pp. 1330-1342, 2020.

[24] T. Demiray, G. Andersson, and L. Busarello, "Evaluation study for the simulation of power system transients using dynamic phasor models," in *2008 IEEE/PES Transmission and Distribution Conference and Exposition: Latin America,* 13-15 Aug. 2008 2008, pp. 1-6.

[25] M. A. Hannan and K. W. Chan, "Modern power systems transients studies using dynamic phasor models," in *2004 International Conference on Power System Technology, 2004. PowerCon 2004.*, 21-24 Nov. 2004 2004, vol. 2, pp. 1469-1473 Vol.2.

[26] H. Shengli, S. Ruihua, and Z. Xiaoxin, "Analysis of balanced and unbalanced faults in power systems using dynamic phasors," in *Proceedings. International Conference on Power System Technology,* 13-17 Oct. 2002 2002, vol. 3, pp. 1550-1557 vol.3.

[27] P. Zhang, J. R. Marti, and H. W. Dommel, "Induction Machine Modeling Based on Shifted Frequency Analysis," *IEEE Transactions on Power Systems,* vol. 24, no. 1, pp. 157-164, 2009.

[28] A. M. Stankovic, S. R. Sanders, and T. Aydin, "Dynamic phasors in modeling and analysis of unbalanced polyphase AC machines," *IEEE Transactions on Energy Conversion,* vol. 17, no. 1, pp. 107-113, 2002.

[29] S. Fan and H. Ding, "Time Domain Transformation Method for Accelerating EMTP Simulation of Power System Dynamics," *IEEE Transactions on Power Systems,* vol. 27, no. 4, pp. 1778-1787, 2012.

[30] J. Mahseredjian, S. Dennetière, L. Dubé, B. Khodabakhchian, and L. Gérin-Lajoie, "On a new approach for the simulation of transients in power systems," *Electric Power Systems Research,* vol. 77, no. 11, pp. 1514-1520, 2007/09/01/ 2007.

[31] L. O. Chua and P. M. Lin, *Computer aided analysis of electronic circuits, algorithms and computational techniques*. Prentice-Hall, 1975.

[32] H. Chung-Wen, A. Ruehli, and P. Brennan, "The modified nodal approach to network analysis," *IEEE Transactions on Circuits and Systems,* vol. 22, no. 6, pp. 504-509, 1975, doi: 10.1109/tcs.1975.1084079.

[33] F. Milano and A. O. Manjavacas, "Frequency-Dependent Model for Transient Stability Analysis," *IEEE Transactions on Power Systems,* vol. 34, no. 1, pp. 806-809, 2019, doi: 10.1109/tpwrs.2018.2871639.

[34] P. Kundur, N. J. Balu, and M. G. Lauby, *Power system stability and control*. New York: McGraw-Hill (in English), 1994.

[35] I. M. Canay, "Causes of Discrepancies on Calculation of Rotor Quantities and Exact Equivalent Diagrams of the Synchronous Machine," *IEEE Transactions on Power Apparatus and Systems,* vol. PAS-88, no. 7, pp. 1114-1120, 1969.

[36] P. C. Krause, *Analysis of electric machinery*. New York: McGraw-Hill, 1986.

[37] P. W. Sauer, M. A. Pai, and J. H. Chow, *Power system dynamics and stability : with synchrophasor measurement and power system toolbox*. Hoboken, NJ, USA: Wiley, 2017.

[38] T. Tshibungu, "Dynamic phasor simulation of power system."

[39] W. Gautschi, *Numerical Analysis*. 2012.

[40] A. Haddadi, R. Hassani, J. Mahseredjian, L. Gérin-Lajoie, and A. Rezaei-Zare, "Evaluation of Simulation Methods for Analysis of Geomagnetic Disturbance System Impacts," *IEEE Transactions on Power Delivery,* vol. 36, no. 3, pp. 1509-1516, 2021.

[41] A. Haddadi, A. Rezaei-Zare, L. Gérin-Lajoie, R. Hassani, and J. Mahseredjian, "A Modified IEEE 118-Bus Test Case for Geomagnetic Disturbance Studies-Part I: Model Data," *IEEE Transactions on Electromagnetic Compatibility,* vol. 62, no. 3, pp. 955-965, 2020.

[42] A. Haddadi, L. Gérin-Lajoie, A. Rezaei-Zare, R. Hassani, and J. Mahseredjian, "A Modified IEEE 118-Bus Test Case for Geomagnetic Disturbance Studies-Part II: Simulation Results," *IEEE Transactions on Electromagnetic Compatibility,* vol. 62, no. 3, pp. 966-975, 2020.

[43] R. Horton, D. Boteler, T. J. Overbye, R. Pirjola, and R. C. Dugan, "A Test Case for the Calculation of Geomagnetically Induced Currents," *IEEE Transactions on Power Delivery,* vol. 27, no. 4, pp. 2368-2373, 2012.

[44] D. H. Boteler, "The use of linear superposition in modelling geomagnetically induced currents," in *2013 IEEE Power & Energy Society General Meeting*, 21-25 July 2013 2013, pp. 1-5.

[45] V. D. Albertson, J. G. Kappenman, N. Mohan, and G. A. Skarbakka, "Load-Flow Studies in the Presence of Geomagnetically-Induced Currents," *IEEE Transactions on Power Apparatus and Systems*, vol. PAS-100, no. 2, pp. 594-607, 1981.

[46] T. J. Overbye, T. R. Hutchins, K. Shetye, J. Weber, and S. Dahman, "Integration of geomagnetic disturbance modeling into the power flow: A methodology for large-scale system studies," in *2012 North American Power Symposium (NAPS)*, 9-11 Sept. 2012 2012, pp. 1-7.

[47] Y. Zhang, K. S. Shetye, R. H. Lee, and T. J. Overbye, "Impact of Geomagnetic Disturbances on Power System Transient Stability," in *2018 North American Power Symposium (NAPS)*, 9-11 Sept. 2018 2018, pp. 1-6.

[48] T. R. Hutchins and T. J. Overbye, "Power system dynamic performance during the late-time (E3) high-altitude electromagnetic pulse," in *2016 Power Systems Computation Conference (PSCC)*, 20-24 June 2016 2016, pp. 1-6.

[49] J. Mahseredjian, S. Lefebvre, and X.-D. Do, "A New Method for Time-Domain Modelling of Nonlinear Circuits in Large Linear Networks," in *11th Power Systems Computation conference (PSCC)*, August 1993 1993, vol. Proceedings Vol. 2, pp. 915-922.

[50] T. Noda and T. Kikuma, "A robust and efficient iterative scheme for the EMT simulations of nonlinear circuits," in *2012 IEEE Power and Energy Society General Meeting*, 22-26 July 2012 2012, pp. 1-1.

[51] L. O. Chua and P.-M. Lin, *Computer-aided analysis of electronic circuits : algorithms and computational techniques*. Englewood Cliffs, N.J. , USA: Prentice-Hall, 1975.